

ASSESSMENT OF DIFFUSIVE AND CONVECTIVE MECHANISMS
DURING CARBON DIOXIDE SEQUESTRATION INTO DEEP SALINE
AQUIFERS

A THESIS SUBMITTED TO
THE GRADUATE SCHOOL OF NATURAL AND APPLIED SCIENCES
OF
MIDDLE EAST TECHNICAL UNIVERSITY

BY

EMRE ÖZGÜR

IN PARTIAL FULFILLMENT OF THE REQUIREMENTS
FOR
THE DEGREE OF MASTER OF SCIENCE
IN
PETROLEUM AND NATURAL GAS ENGINEERING

DECEMBER 2006

Approval of the Graduate School of Natural and Applied Sciences

Prof. Dr. Canan Özgen
Director

I certify that this thesis satisfies all the requirements as a thesis for the degree of Master of Science.

Prof. Dr. Mahmut Parlaktuna
Head of Department

This is to certify that we have read this thesis and that in our opinion it is fully adequate, in scope and quality, as a thesis for the degree of Master of Science

Prof. Dr. Fevzi Gümrah
Supervisor

Examining Committee Members

Prof. Dr. Mahmut Parlaktuna (METU,PETE) _____

Prof. Dr. Fevzi Gümrah (METU,PETE) _____

Prof. Dr. Birol Demiral (METU,PETE) _____

Prof. Dr. Nurkan Karahanoğlu (METU,GEOE) _____

Assist. Prof. Dr. M. Evren Özbayoğlu (METU,PETE) _____

I hereby declare that all information in this document has been obtained and presented in accordance with academic rules and ethical conduct. I also declare that, as required by these rules and conduct, I have fully cited and referenced all material and results that are not original to this work.

Name, Last name : EMRE ÖZGÜR

Signature:

ABSTRACT

ASSESSMENT OF DIFFUSIVE AND CONVECTIVE MECHANISMS DURING CARBON DIOXIDE SEQUESTRATION INTO DEEP SALINE AQUIFERS

Özgür, Emre

M.S., Department of Petroleum and Natural Gas Engineering

Supervisor: Prof. Dr. Fevzi Gümrah

December 2006, 99 pages

The analytical and numerical modeling of CO₂ sequestration in deep saline aquifers having different properties was studied with diffusion and convection mechanisms. The complete dissolution of CO₂ in the aquifer by diffusion took thousands, even millions of years. In diffusion dominated system, an aquifer with 100 m thickness saturated with CO₂ after 10,000,000 years. It was much earlier in convective dominant system. In diffusion process, the dissolution of CO₂ in aquifer increased with porosity increase; however, in convection dominant process dissolution of CO₂ in aquifer decreased with porosity increase. The increase in permeability accelerated the dissolution of CO₂ in aquifer significantly, which was due to increasing velocity. The dissolution process in the aquifer realized faster for the aquifers with lower dispersivity. The results of convective dominant mechanism in aquifers with 1md and 10 md permeability

values were so close to that of diffusion dominated system. For the aquifer having permeability higher than 10 md, the convection mechanism began to dominate gradually and it became fully convection dominated system for 50 md and higher permeability values. These results were also verified with calculated Rayleigh number and mixing zone lengths. The mixing zone length increased with increase in porosity and time in diffusion dominated system. However, the mixing zone length decreased with increase in porosity and it increased with increase in dispersivity and permeability higher than 10 md in convection dominated system.

Keywords: CO₂ sequestration, deep saline aquifer, diffusion, convection, analytical modeling, numerical modeling

ÖZ

DERİN TUZLU AKİFERLERE KARBONDİOKSİT TECRIDİNDE, DİFÜZYON VE KONVEKSİYON MEKANİZMALARININ DEĞERLENDİRİLMESİ

Özgür, Emre

Yüksek Lisans, Petrol ve Doğal Gaz Mühendisliği Bölümü

Tez Yöneticisi: Prof. Dr. Fevzi Gümrah

Aralık 2006, 99 sayfa

Karbondioksitin değişik özelliklere sahip derin tuzlu akiferlerde tecridinin difüzyon ve konveksiyon mekanizmaları dikkate alınarak analitik ve nümerik yaklaşımlarla modellenmesi yapıldı. Karbondioksitin sadece difüzyon mekanizmasıyla akiferde çözünmesi binlerce yıl hatta milyonlarca yıl aldı. Difüzyonun baskın olduğu sistemlerde, 100 metre boyundaki bir akiferin karbondioksit ile doyması yaklaşık 10,000,000 yıl almaktaydı. Fakat bu süre konveksiyon mekanizmasının baskın olduğu sistemlerde daha erken gerçekleşti. Difüzyon mekanizmasının baskın olduğu sistemlerde, çözünme gözeneklilik artışıyla birlikte arttı, fakat konveksiyon mekanizmalarının baskın olduğu sistemlerde bunun tam tersi gerçekleşti. Geçirgenlik artışında karbondioksitin akiferlerde çözünmesini, hız artışından dolayı ciddi derece de arttıran bir faktördü. Çözünme işlemi düşük yayınlı akiferlerde daha erken gerçekleşti. 1md ve 10md geçirgenliğine sahip akiferlerdeki konveksiyon mekanizmalarına göre hesaplanan sonuçlar hemen hemen difüzyon sistemindeki gibi aynı değerlerdeydi. 10md geçirgenlik değerinden yüksek olan akiferlerde, yavaş yavaş konveksiyon mekanizması etkili olmaya başladı ve 50md ve daha yukarı geçirgenlik değerlerinde ise tamamen konveksiyon mekanizması baskın hale

geldi. Bu sonuçlar Rayleigh sayılarıyla ve karışım bölgesinin uzunluğuyla da doğrulandı. Difüzyonun baskın olduğu sistemlerde karışım bölgesinin uzunluğu gözeneklilik ve zaman artışıyla arttı. Fakat, karışım bölgesinin uzunluğu konveksiyon baskın sistemlerde gözeneklilik arttıkça azaldı ve yayılım ve geçirgenlik artışıyla 10md'den sonra artmaya başladı.

Anahtar Kelimeler: CO₂ tecridi, derin tuzlu akifer, difüzyon, konveksiyon, analitik modelleme, nümerik modelleme

ACKNOWLEDGMENTS

I would like to express my gratitude to Prof. Dr. Fevzi GÜMRAH for his guidance, continuous encouragement and supervision in completing this study. I would like to thank also to Middle East Technical University for the financial support provided in my thesis study.

Thanks are extended to my colleagues; Çiğdem, Mehmet, and Sevtaç for their helps while studying my thesis.

Finally I also would like to express my biggest thanks to my family and my aunt for their endless supports during my thesis study.

TABLE OF CONTENTS

PLAGIARISM.....	iii
ABSTRACT.....	iv
ÖZ.....	vi
ACKNOWLEDGEMENTS.....	viii
TABLE OF CONTENTS.....	ix
LIST OF FIGURES.....	xiii
LIST OF TABLES.....	xviii
NOMENCLATURE.....	xix
CHAPTER	
1. INTRODUCTION.....	1
2. WORLD CLIMATE AND CO ₂ SEQUESTRATION.....	3
2.1 Climate Change.....	3
2.2 CO ₂ Sequestration in Deep Saline Aquifers.....	6
3. SOLUTE TRANSPORT IN AQUIFERS.....	9
3.1 Aquifers.....	9
3.2 Transport Mechanisms.....	11
3.3 Molecular Diffusion.....	11
3.4 Measurement Techniques for Diffusion Coefficient of Gases in Liquids.....	13
3.5 CO ₂ Diffusion Coefficient in Water.....	14
3.5.1 Temperature Effect.....	14
3.5.2 Pressure Effect.....	15
3.5.3 Concentration Effect.....	16
3.6 Convection.....	16
3.7 Dispersion.....	18
3.8 Aquifer Properties.....	20

3.8.1 Porosity.....	20
3.8.2 Permeability.....	20
3.8.3 Hydraulic Conductivity.....	20
3.8.4 Dispersivity.....	21
3.9 Physical Properties of CO ₂ -Brine System.....	24
3.9.1 Physical Properties of Carbon Dioxide.....	24
3.9.2 CO ₂ Solubility in Water.....	26
3.9.2.1 Salinity Effect.....	26
3.10 Density of Brine.....	28
3.11 Viscosity of Brine.....	29
3.12 Density of Water with CO ₂	31
3.13 Viscosity of Water with CO ₂	33
4. STATEMENT OF PROBLEM.....	34
5. METHODOLOGY.....	35
5.1 Analytical Modeling.....	35
5.2 Numerical Modeling.....	40
5.2.1 Numerical Simulator.....	41
5.3 Previous Studies Conducted on CO ₂ Sequestration in Deep Saline Aquifers at Petroleum and Natural Gas Engineering Department of METU.....	42
6. RESULTS AND DISCUSSION.....	43
6.1 The Results of Analytical Modeling Study.....	45
6.1.1 Analytical Modeling of Molecular Diffusion Mechanism.....	45
6.1.1.1 Effect of Duration on CO ₂ Saturation (analytical model).....	45
6.1.1.2 Effect of Porosity on CO ₂ Saturation (analytical model).....	45
6.1.2 Analytical Modeling of Convection Dominant Process	46

6.1.2.1 Effect of Dispersivity on CO ₂ Saturation (analytical modeling).....	47
6.1.2.2 Effect of Permeability on CO ₂ Saturation (analytical modeling).....	50
6.1.2.3 Effect of Porosity on CO ₂ Saturation (analytical model).....	50
6.2 The Results of Numerical Modeling Study.....	51
6.2.1 Numerical Modeling of Molecular Diffusion Process....	51
6.2.1.1 Effect of Duration on CO ₂ Saturation (numerical model).....	51
6.2.1.2 Effect of Porosity on CO ₂ Saturation (numerical model).....	55
6.2.2 Numerical Modeling of Convection Dominant Process.....	57
6.2.2.1 Effect of Dispersivity on CO ₂ Saturation (numerical model).....	57
6.2.2.2 Effect of Permeability on CO ₂ Saturation (numerical model).....	64
6.2.2.3 Effect of Porosity on CO ₂ Saturation (numerical model).....	67
6.3 Comparison of Analytical and Numerical Models.....	69
6.3.1 Molecular Diffusion Process.....	69
6.3.1.1 Effect of Duration on CO ₂ Saturation.....	69
6.3.1.2 Effect of Porosity on CO ₂ Saturation.....	70
6.3.2 Convection Dominated Process.....	71
6.3.2.1 Effect of Dispersivity on CO ₂ Saturation.....	71
6.3.2.2 Effect of Permeability on CO ₂ Saturation.....	74
6.3.2.3 Effect of Porosity on CO ₂ Saturation.....	76
6.3.2.4 Root Mean Square Error (RMSE).....	77

6.4 Determination of Mixing Zone Length by Using the Results of Analytical Modeling.....	78
6.4.1 Molecular Diffusion Process.....	78
6.4.1.1 Effect of Time on Mixing Zone Length.....	78
6.4.1.2 Effect of Porosity on Mixing Zone Length.....	79
6.4.2 Convection Process.....	79
6.4.2.1 Effect of Dispersivity on Mixing Zone Length....	79
6.4.2.2 Effect of Permeability on Mixing Zone Length....	80
6.4.1.3 Effect of Porosity on Mixing Zone Length.....	81
6.5 CO ₂ Saturated Part of the Aquifer.....	81
6.6 Rayleigh and Peclet Numbers.....	82
6.7 Comparison between Numerical Results of Molecular Diffusion and Dispersion.....	84
7. CONCLUSION.....	88
RECOMMENDATIONS.....	90
REFERENCES.....	91
APPENDIX.....	96

LIST OF FIGURES

Figure 2. 1. - The image of Arctic Sea Ice in 1979.....	4
Figure 2. 2. - The image of Arctic Sea Ice in 2003.....	5
Figure 2. 3. - Geological formations for the sequestration of CO ₂	6
Figure 2. 4. - Storage mechanisms in the sequestrating of CO ₂ in the aquifer.....	7
Figure 3. 1. - Cross-section of a typical groundwater system.....	10
Figure 3. 2. - CO ₂ Diffusion coefficients in pure water at atmospheric pressure.....	14
Figure 3. 3. - CO ₂ Diffusion coefficients in pure water at 13° C.....	15
Figure 3. 4. - Dispersion due to velocity profile in pores.....	18
Figure 3. 5. - Dispersion due to different velocities in different pores.....	18
Figure 3. 6. - Dispersion due to tortuosity.....	19
Figure 3. 7. - Longitudinal dispersivity based on aquifer depth.....	22
Figure 3. 8. - Longitudinal dispersivity values based on 10% trend and Neuman's equation.....	23
Figure 3. 9. - Vertical transverse dispersivity values based on 1% trend....	24
Figure 3. 10. - Phase behavior of CO ₂	25
Figure 3. 11. - Solubility of CO ₂ in distilled water.....	27
Figure 3. 12. - CO ₂ Solubility in brine for different salinity values.....	28
Figure 3. 13. - Brine density as a function of pressure, temperature and salinity.....	29
Figure 3. 14. - Brine viscosity as a function of pressure, temperature and salinity.....	31
Figure 3. 15. - Effect of CO ₂ on brine density at 50° C and 100000 ppm.....	33
Figure 3. 16. - Viscosity of water with dissolved CO ₂	33
Figure 5. 1. - Geometry and boundary conditions of the model.....	36

Figure 6. 1. - Effect of Duration on CO ₂ Saturation (analytical model).....	45
Figure 6. 2. - Effect of Porosity on CO ₂ Saturation (analytical model).....	46
Figure 6. 3. - Mean Velocity Calculation for Analytical Modeling.....	47
Figure 6. 4. - Effect of Dispersivity on CO ₂ Saturation (200 years, analytical model).....	48
Figure 6. 5. - Effect of Dispersivity on CO ₂ Saturation (750 years, analytical model).....	49
Figure 6. 6. - Effect of Dispersivity on CO ₂ Saturation (6000 years, analytical model).....	49
Figure 6. 7. - Effect of Permeability on CO ₂ Saturation (1000 years, analytical model).....	49
Figure 6. 8. - Effect of Porosity on CO ₂ Saturation (200 years, analytical model).....	51
Figure 6. 9. - Effect of Duration on CO ₂ Saturation ($\phi=0.2$, numerical model).....	51
Figure 6. 10. - Map of CO ₂ Saturation in an Aquifer for Run 1a, t=5000 years (numerical modeling).....	52
Figure 6. 11. - Map of CO ₂ Saturation in an Aquifer for Run 1b, t=10000 years (numerical modeling).....	53
Figure 6. 12. - Map of CO ₂ Saturation in an Aquifer for Run 1c, t=20000 years (numerical modeling).....	53
Figure 6. 13. - Map of CO ₂ Saturation in an Aquifer for Run 1d, t=100000 years (numerical modeling).....	54
Figure 6. 14. - Map of CO ₂ Saturation in an Aquifer for Run 1e, t=1000000 years (numerical modeling).....	54
Figure 6. 15. - Effect of Porosity on CO ₂ Saturation ($\phi=0.2$, numerical model).....	55
Figure 6. 16. - Map of CO ₂ Saturation in an Aquifer for Run 2a, $\phi=0.1$ ($2 \cdot 10^4$ years, numerical modeling).....	56

Figure 6. 17. - Map of CO ₂ Saturation in an Aquifer for Run 2b, $\phi=0.3$ ($2 \cdot 10^4$ years, numerical modeling).....	56
Figure 6. 18. - Effect of Dispersivity on CO ₂ Saturation ($t=200$ years, numerical model).....	58
Figure 6. 19. - Map of CO ₂ Saturation in an Aquifer for Run 3a, $\alpha=1$ m (200 years, numerical model).....	58
Figure 6. 20. - Map of CO ₂ Saturation in an Aquifer for Run 3b, $\alpha=10$ m (200 years, numerical model).....	59
Figure 6. 21. - Map of CO ₂ Saturation in an Aquifer for Run 3c, $\alpha=20$ m (200 years, numerical model).....	59
Figure 6. 22. - Effect of Dispersivity on CO ₂ Saturation ($t=750$ years, numerical model).....	60
Figure 6. 23. - Map of CO ₂ Saturation in an Aquifer for Run 4a, $\alpha=1$ m (750 years, numerical model).....	60
Figure 6. 24. - Map of CO ₂ Saturation in an Aquifer for Run 4b, $\alpha=10$ m (750 years, numerical model).....	61
Figure 6. 25. - Map of CO ₂ Saturation in an Aquifer for Run 4c, $\alpha=20$ m (750 years, numerical model).....	61
Figure 6. 26. - Effect of Dispersivity on CO ₂ Saturation ($t=6000$ years, numerical model).....	62
Figure 6. 27. - Map of CO ₂ Saturation in an Aquifer for Run 5a, $\alpha=1$ m (6000 years, numerical model).....	62
Figure 6. 28. - Map of CO ₂ Saturation in an Aquifer for Run 5b, $\alpha=10$ m (6000 years, numerical model).....	63
Figure 6. 29. - Map of CO ₂ Saturation in an Aquifer for Run 5c, $\alpha=20$ m (6000 years, numerical model).....	63
Figure 6. 30. - Effect of Permeability on CO ₂ Saturation ($t=1000$ years, numerical model).....	64

Figure 6. 31. - Map of CO ₂ Saturation in an Aquifer for Run 6a, k=1 md (1000 years, numerical model).....	65
Figure 6. 32. - Map of CO ₂ Saturation in an Aquifer for Run 6b, k=10 md (1000 years, numerical model).....	65
Figure 6. 33. - Map of CO ₂ Saturation in an Aquifer for Run 6c, k=100 md (1000 years, numerical model).....	66
Figure 6. 34. - Map of CO ₂ Saturation in an Aquifer for Run 6d, k=1000 md (1000 years, numerical model).....	66
Figure 6. 35. - Effect of Porosity of CO ₂ Saturation (t=200 years, numerical model).....	67
Figure 6. 36. - Map of CO ₂ Saturation in an Aquifer for Run 7a, $\phi=0.1$ (200 years, numerical modeling).....	68
Figure 6. 37. - Map of CO ₂ Saturation in an Aquifer for Run 3b, $\phi=0.2$ (200 years, numerical modeling).....	68
Figure 6. 38. - Map of CO ₂ Saturation in an Aquifer for Run 7b, $\phi=0.3$ (200 years, numerical modeling).....	69
Figure 6. 39. - Effect of Duration ($\phi=0.2$, comparison).....	70
Figure 6. 40. - Effect of Porosity (2.10 ⁴ years, comparison).....	70
Figure 6. 41. - Effect of Dispersivity (200 years, comparison).....	72
Figure 6. 42. - Effect of Dispersivity (750 years, comparison).....	72
Figure 6. 43. - Effect of Dispersivity (750 years, comparison).....	73
Figure 6. 44. - Effect of Dispersivity (750 years, comparison).....	73
Figure 6. 45. - Effect of Dispersivity (6000 years, comparison).....	74
Figure 6. 46. - Effect of Permeability (1000 years, comparison).....	75
Figure 6. 47. - Effect of Permeability (1000 years, comparison).....	75
Figure 6. 48. - Effect of Porosity (200 years, comparison).....	76
Figure 6. 49. - Variation of Mixing Zone with Time for Diffusion Dominated System.....	78
Figure 6. 50. - Variation of Mixing Zone with Porosity for Diffusion Dominated System (20000 years).....	79

Figure 6. 51. - Variation of Mixing Zone with Dispersivity for Convection Dominated System.....	80
Figure 6. 52. - Variation of Mixing Zone with Permeability for Convection Dominated System (1000 years).....	80
Figure 6. 53. - Variation of Mixing Zone with Porosity for Convection Dominated System (200 years).....	81
Figure 6. 54. - Comparison of Results for Runs 8a and 9a, $t=10000$ y and $k=1$ md.....	84
Figure 6. 55. - Comparison of Results for Runs 8b and 9b, $t=1000$ y and $k=10$ md.....	85
Figure 6. 56. - Comparison of Results for Runs 8c and 9c, $t=500$ y and $k=20$ md.....	85
Figure 6. 57. - Comparison of Results for Runs 8d and 9d, $t=200$ y and $k=50$ md.....	86
Figure 6. 58. - Comparison of Results for Runs 8e and 9e, $t=100$ y and $k=100$ md.....	86
Figure 6. 59. - Comparison of Results for Runs 8d and 9d, $t=10$ y and $k=1000$ md.....	87
Figure A.1. - Input Data for Run 3b.....	96
Figure A.2. - Input Data for all Density-dependent Runs.....	97
Figure A.3. - Options for layers of Aquifer about dispersivity and diffusion coefficient terms.....	97
Figure A.4. - User Interface Screen to Enter Inputs.....	98
Figure A.5. - User Interface Screen to Enter Inputs.....	98
Figure A.6. - Engine to Run the Given Inputs.....	99
Figure A.7 - Hydraulic Conductivities for Each Run.....	99

LIST OF TABLES

Table 2.1 - Natural Reservoirs for the storage of CO ₂	7
Table 6.1 - Common data to all runs given in tables 6.2, 6.3, 6.4, 6.5.....	43
Table 6.2 - Run conditions for analytical and numerical modeling with only molecular diffusion.....	43
Table 6.3 - Run conditions for analytical and numerical modeling with dispersion.....	44
Table 6.4 - Run conditions for numerical modeling with dispersion and molecular diffusion.....	44
Table 6.5 - Maximum Velocities Occured in the Runs.....	47
Table 6.6 - RMSE values for Runs.....	77
Table 6.7 - Constants for Polynomial Equation of C _D vs z _D Curves.....	82
Table 6.8 - CO ₂ Saturated Part of the aquifer (fraction), analytical modeling.....	82
Table 6.9 - Rayleigh Numbers.....	83
Table 6.10 - Peclet Numbers.....	83

NOMENCLATURE

Greek Symbols

α	Dispersivity (cm)
\emptyset	Porosity of reservoir, fraction
τ	Tortuosity
μ	Viscosity (cp)
$\Delta\rho$	Density difference (g/cm ³)
ρ	Fluid density (g/cm ³)

Abbreviations

TDS	Total dissolved solids concentration (weight percent)
Pe	Peclet Number
Ra	Rayleigh Number

Latin Symbols

C_{CO_2}	Concentration of CO ₂ in aquifer (mol/cm ³)
$C_{CO_2,sat}$	Concentration of CO ₂ in saturated aquifer at aquifer conditions (mol/cm ³)
C_D	Dimensionless Concentration
D_e	Effective diffusivity coefficient (cm ² /s)
D_o	Molecular Diffusion coefficient (cm ² /s)
g	Gravitational Acceleration (cm/s ²)
J	Diffusion Flux (mol/cm ² .s)
H	Thickness (cm)
K	Hydraulic Conductivity (cm/s)

k	Permeability (cm ²)
L	Length (cm)
M	Molecular Weight (gram/mole)
P	Pressure (atm)
S	Salinity (weight percent)
t	Time (second)
t_D	Dimensionless Time
T	Temperature (°C)
u	Superficial velocity (Darcy velocity) (cm/s)
V_o	Apparent molar volume (cm ³ /mol)
v_o	Interstitial velocity (cm/s, u/ϕ)
W	Weight (weight)
z	Depth below the interface (cm)
Z_D	Dimensionless Length

Subscripts

b	Brine
c	Critical
D	Dimensionless
H	Horizontal
L	Longitudinal
T	Transverse
w	Water

CHAPTER 1

INTRODUCTION

Consuming fossil fuels, industrial activities, and deforestation of lands are day by day increasing the atmospheric concentrations of carbon dioxide, methane, nitrous oxide, hydrofluorocarbons, perfluorocarbons, and sulfur hexafluoride. These main gases are accepted to be the responsible of global warming and are called “greenhouse gases”. Among the greenhouse gases, CO₂ is the major contributor to the global warming.

One way to protect the climate of our world is to prevent the release of CO₂ to the atmosphere or decrease its amount in the atmosphere by storing it in geological reservoirs. There are many options to store CO₂ in geological reservoirs, such as, depleted oil and gas reservoirs, coal beds, and deep saline aquifers. Deep saline aquifers have the potential to provide very large storage capacity worldwide at relatively low cost. There are a number of locations where deep saline aquifers have been used for natural gas storage, giving confidence that CO₂ could be stored safely for thousands of years in carefully selected saline aquifers [1, 2].

Aquifers are the underground layers of rock sufficiently porous to store water and permeable enough to allow water to flow through them in considerable amounts. There are two types of aquifers: unconfined and confined.

There are three main trapping mechanisms for the immobilization of CO₂ in deep saline aquifers; gaseous phase storage under caprock, which is called hydrodynamic trapping; trapping of CO₂ as dissolved solute in the aqueous phase,

which is called solubility trapping; and trapping of CO₂ in stable minerals due to the reactions in the aquifer, which is called mineral trapping [3].

In this study, the transport of CO₂ dissolved in brine is examined by molecular diffusion and mechanical dispersion mechanisms. The effect of aquifer properties on the transportation of injected CO₂ is analyzed with analytical and numerical modeling approaches.

CHAPTER 2

WORLD CLIMATE AND CO₂ SEQUESTRATION

2.1. Climate Change

There is a general consensus among the scientists that human activities are leading to an increase in the global average temperatures. Global temperatures have already risen 0.6°C in the last 100 years, and, according to model predictions, may continue to rise from as little as 1.8°C to as much as 7.1°C over the next 100 years. Burning of fossil fuels, industrial activities, and deforestation of lands are day by day increasing the atmospheric concentrations of carbon dioxide (CO₂), methane (CH₄), nitrous oxide (N₂O), hydrofluorocarbons (HFCs), perfluorocarbons (PFCs), and sulfur hexafluoride (SF₆). These main gases are accepted for the responsible of global warming and are called “greenhouse gases”. Among the greenhouse gases, CO₂ is the major contributor to the global warming. The atmospheric concentrations of carbon dioxide (CO₂) has increased by 35% from pre-industrial time values of 280 ppm to 378 ppm over the past 150 years and CO₂ is now responsible about 60% of the total radiative forcing of Earth by long-lived greenhouse gases. Consequently, the increased concentration of CO₂ arises the degree of the greenhouse effect and the global warming issue. The global warming may cause disruption in the chemical composition and physical dynamics of Earth’s atmosphere, leading to the distribution of heat or energy around atmosphere abnormally [4].

The increase in global temperatures is expected to cause environmental changes, such as, rises in sea levels, melting in glaciers and changes in the amount and pattern of precipitation. Such changes may increase the occurrence and strength of extreme weather events such as floods, hurricanes, and droughts. Although

global warming is expected to trigger many abnormal events, it is difficult to set up a relation between any particular event and global warming [5].

The effect of global warming on our earth could be seen in the images taken from NASA (National Aeronautics and Space Administration) [6]. In Figures 2.1 and 2.2, considerable changes in Arctic Ice could be seen between the years, 1979 and 2003. NASA created these images by the use of several data obtained from its satellites. The satellites include the scanning multi-channel microwave radiometer and the special sensor microwave imagers. The images show the minimum sea ice concentrations in Arctic Sea Ice for the years, 1979 and 2003.



Figure 2. 1. The image of Arctic Sea Ice in 1979 (NASA) [6]



Figure 2. 2. The image of Arctic Sea Ice in 2003 (NASA) [6]

There are many ways to combat against global warming and reduce CO₂ emissions, such as usage of renewable energy sources, increasing the efficiency of energy systems or by switching from solid fuels (e.g. coal) to liquid or gaseous fuels (e.g. oil or natural gas). However, many predictions indicate that these steps alone will not be able to achieve the required reductions in CO₂ emissions. The capture and storage of CO₂ in geological formations at the high emission points, such as industrial sources, could play an important role in solving this problem. The extensive usage of this technique could be achieved without the need for rapid change in the energy supply infrastructure. Several million tonnes of CO₂ are emitted annually due to the usage of fossil fuels in electricity production, oil refineries, cement works, and iron and steel production. The emissions of these industrial sources could be lowered significantly, without making major changes to the main processes, by capturing and sequestering the CO₂. Other sources of emissions, such as transport and domestic buildings, can not be controlled in the same way because of the large number of small sources of CO₂ [1].

2.2. CO₂ Sequestration in Deep Saline Aquifers

There are many alternatives to sequester CO₂ in geological reservoirs (Figure 2.3). CO₂ could be injected to depleted oil and gas reservoirs, coal beds, and deep saline aquifers for the sequestration. Among these geological reservoirs, the deep saline aquifer is the most promising one due to its high storage capacity. Sedimentary rocks such as sandstone and limestone have many small spaces or pores and many of them contain salt water that are called as saline aquifers. These aquifers are generally trapped by an overlying layer of impermeable rock. If CO₂ is injected into these aquifers, some will dissolve in the saline water and disperse widely in the aquifer. CO₂ can also react with the minerals within the aquifer and remain fixed for eternity. The most suitable aquifers for CO₂ sequestration are those at the location deeper than 800m, as the CO₂ will behave more like a liquid than a gas, enabling much more to be stored [7].

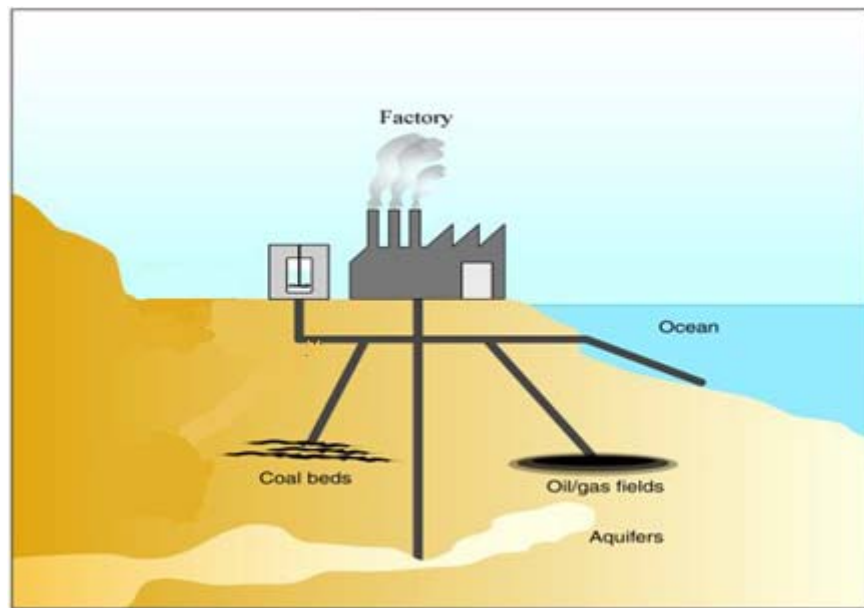


Figure 2. 3. Geological formations for the sequestration of CO₂ [7]

According to the estimation of International Energy Agency (IEA) Greenhouse Gas R&D Programme in the early 1990s, the global potential for storage of CO₂ in deep saline reservoirs is in the range of 400 and 10 000 Gtonne CO₂. Recent studies show that the storage capacity in geological reservoirs in Northwest Europe alone could be as high as 800 Gtonne CO₂ (most of this is deep saline aquifers). Research activities are ongoing in Europe and Australia to measure the storage capacity of offshore saline aquifers while similar research in Canada and the USA is looking at onshore saline aquifers. The global capacity of geological storage places are given in Table 2.1 to show the significance of deep saline aquifers.

Table 2.1, Natural Reservoirs for the Storage of CO₂ [7]

Sequestration Option	Worldwide Capacity (Gt CO ₂)
Deep Saline Aquifers	400 - 10,000
Depleted Oil and Gas Fields	920
Unminable Coal Seams	>15

CO₂ can be sequestered in saline aquifer by means of three mechanisms, also shown in Figure 2. 4 [3]:

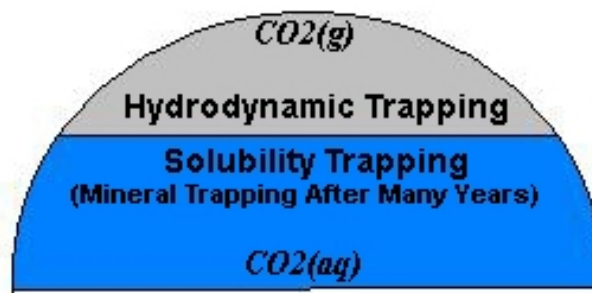


Figure 2. 4. Storage mechanisms in the sequestrating of CO₂ in the aquifer

- I. CO₂ can be trapped as a gaseous phase forming a gas cap over brine column after an injection process or supercritical fluid under a low-permeability or impermeable caprock, which is called hydrodynamic trapping.

- II. CO₂ can be trapped as dissolved solute in brine. The dissolution of gaseous CO₂ into brine in the aquifer increases the density of brine. The denser brine column begins to move vertically downward. This convection process increases the dissolution rate of CO₂ in brine. The presence of CO₂ in an aqueous phase is called solubility trapping.

- III. CO₂ can react with other compounds or ions in saline aquifers to become a part of the solid, which is called mineral trapping. Precipitation of dissolved CO₂ as mineral is an example of this trapping; such as formation of carbonate minerals (calcite). However, these reactions are very slow and thousands of years should pass for mineral trapping.

CHAPTER 3

SOLUTE TRANSPORT IN AQUIFERS

3.1 Aquifers

If the values of medium properties (permeability, porosity, and etc.) are constant throughout an aquifer domain, the domain is homogeneous. If the values of medium properties vary through space, the aquifer is heterogeneous. Heterogeneity may be caused by stratigraphic layering, deposition, erosion, weathering, lithification, folding, faulting, or other geologic trends [8].

If the values of medium properties are constant in all directions at a measurement point in an aquifer, the aquifer is called isotropic aquifer. If medium properties vary with direction, the aquifer is called anisotropic aquifer. Anisotropy could be caused by grain-size distribution, stratigraphic layers, faults and etc. Horizontal values of medium properties usually exceed vertical values of medium properties due to the nature of rocks. Because rocks are generally layered in horizontal position underground as stated before [8].

Aquifers are the underground layers of rock sufficiently porous to store water and permeable enough to allow water to flow through them in considerable amounts (Figure 3.1) [9]. They are generally composed of permeable mixtures of unconsolidated materials such as; gravel, sand, silt, or clay. Some productive aquifers are also found in fractured rocks such as; carbonate rock, basalt, or sandstone [10]. There are two types of aquifers: unconfined and confined (Figure 3. 1).

Unconfined aquifers are similar to underground lakes in porous materials. There is no impermeable material at the top of the groundwater, so that groundwater levels are free to rise or fall. The top of an unconfined aquifer is the water table and open to the atmosphere. Thus, groundwater pressures are equal to the atmospheric pressure [11].

A confined aquifer is covered with an impermeable top and possibly bottom boundaries. Confined aquifers are completely filled with groundwater, and they do not have a free water table [11]. Shortly, aquifers are formations which allow the flow of water; such as, sandstone. Aquitards and aquicludes are also typical examples of confined aquifers. Aquitards have considerable porosity saturated with water but do not allow the flow of water due to low permeability characteristic. This type of confining aquifers is seen in shaly systems. Aquicludes are formations which have low porosity with low permeability; such as, igneous rocks [9].

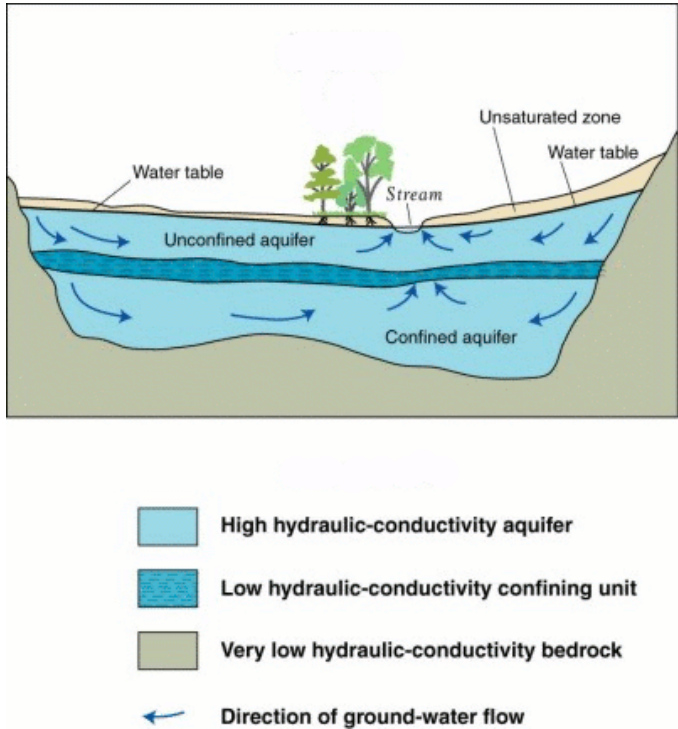


Figure 3. 1. Cross-section of a typical groundwater system [10]

3.2 Transport Mechanisms

Solutes dissolved in groundwater are transported by three mechanisms : molecular diffusion, mechanical dispersion, and convection. The sum of the molecular diffusion and mechanical dispersion are called as hydrodynamic dispersion. All three mechanisms may operate simultaneously or individually in flowing groundwater [8].

3.3 Molecular Diffusion

Molecular Diffusion is mixing caused by random molecular motions due to thermal kinetic energy of the solute [12]. The behavior of diffusion is explained by Adolf Fick in the year 1855 with his laws, known as Fick's laws. Fick's First Law is used in steady state diffusion as written in equation 3. 1. In this situation the concentration within the diffusion volume does not change with respect to time [13].

$$J = -D_e \cdot \frac{\partial c}{\partial z} \quad (3.1)$$

Where,

J: Diffusion flux (mol/cm².s)

D_e: Effective diffusion coefficient (cm²/s)

c: Concentration (mol/cm³)

z: Depth (cm)

Fick's Second Law is used in non-steady diffusion as written in equation 3. 2. In non-steady diffusion process, the concentration within the diffusion volume changes with respect to time [13]. In natural systems, the diffusion occurs in non-steady state generally.

$$D_e \frac{\partial^2 c}{\partial z^2} = \frac{\partial c}{\partial t} \quad (3.2)$$

Where,

t: time

The diffusion coefficient of a solute in water in a porous medium is smaller than in pure liquids. As the porosity of the medium decreases, the diffusion coefficient of a solute in water in a porous medium decreases. This is primarily due to the collision of solutes with the solids of the medium which makes diffusion difficult in porous medium [8]. The effects of porosity and longer pores are often lumped together in the definition of an effective molecular diffusion coefficient (D_e) in equation 3.3 [14].

$$D_e = \frac{D_o \phi}{\tau} \quad (3.3)$$

In which D_e is the effective diffusion coefficient within pores, D_o is the molecular diffusion coefficient within pores, ϕ is porosity, and τ is the tortuosity. The tortuosity attempts to account for the longer distance traversed in the pores. Tortuosity values usually range between two and six, averaging about three in real systems but for homogeneous straight line medium its value is one.

3.4 Measurement Techniques for Diffusion Coefficient of Gases in Liquids

To measure the diffusion coefficient of gases in liquids, there exists various methods; such as, usage of basic volumetric techniques, spectroscopy, radiotracers, and conductivity meters. Many experimental data about the diffusion coefficient of CO₂ in water in the literature are present. Most of them are obtained from different measurement methods based on same principles. For example, Unver and Himmelblau (1964) used laminar falling jet method to find the effect of temperature on the diffusion coefficient of CO₂ in water [15]. This method is based on the absorption of a solute gas in a laminar flowing solvent and the observation of the absorbed amount of gas to find the diffusion coefficient. Hirai et al. (1997) used laser-induced fluorescence for measuring CO₂ diffusion coefficient in water at high pressures [16]. The diffusion coefficient is estimated by measuring the CO₂ dissolution rate and using the empirical mass transfer coefficient. Laser-induced fluorescence is a spectroscopic method. In this method, the light is sent to the solution and emitted light from solution is measured with a detector. This method has greater sensitivity than other methods. The advantage over absorption spectroscopy is that two and three dimensional images could be obtained since fluorescence takes place in all directions due to its property of not being polarized [17].

3.5 CO₂ Diffusion Coefficient in Water

3.5.1 Temperature Effect

Unver and Himmelblau (1964) developed the quadratic molecular diffusion coefficient (D_o) equation (equation 3.4) for the temperature range 6°C to 65°C at atmospheric pressure [15].

$$D_o (m^2 / s) = (A + BT + CT^2)10^{-9} \quad (3.4)$$

Where the constants for CO₂ are; A = 0.95893, B = 0.024161, C = 0.00039813 and T in °C

Although Figure 3.2 is valid at an atmospheric pressure, the trend is similar with temperature change at different pressures.

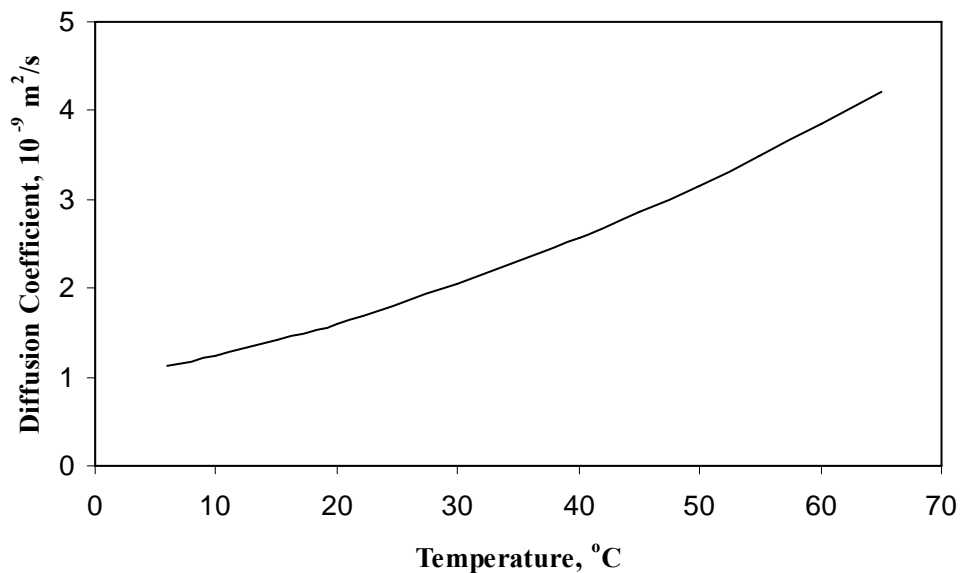


Figure 3. 2. CO₂ Diffusion coefficients in pure water at atmospheric pressure [15]

3.5.2 Pressure Effect

In the literature, there are few studies about the effect of pressure on diffusion coefficient of CO₂-H₂O system. According to the work of Hirai et al. (1997), the diffusion coefficient between the gaseous CO₂ and liquid water changes with pressure very little as seen in Figure 3.3 [16].

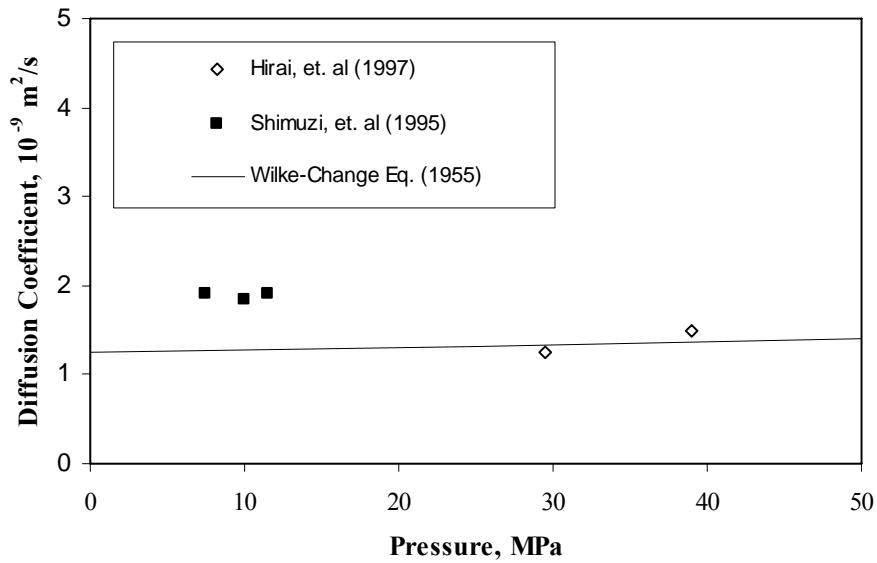


Figure 3. 3. CO₂ Diffusion coefficients in pure water at 13° C [16]

All shown measurements in Figure 3.3 by Wilke-Chang (1955), Shimizu et al. (1995), and Hirai et al. (1997) are at a temperature of 13° C [16, 18, 19]. The measured values of Shimizu et al. (1995) are 40% larger than that of Wilke-Chang equation (1955), whereas Hirai et al.'s (1997) measured diffusion coefficients agree with the Wilke-Chang equation (1955) fairly well. Although there are some differences between the results, it could be said that the diffusion coefficient of CO₂-H₂O system changes with pressure insignificantly. The trend is also similar for different temperatures based on Wilke-Chang equation. So the effect of pressure to diffusion coefficient of CO₂ is neglected in this thesis.

3.5.3 Concentration Effect

The driving force for molecular diffusion in aqueous systems is concentration gradient. Although the behavior of solute transport by diffusion is explained with Fick's Equation as an analytical approach, the effect of concentration gradient on diffusion coefficient in the equation is neglected; in other words, the diffusion coefficient is assumed as constant throughout the transport. However, in real systems the diffusion coefficient could not be a constant and it could change always due to the variation in concentration gradient in the system. According to Cussler (1999), the diffusion coefficient of solutes in liquids could vary with concentration gradient considerably, frequently by several hundred percent [14]. However, this is not valid for all solute types and according to the published results of Onda et al. (1960) and Tang and Himmelblau (1965), the effect of concentration gradient CO_2 diffusion coefficient in water is quite small and so negligible [20, 21]. As a matter of fact, constant diffusion coefficient is used as an input data in analytical solution as made in the numerical solution part in this thesis.

3.6 Convection

Convection is the movement of dissolved solutes with flowing stream in porous media [22]. When only convection process is considered, solutes move at the same rate with flowing stream without dispersing. But this is not possible in porous media due to the velocity profile of water in pores and heterogeneities in the medium, therefore dispersion occurs when convection takes place in porous media. Sometimes, the term "advection" could be encountered in the literature when dealing with groundwater systems. The term advection is generally used for the horizontal movement of groundwater in porous media and the term convection is used for the vertical movement of groundwater in porous media.

In the aquifer, molecular diffusion normally arises due to the concentration difference (Δc) in brine. But for the occurrence of convection, concentration difference or density difference ($\Delta\rho$) in the brine is not enough due to other parameters of the reservoir; such as, permeability (k), porosity (ϕ), aquifer height (H) and fluid properties, such as viscosity (μ). The height of the aquifer has an important effect on the velocity of the brine column during natural convection. The Darcy velocity of the brine column could be determined from equation 3.5 in terms of known data.

$$u = \frac{k \cdot g \cdot \Delta\rho}{\mu} \quad (3.5)$$

The occurrence of convection could be determined by the dimensionless solutal Rayleigh number (Ra) (equation 3.6). The equation consists parameters that form velocity term. Solutal Rayleigh number (Ra) determines if convection will begin or not. After a critical solutal Rayleigh number (Ra_c), convection starts to take place. Critical solutal Rayleigh number depends on the shape of the fluid system and the boundary conditions [23]. For a fluid layer between two boundaries, constant concentration top boundary and impermeable bottom boundary, the critical solutal Rayleigh number has been computed theoretically to be $4\pi^2$ (approximately 39.48) for the occurrence of convection process [23]. When convection started, then Peclet number (equation 3.7) is important to determine the ratio of the convection to dispersion in the transport.

$$Ra = \frac{k g \Delta\rho H}{D_o \mu \phi} \quad (3.6)$$

$$Pe = \frac{u H}{D_e \phi} \quad (3.7)$$

Where, for convection dominated systems D_e ,

$$D_e = \frac{D_o \cdot \phi}{\tau} + \alpha \cdot v \quad (3.8)$$

Where,

v : pore velocity (u / ϕ , cm/s)

3.7 Dispersion

There are three basic causes of pore-scale longitudinal dispersion [24]: (i) As groundwater moves through pores, it will move faster through the center of the pore than along the edges (figure 3.4). (ii) Fluid that travels through larger pores will travel faster than fluid moving in smaller pores (figure 3.5). (iii) Some of the fluid will travel in longer pathways than other fluid. The longer pathways are caused due to the tortuosity of an aquifer and in more tortuous aquifer dispersion increases (figure 3.6).

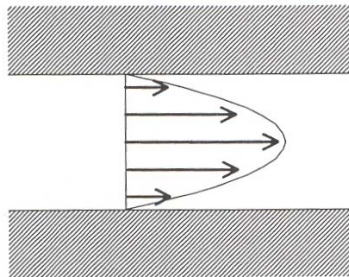


Figure 3. 4. Dispersion due to velocity profile in pores [25]

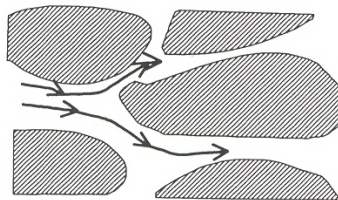


Figure 3. 5. Dispersion due to different velocities in different pores [25]

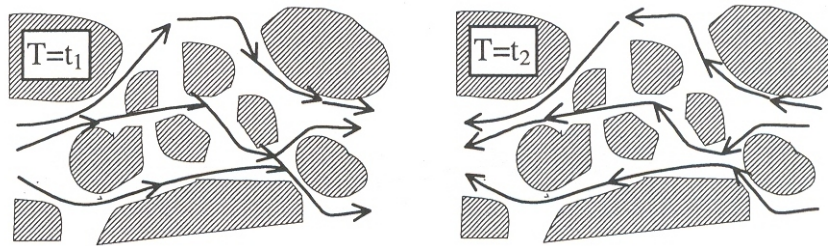


Figure 3. 6. Dispersion due to tortuosity [25]

The behaviour of dispersion in the aquifer could be explained by equation 3. 9. As shown in equation 3.9, the dispersion behaviour depends on the velocity of the fluid column and dispersivity of the aquifer. In other words, it is dependent on both fluid and rock property. The dispersion term is added to the diffusion equation when dispersion has effect in the aquifer. If the effect of dispersion is high, the molecular diffusion could be neglected beside the high dispersion.

$$D^* = \alpha \cdot v \quad (3.9)$$

Dispersion could take place in all directions or in one direction according to the aquifer and boundary conditions. The equation 3.9 could be used for the solution of dispersion in all directions rearranging the dispersivity (α) and pore velocity (v) values for the desired direction. It could occur in the transverse (horizontal) direction even the flow direction is in vertical. However, when the flowing groundwater column enters over a broad front, the effects of transverse dispersion within the zone cancel each other due to the absence of concentration gradient, and only longitudinal dispersion needs to be considered as if one dimensional flow is occurring [11].

3.8 Aquifer Properties

3.8.1 Porosity

Porosity is defined as the ratio of pore (non-solid) volume to the total volume of a material [26]. Porosity is a property of the medium like permeability, not the fluid. High porosity aquifers are good candidate for CO₂ sequestration because of their large volume.

3.8.2 Permeability

Permeability is a measure of the ability of a rock to transmit fluids through it. It is of great importance in determining the flow characteristics of hydrocarbons in oil and gas reservoirs, and of groundwater in aquifers. Permeability is a property of the porous medium only, not the fluid. The usual unit for permeability is the “darcy”, or more commonly the “mili-darcy” (md) [27].

3.8.3 Hydraulic Conductivity

The hydraulic conductivity, as defined in equation 3.10, of a soil or rock depends on a variety of physical factors and is an indication of an aquifer’s capacity to transmit water [22]. Permeability and hydraulic conductivity are often used interchangeably. The term permeability is generally used in oil sector by petroleum engineers and hydraulic conductivity term is used in geology science by groundwater hydrogeologists. Technically speaking, an aquifer has a permeability that is a function of the medium property only (shown with a unit of “mildarcy”), whereas hydraulic conductivity is a function of both medium and fluid properties (shown with a unit of length per time). The pore velocity of brine column could also be calculated from hydraulic conductivity and hydraulic gradient terms as shown in equation 3.11.

$$K = \frac{k \cdot \rho \cdot g}{\mu} \quad (3.10)$$

$$v = \frac{K \cdot \nabla \Phi}{\phi} \quad (3.11)$$

Where,

$\nabla \Phi$: Hydraulic Gradient (dimensionless)

3.8.4 Dispersivity

Dispersivity is a property of an aquifer. There are many definitions about dispersivity term in the literature. For example, Lake defined the dispersivity as “a measure of the local heterogeneity scale” [28]. Dispersivity is defined by Nofziger and Wu [29]. They stated that “Dispersivity is a geometrical proportionality constant of a porous medium. It is determined by the pore-size distribution of the channels participating in the transmission of a bulk solution. It measures the spreading of a solute across the front of an average bulk flow”. Increasing anisotropy and heterogeneity increases the magnitude of dispersion.

The dispersivity in the flow direction is called longitudinal dispersivity (α_L). There are many data about dispersivity values in the literature. According to the studies of Anderson (1984) and Gelher et al. (1982), the value of longitudinal dispersivity could be accepted as the 10% of flow length despite some scatters as given in the equation 3.12 [30, 31]. Also, there are different works in the literature.

$$\alpha_L = 0.1 L \quad (3.12)$$

According to the study of Neuman (1990), the trend is different than that of 10% trend as given in the empirical equation of Neuman (equation 3.13) which is valid for lengths less than 3,500 meters [32]. In Figure 3. 7, some measured longitudinal dispersivity values of Anderson (1984) are given to show the variation of dispersivity with distance and in Figure 3. 8, the comparison is made between 10% trend in dispersivity and Neuman’s equation.

$$\alpha_L = 0.0175 L^{1.46} \tag{3.13}$$

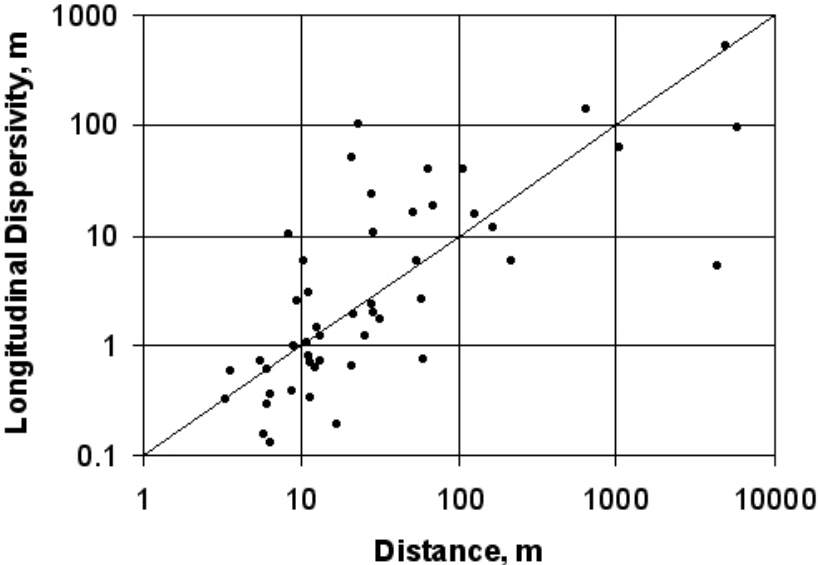


Figure 3.7. Longitudinal dispersivity based on distance [30]

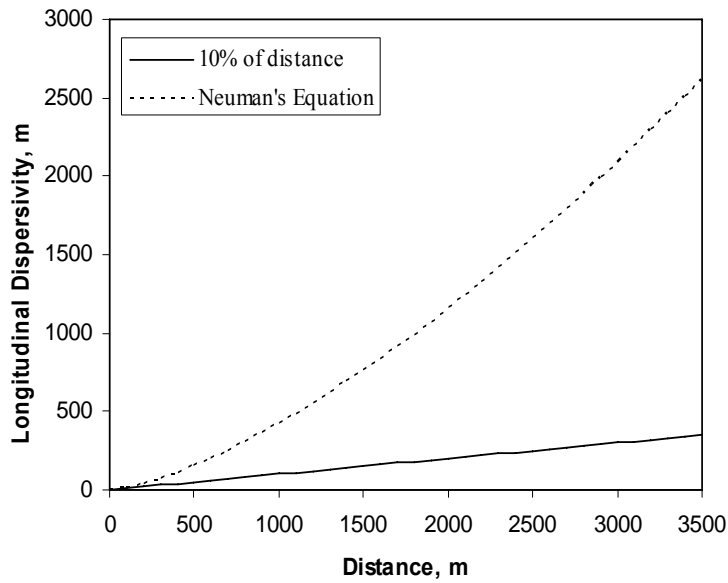


Figure 3. 8. Longitudinal dispersivity values based on 10% trend and Neuman’s equation [30, 31, 32]

The transverse dispersivity (α_T) , dispersivity normal to the flow direction, is 10% of longitudinal dispersivity if the transverse is in horizontal direction but 1% of longitudinal dispersivity if the transverse is in vertical direction in general (equation 3. 14) [9]. The variation of vertical transverse dispersivity could be observed in Figure 3. 9.

$$\alpha_T = 0.01 L \tag{3.14}$$

where L is in ft or m and α_T is in ft or m.

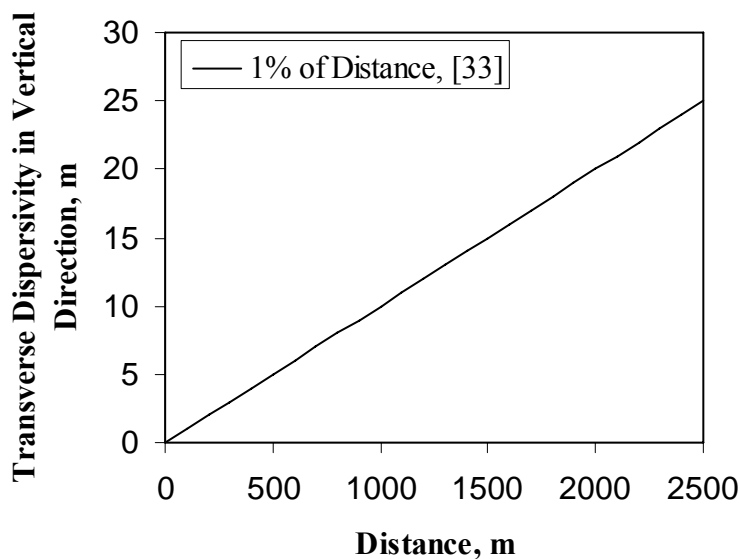


Figure 3. 9. Vertical transverse dispersivity values based on 1% trend [9]

As stated, dispersion not only occurs in the flow direction but also in the transverse direction. However due to different dispersivity and velocity values in horizontal and vertical directions, the effect of dispersion is different in horizontal and vertical directions. Finally, in general horizontal dispersivity values are higher than the vertical dispersivity values in groundwater systems because natural systems extends horizontally mostly [33].

3.9 Physical Properties of CO₂-Brine System

3.9.1 Physical Properties of Carbon Dioxide

Carbon dioxide (CO₂) is a chemical compound composed of two carbon atoms and one oxygen atom. Its concentration in the atmosphere is about 330 ppm (0.033% by volume). CO₂ has a slightly irritating odour, is colourless and is denser than air [34]. At normal temperature and pressure, carbon dioxide is

present as a gas. The phase behavior of CO₂ could be interpreted from Figure 3. 10. At a temperature above 31.1 °C (the temperature at the critical point) and for the pressure above 73.9 bar (the pressure at the critical point), CO₂ behaves as supercritical fluid [34]. Ebbing and Gammon (1999) stated that “supercritical fluid is the name given to a substance that is at a temperature and pressure above the critical point , supercritical fluids have unique properties that lie between that of a liquid and that of a gas: polarity, viscosity, diffusivity, and density” [34]. This is an important aspect of CO₂’s behaviour and is particularly relevant for its storage.

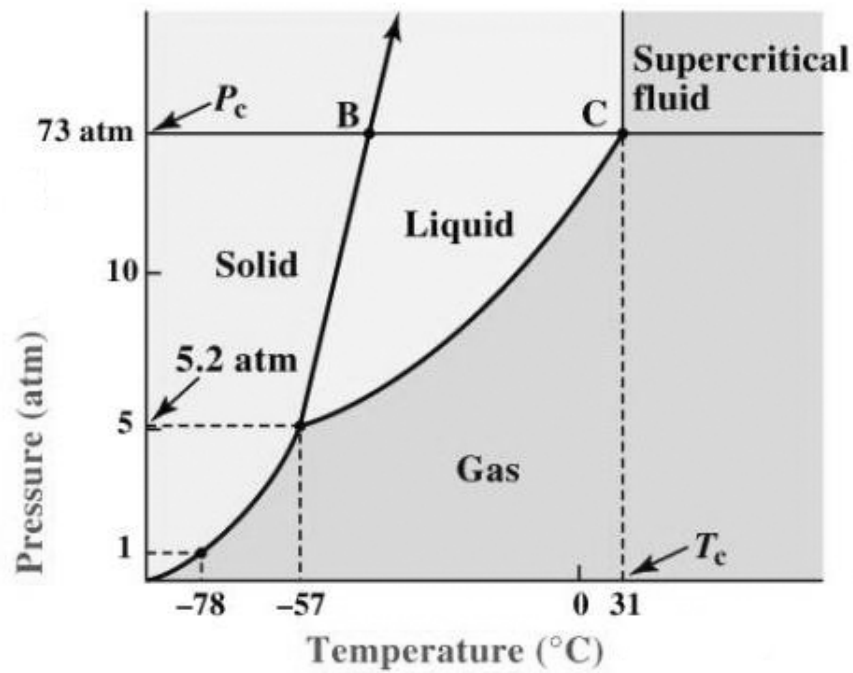


Figure 3. 10. Phase behavior of CO₂ [35]

3.9.2 CO₂ Solubility in Water:

The solubility of CO₂ in water changes with respect to aquifer conditions. Temperature, pressure and salinity have very effective role on the solubility of CO₂. At aquifer conditions, 3 to 4% weight percentage of CO₂ may dissolve in brine. Dissolved CO₂ has the effect of increasing water density, by up to 3% in the temperature range of 5–300 °C [36].

3.9.2.1 Salinity Effect

According to the study of Enick and Klara (1990), the effect of salinity on CO₂ solubility in brine ($Y_{CO_2,brine}$) could be obtained from equation 3.15 with a temperature range of 25 to 250° C and a pressure range of 30 to 838 atm (3 to 85 Mpa) [36].

$$Y_{CO_2,brine} = Y_{CO_2,pure-w} \times (1 - 4,893414 \times 10^{-2} S + 0,1302838 \times 10^{-2} S^2 - 0,1871199 \times 10^{-4} S^3) \quad (3.15)$$

Where,

S : water salinity (weight percent)

$Y_{CO_2,pure\ water}$: CO₂ solubility in pure water (mass fraction)

$Y_{CO_2,brine}$: CO₂ solubility in brine (mass fraction)

The required CO₂ solubility values in distilled water ($Y_{CO_2,water}$) could be obtained from Figure 3.11 for different temperature and pressure values [37]. The increase in salinity decreases CO₂ solubility in brine. From the empirical equation of Enick and Klara (1990), the solubility of CO₂ in brine changes with salinity as seen in Figure 3.12 [36].

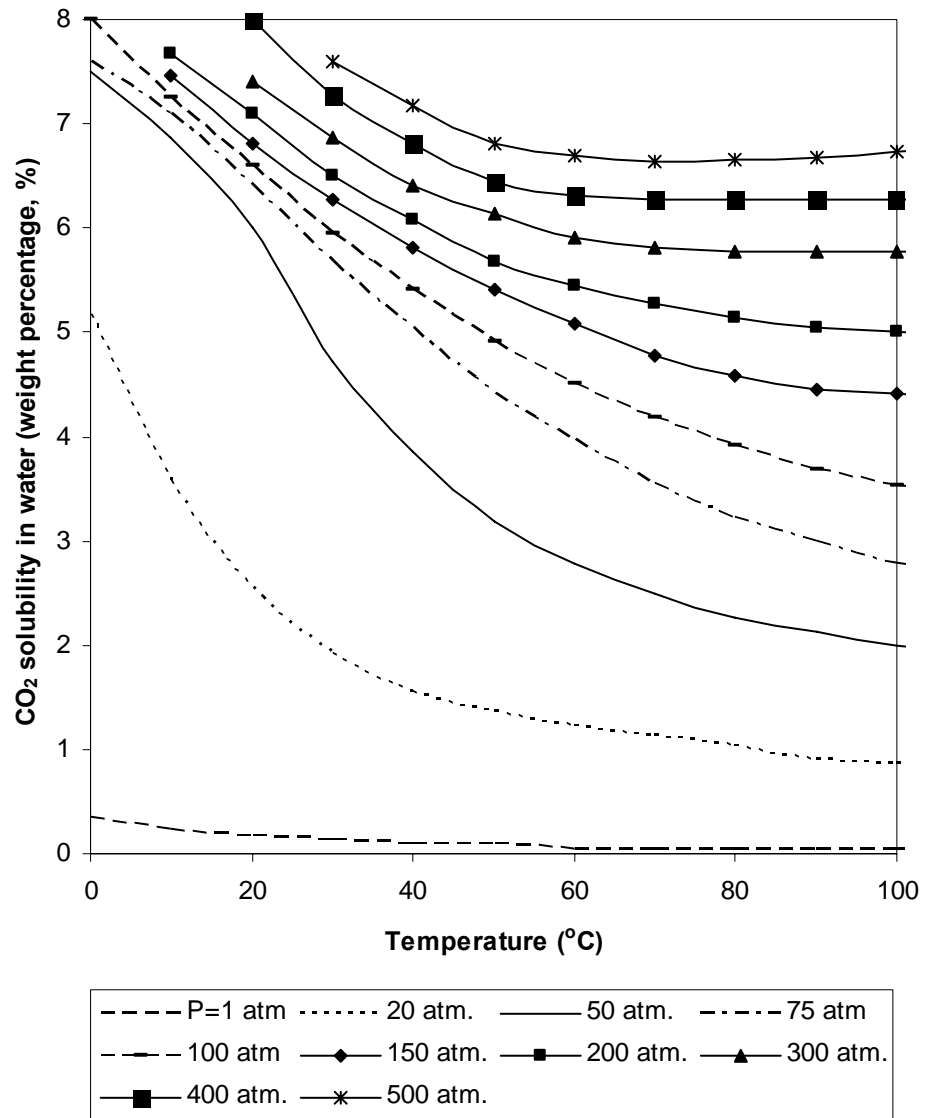


Figure 3. 11. Solubility of CO₂ in pure water ($Y_{CO_2, \text{purewater}}$) [37]

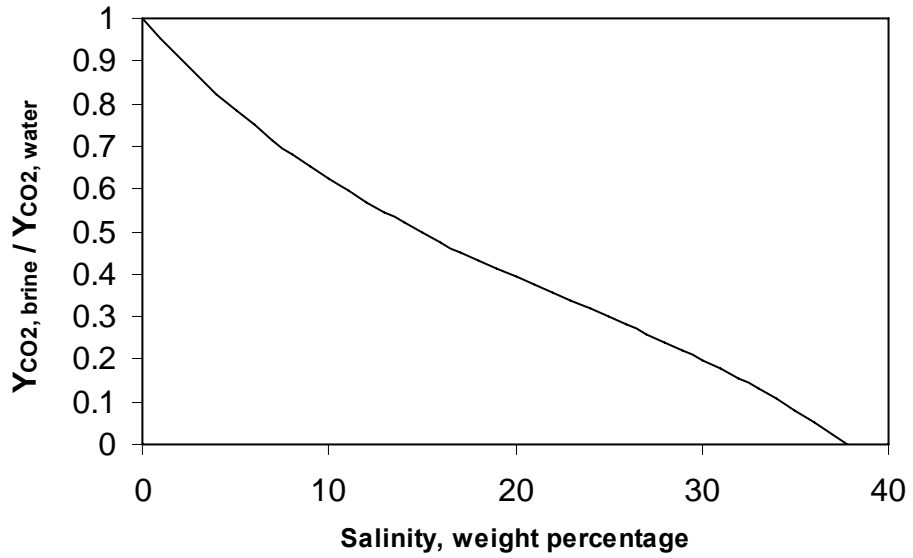


Figure 3. 12. CO₂ Solubility in brine for different salinity values [36]

3.10 Density of Brine

The density of brine could be found approximately with equations 3.16 and 3.17 [38]. The equations are valid for the temperature range of 25 – 350 °C and up to the 98.1 MPa pressure (Figure 3.13). Although the pressure parameter in the brine density equation is included, the effect of pressure on brine density is negligible.

$$\rho_{purewater}(kg/m^3) = 1000 + 1 \times 10^{-3} (-80T - 3.3T^2 + 0.00175T^3 + 489P - 2T \times P + 0.016T^2 \times P - 1.3 \times 10^{-5} T^3 \times P - 0.333P^2 - 0.002T \times P^2) \quad (3.16)$$

$$\rho_{brine}(kg/m^3) = \rho_{purewater} + 1000S \left\{ 0.668 + 0.44S + 1 \times 10^{-6} [300P - 2400PS + T(80 + 3T - 3300S - 13P + 47PS)] \right\} \quad (3.17)$$

Where, T is in °C, P is in MPa, and S is in weight fraction of water salinity.

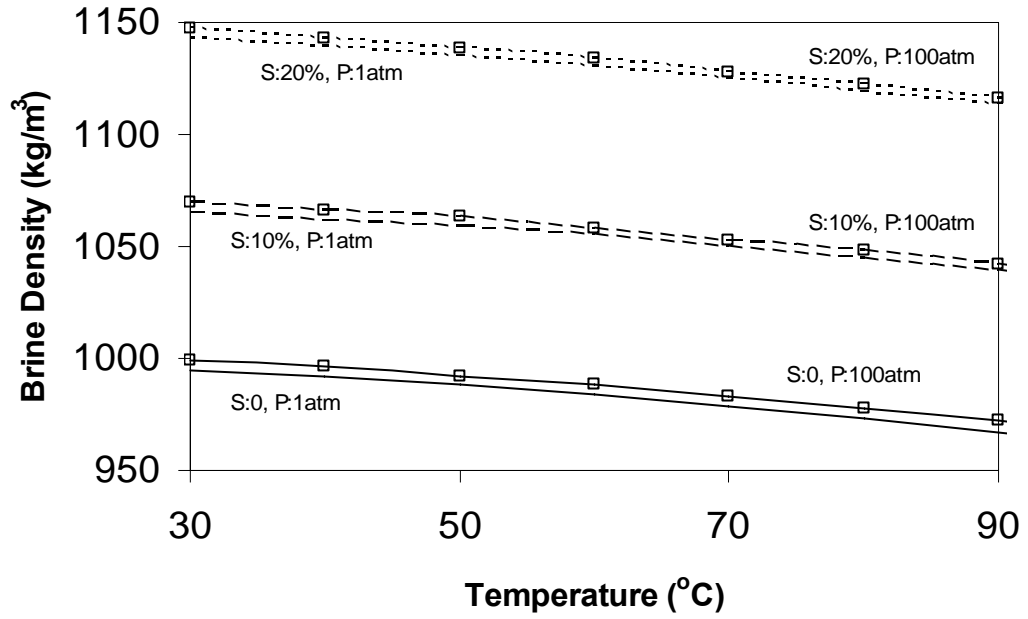


Figure 3. 13. Brine density as a function of pressure, temperature and salinity [38]

3.11 Viscosity of brine

The brine viscosity at aquifer conditions could be estimated by equation 3.18 [39].

$$\mu_{brine}(cp) = \mu_{brine1} (0.9994 + 4.0295 \times 10^{-5} P + 3.1062 \times 10^{-9} P^2) \quad (3.18)$$

$$\mu_{brine1}(cp) = AT^{-B} \quad (3.19)$$

Where,

$$A = 109.574 - 8.40564S + 0.313314S^2 + 8.72213 \times 10^{-3} S^3 \quad (3.20)$$

$$B = 1.12166 - 2.63951 \times 10^{-2} S + 6.79461 \times 10^{-4} S^2 + 5.47119 \times 10^{-5} S^3 - 1.55586 \times 10^{-6} S^4 \quad (3.21)$$

μ_{brine} : brine viscosity at P (psia) and T ($^{\circ}\text{F}$), cp

μ_{brine1} : brine viscosity at P = 14.7 psia and T ($^{\circ}\text{F}$), cp

T : temperature of brine ($^{\circ}\text{F}$)

P : pressure of brine (psia)

Equation 3.19, which gives the viscosity of brine (μ_{brine1}) at aquifer temperature and atmospheric pressure, is valid for the temperatures between 100 and 400 $^{\circ}$ F and salinities to 26 weight percentage with 5% error. Equation 3.18 is valid for the temperatures between 86 to 167 $^{\circ}$ F and pressures below 10000 psia with 4% error; for pressures between 10000 and 15000 psia with 7% error.

The required brine viscosity values for salinity, pressure, and temperature parameters could also be obtained from Figure 3.14 based on equation 3.18.

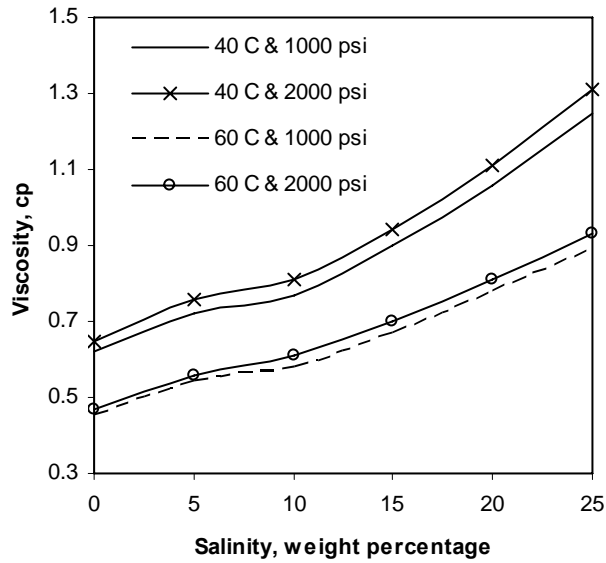


Figure 3. 14. Brine viscosity as a function of pressure, temperature and salinity [39]

3.12 Density of Water with CO₂

Dissolved CO₂ has the effect of increasing water density, by up to 2–3% in the temperature range of 5-300° C [36]. Garcia (2001) found a relationship for the apparent molar volume of CO₂ for the temperatures lower than 300° C on the basis of 53 data points where the effect of pressure is negligible [40]. At aquifer conditions the dissolved CO₂ in brine causes 1% change in brine density.

The density of aqueous solutions with a single solute dissolved in pure water could be defined as in equation 3.22.

$$\rho_{aq} = \frac{\rho_w}{1 - X_{sol} \left(1 - \frac{V_\phi}{M} \rho_w\right)} \quad (3.22)$$

The apparent molar volume (V_{ϕ}) for CO_2 in equation 3.22 could be calculated from equation 3.23 according to the expression of Garcia (2001) on the basis of 53 data [40].

$$V_{\phi} = 37.51 - 9.585 \times 10^{-2} T + 8.740 \times 10^{-4} T^2 - 5.044 \times 10^{-7} T^3 \quad (3.23)$$

To find the effect of solute on brine density, Bachu and Adams (2003) used the mass conservation principle [41]. The apparent molar volume of solute in brine could be obtained from equation 3.24.

$$V_{\phi,b} \rho_b = V_{\phi} \rho_w \quad (3.24)$$

After rearranging the terms, the effect of dissolved CO_2 on brine density could be obtained from equation 3.25.

$$\rho_{aq,CO_2} = \frac{\rho_b}{1 - Y_{CO_2} \left(1 - \frac{V_{\phi,b}}{M} \rho_b\right)} \quad (3.25)$$

where,

ρ_{aq,CO_2} : brine density (g/cm^3)

ρ_b : brine density without CO_2 (g/cm^3)

Y_{CO_2} : dissolved CO_2 mass fraction

$V_{\phi,b}$: apparent molar volume of CO_2 in brine (cm^3/mol)

M : molecular weight of CO_2 (gram/mole)

T is in $^{\circ}\text{C}$

After all, the variation of brine density with CO₂ could be observed from Figure 3.15 based on equation 3.25.

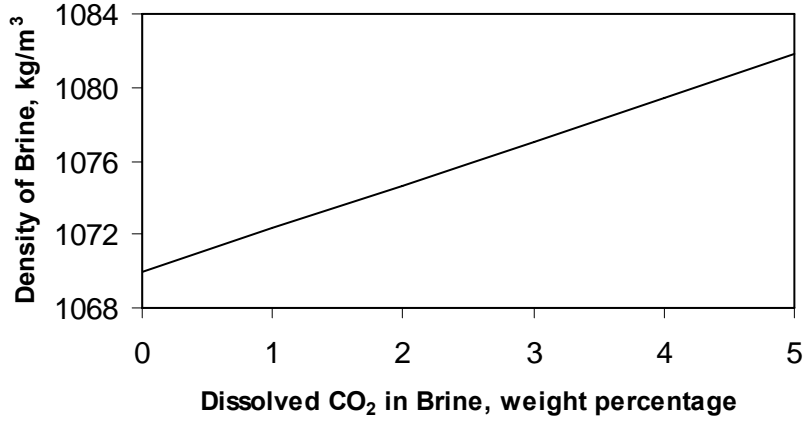


Figure 3. 15. Effect of CO₂ on brine density at 50° C and 100000 ppm [36]

3.13 Viscosity of Water with CO₂

There is no empirical equation in the literature for the effect of dissolved CO₂ on water viscosity. Tumasjan et al. (1969) published their experimental results for the water viscosity change with CO₂ [42]. The change in the viscosity of water with CO₂ according to the study of Tumasjan et al. could be seen in Figure 3.16.

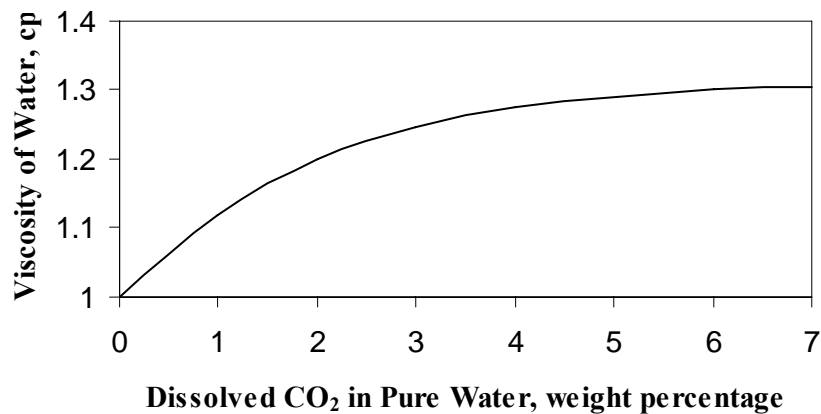


Figure 3. 16. Viscosity of pure water with dissolved CO₂ [42]

CHAPTER 4

STATEMENT OF THE PROBLEM

Global temperature is increasing every year due to anthropogenic activities and the main reason of this global warming issue is CO₂ emissions. To decrease the concentration of CO₂ in the atmosphere, CO₂ could be sequestered in deep saline aquifers. Deep saline aquifers are the best alternative among geological places due to its high capacity around worldwide and containing unusable water.

For this reason, the transport of CO₂ in a deep saline aquifer having different properties will be investigated in this study. The transport mechanisms of CO₂ sequestered in a deep saline aquifer will be modelled in one dimensional vertical system by solving the diffusion-convection equation analytically while making an allowance for the CO₂ cap – brine interface as a boundary condition. The simulator will also be used to verify the numerical results with that of analytical modelling.

CHAPTER 5

METHODOLOGY

5.1 Analytical Modeling

The transport of CO₂ in an aquifer is analyzed with diffusion-convection equation 5.1. The reasonable assumptions are done for the calculation of CO₂ distribution in the aquifer to simplify the problem.

By considering the CO₂ cap as a boundary condition, the flow is assumed to be one-dimensional vertical flow in the aquifer. The pressure of CO₂ cap is also assumed as constant throughout the transport to develop an analytical solution for the diffusive and convective mixing process. The temperature along the aquifer is taken as constant. Besides, the velocity of brine column arised from density difference is assumed as constant to develop an analytical solution for convective mixing process in analytical modeling part. Chemical reactions that could occur between brine-CO₂-rock are neglected in the study, because these processes take place generally in very long period and the assumption is also made for the simplicity to enable the comparison between analytical and numerical modeling in the study.

$$D_e \frac{\partial^2 c}{\partial z^2} - \frac{u}{\phi} \frac{\partial c}{\partial z} = \frac{\partial c}{\partial t} \quad (5.1)$$

The hypothetical model is shown in Figure 5.1. There is a gas cap formed of CO₂ above the brine in the aquifer. The CO₂ diffuses into brine by time and the density of brine increases due to saturation by CO₂. The density increase in the upper layer of brine causes convection effect by the movement of layers. Beside this, it is assumed that CO₂ is injected periodically into gas cap to keep the pressure of the gas cap constant.

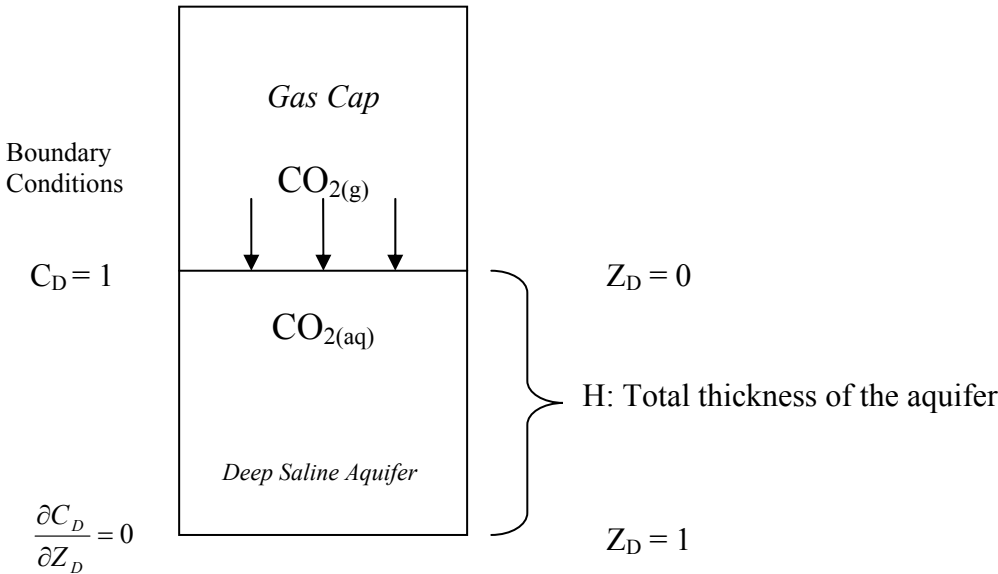


Figure 5. 1. Geometry and boundary conditions of the model

The following assumptions are considered for the development of an analytical model:

- Isotropic homogenous medium
- One dimensional diffusion in vertical direction.
- Gas cap is formed due to CO₂ injection.
- Initial CO₂ concentration is zero in the aquifer.
- Possible chemical reactions in the aquifer are neglected

- Gravity tonguing and viscous fingering effects are neglected
- Upper boundary's CO₂ concentration and pressure are taken as constant assuming gas cap is filled with CO₂ periodically.
- Temperature is constant in the model of environment
- The water in the medium and CO₂ in the gas cap cannot escape through the boundaries of the aquifer.
- The velocities are in terms of average values and 1% brine density difference for convection is used in the calculation of maximum velocity.

For only diffusion dominant process in the aquifer, the behavior of molecular diffusion could be expressed with the equation known as Fick's Diffusion Equation 5.2.

$$D_e \frac{\partial^2 c}{\partial z^2} = \frac{\partial c}{\partial t} \quad (5.2)$$

Where,

D_e : effective diffusion coefficient (cm²/s)

C : concentration (mol/cm³)

z : vertical distance (cm)

t : time (s)

The analytical solution of equation 5.2 is given in equation 5.3.

$$\frac{C(z,t)}{C_o} = \operatorname{erfc} \left[\frac{z}{2\sqrt{D_e t}} \right] \quad (5.3)$$

If there is a vertical convection, then the velocity term is added to the Fick's Diffusion equation 5.2 and equation 5.1 is used as a diffusion-convection equation.

Equation 5.1 could be arranged in dimensionless form to make the equation unique with given boundary conditions as in equation 5.4 [28].

$$\frac{1}{N_{Pe}} \frac{\partial^2 C_D}{\partial Z_D^2} - \frac{\partial C_D}{\partial Z_D} = \frac{\partial C_D}{\partial t_D} \quad (5.4)$$

Where the dimensionless groups are,

$$C_D = \frac{C_{CO_2}}{C_{CO_2,sat}} \quad (5.5)$$

$$Z_D = \frac{z}{H} \quad (5.6)$$

$$t_D = \frac{u.t}{\phi.H} \quad (5.7)$$

$$N_{Pe} = \frac{u.H}{\phi.D_e} \quad (5.8)$$

Where,

H : total thickness of the aquifer (cm)

$C_{CO_2,sat}$: saturation concentration of CO₂ in brine at aquifer conditions (mol/cm³)

C_{CO_2} : concentration of CO₂ in brine at aquifer conditions (mol/cm³)

The initial and boundary conditions are also defined in the hypothetical model for solving the problem.

Initial Condition:

$$C_D=0 \text{ for } t_D = 0 \text{ and for all } Z_D \quad (5.9)$$

Boundary Conditions:

$$\text{At } Z_D=0: C_D=1 \text{ for } t_D > 0 \quad (5.10)$$

$$\text{At } Z_D=1: \frac{\partial C_D}{\partial Z_D} = 0 \quad (5.11)$$

For the given boundary conditions in equations 5.9, 5.10, and 5.11, the final dimensionless CO₂ concentration becomes as in equation 5.12 which is an exact analytic solution for equation 5.4 [28];

$$C_D = \frac{1}{2} \operatorname{erfc} \left(\frac{z_D - t_D}{2 \sqrt{\frac{t_D}{N_{Pe}}}} \right) + \frac{e^{z_D N_{Pe}}}{2} \operatorname{erfc} \left(\frac{z_D + t_D}{2 \sqrt{\frac{t_D}{N_{Pe}}}} \right) \quad (5.12)$$

Where,

$$\text{The error function, } \operatorname{erf}(\beta) = \frac{2}{\sqrt{\pi}} \int_0^{\beta} e^{-t^2} dt \quad (5.13)$$

$$\text{The complementary error function, } \operatorname{erfc}(\beta) = 1 - \operatorname{erf}(\beta) \quad (5.14)$$

The required values of the erf function could be obtained from equation (5.15) [43].

$$erf(x) = 1 - (a_1 w + a_2 w^2 + a_3 w^3 + a_4 w^4 + a_5 w^5) e^{-x^2} \quad (5.15)$$

Where,

$$w = \frac{1}{1 + px}$$

$$a_1 = 0.254829592$$

$$a_2 = -0.284496736$$

$$a_3 = 1.421413741,$$

$$a_4 = -1.453152027$$

$$a_5 = 1.061405429$$

$$p = 0.3275911$$

5.2 Numerical Modeling

The numerical analyses are frequently applied to solve many problems in science and engineering. Although analytical approaches are sometimes applied in the solutions of problems, most partial differential equations can not be solved analytically. To reduce the problems encountered in the solution of these equations, numerical methods can be used. The two most common numerical methods are finite difference and finite element methods. Numerical reservoir simulations are used to combine the geological and engineering data to make estimations about the field performance by using any numerical methods. So, the solutions of problematic cases are easily made with these numerical reservoir simulations.

5.2.1 Numerical Simulator

The numerical solutions of the cases are realised with the computer program SEAWAT. SEAWAT is used for the simulation of transient three-dimensional flow of variable-density groundwater in porous media. SEAWAT-2000 was designed by combining a modified version of MODFLOW-2000 and MT3DMS into a single computer program. The code was developed using the MODFLOW-2000 concept of a process, which is defined as “part of the code that solves a fundamental equation by a specified numerical method.” SEAWAT-2000 contains all of the processes distributed with MODFLOW-2000 and also includes the Variable-Density Flow Process (as an alternative to the constant-density Ground-Water Flow Process) and the Integrated MT3DMS Transport Process [44, 45].

The fundamental concept of the original SEAWAT program was to combine MODFLOW and MT3D into a single program that solves the variable-density ground-water flow and solute-transport equations. SEAWAT uses either an explicit or implicit procedure to couple the ground-water flow equation with the solute-transport equation. With the explicit procedure, the flow equation is solved first for each timestep, and the resulting advective velocity field is then used in the solution to the solute-transport equation. This procedure for alternately solving the flow and transport equations is repeated until the stress periods and simulation are complete. With the implicit procedure for coupling, the flow and transport equations are solved multiple times for the same time step until the maximum difference in fluid density between consecutive iterations is less than a user-specified tolerance [44, 45].

In this study, the numerical runs are based on finite difference method and implicit technique.

5.3 Previous Studies Conducted on CO₂ Sequestration in Deep Saline Aquifers at Petroleum and Natural Gas Engineering Department of METU

There were three studies about the sequestration of CO₂ in a deep saline aquifer in Petroleum and Natural Gas Engineering Department of Middle East Technical University up to now.

Dirik et al studied the formation of CO₂ gas bubble in the aquifer by analytical equations [46]. They analyzed the presence of CO₂ from two different aspects, as gas bubble formation and as dissolution in brine. They studied the concentration distribution of CO₂ gas from the injector well in the aquifer. They also checked the effect of reservoir and fluid properties on this distribution.

İzgeç conducted CO₂ injection into a core sample under computerized tomography (CT) system. Then he studied CO₂ sequestration in a deep saline aquifer by using CMG/STARS simulator [47]. He investigated the storage mechanisms of CO₂ in a deep saline aquifer for different cases and effects of CO₂ on an aquifer properties by comparing the results of experimental and numerical model.

Başbuğ studied the numerical modeling of CO₂ sequestration in a deep saline aquifer by using CMG/GEM simulator [48]. He investigated the effects of reservoir and fluid properties on the distribution of CO₂ in an aquifer. He also checked the storage mechanisms in a deep saline aquifer.

CHAPTER 6

RESULTS AND DISCUSSION

The objective of results and discussion part is to model the hypothetical cases with analytical and numerical approaches. After having analytical and numerical solutions, they are compared with each other.

The common data to be used in the analytical and numerical modeling are given in Table 6.1. The conditions for analytical and numerical runs are given in Tables 6.2, 6.3, 6.4, and 6.5. The sample input data for the numerical run 3b is given in Appendix part.

Table 6.1, Common data to all runs given in tables 6.2, 6.3, and 6.4.

Common data to all runs	
Aquifer Thickness, m	100
Viscosity of water, cp	0.7
Temperature, °C	50
Pressure, atm	75
Aquifer top, m	850
Aquifer bottom, m	950
Molecular diffusion coefficient of CO ₂ in water, cm ² /s	3.10 ⁻⁵

Table 6.2, Run conditions for analytical and numerical modeling with only molecular diffusion

Effect of duration (years)					
Data	Run 1a	Run 1b	Run 1c	Run 1d	Run 1e
Time, year	5.10 ³	10 ⁴	2.10 ⁴	10 ⁵	10 ⁷
Molecular diffusion coefficient, cm ² /s	3.10 ⁻⁵				
Porosity, fraction	0.2				
Effect of porosity					
Data	Run 2a	Run 1c	Run 2b		
Porosity, fraction	0.1	0.2	0.3		
Time, year	2.10 ⁴				
Molecular diffusion coefficient, cm ² /s	3.10 ⁻⁵				

Table 6.3, Run conditions for analytical and numerical modeling with dispersion

Effect of dispersivity (m)				
Data	Run 3a	Run 3b	Run 3c	
Dispersivity, m	1	10	20	
Permeability, md	100			
Time, year	200			
Porosity, fraction	0.2			
Effect of dispersivity (m)				
Data	Run 4a	Run 4b	Run 4c	
Dispersivity, m	1	10	20	
Permeability, md	100			
Time, year	750			
Porosity, fraction	0.2			
Effect of dispersivity (m)				
Data	Run 5a	Run 5b	Run 5c	
Dispersivity, m	1	10	20	
Permeability, md	100			
Time, year	6000			
Porosity, fraction	0.2			
Effect of permeability (md)				
Data	Run 6a	Run 6b	Run 6c	Run 6d
Permeability, md	1	10	100	1000
Time, year	1000			
Porosity, fraction	0.2			
Dispersivity, m	10			
Effect of porosity				
Data	Run 7a	Run 3b	Run 7b	
Porosity, fraction	0.1	0.2	0.3	
Permeability, md	100			
Time, year	200			
Dispersivity, m	10			

Table 6.4, Numerical Run conditions for dispersion and molecular diffusion

Long and short duration dispersion						
Data	Run 8a	Run 8b	Run 8c	Run 8d	Run 8e	Run 8f
Permeability, md	1	10	20	50	100	1000
Time, year	10000	1000	500	200	100	10
Porosity, fraction	0.2					
Dispersivity, m	10					
Molecular Diffusion						
Data	Run 9a	Run 9b	Run 9c	Run 9d	Run 9e	Run 9f
Molecular diffusion coefficient, cm ² /s	3.10 ⁻⁵					
Time, year	10000	1000	500	200	100	10
Porosity, fraction	0.2					

6.1 The Results of Analytical Modeling Study

6.1.1 Analytical Modeling of Molecular Diffusion Mechanism

Equation 5.3 is used for the solution of the cases in which only the molecular diffusion mechanism is considered.

6.1.1.1 Effect of Duration on CO₂ Saturation (analytical model)

In Figure 6.1, the distribution of CO₂ in aquifer for a diffusion dominated process is presented. The dissolved amount of CO₂ increases with time. However, due to diffusion dominated system the dissolution rate is very slow. Even after 10,000,000 years the aquifer is not fully saturated with CO₂.

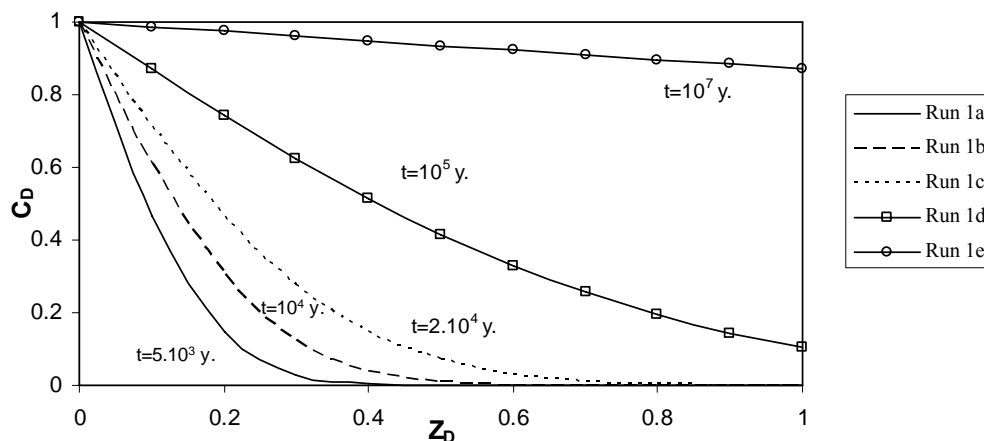


Figure 6. 1. Effect of Duration on CO₂ Saturation ($\phi=0.2$, analytical model)

6.1.1.2 Effect of Porosity on CO₂ Saturation (analytical model)

In Figure 6.2, the effect of porosity for a diffusion dominated system is presented. When the porosity of aquifer increases, the effective diffusion coefficient of solute in the brine increases (equation 3.3). So, the diffusion rate is higher at higher porosity systems and the aquifer with higher porosity is saturated with CO₂ faster as shown in Figure 6.2.

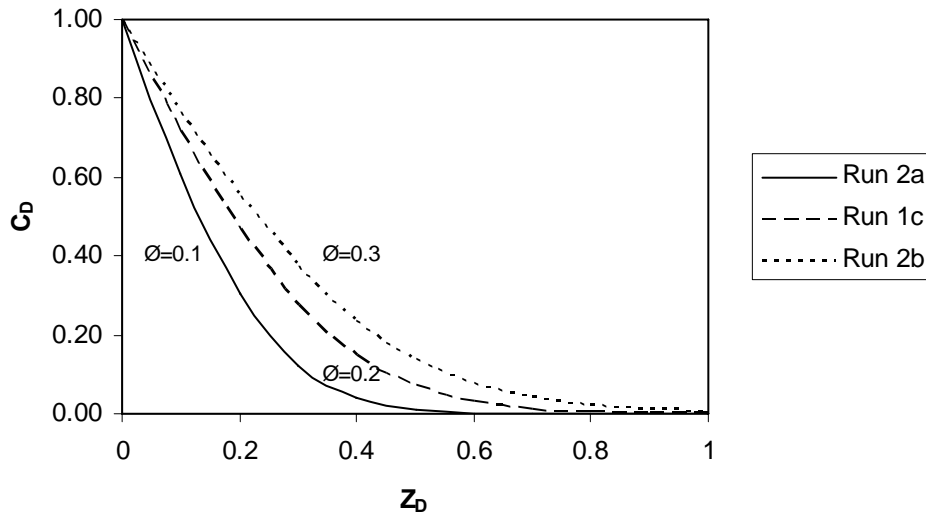


Figure 6. 2. Effect of Porosity on CO₂ Saturation (2.10⁴ years, analytical model)

6.1.2 Analytical Modeling of Convection Dominant Mechanism

In the convection dominant process, Equation 5.12 is used for the solution of the run cases. The only different parameter in this equation between analytical and numerical approach is the velocity parameter. In numerical part, the velocity is calculated according to the varying concentration difference. On the other hand, for analytical part this velocity is taken as a constant value. The constant velocity is the average value of the varying velocity in the aquifer. It is calculated based on the geometric mean. The geometric mean is a measure of central tendency, Equation 6.1. To take the effect of V_{\min} ($V=0$) into account in geometric series, minimum velocity (zero velocity) is set to very small value, 10^{-18} cm/s shown in Figure 6. 3. The maximum velocity values are in the order 10^{-5} cm/s and 10^{-8} cm/s in run cases. So, the minimum value is taken as the 10^{10} times smaller of the maximum velocity.

$$GeometricMean = \frac{1}{n} \sqrt[n]{a_1 \cdot a_2 \dots a_n} \quad (6.1)$$

V	ΔC_D
V_{max}	1
$0.9V_{max}$	0.9
$0.8V_{max}$	0.8
$0.7V_{max}$	0.7
$0.6V_{max}$	0.6
$0.5V_{max}$	0.5
$0.4V_{max}$	0.4
$0.3V_{max}$	0.3
$0.2V_{max}$	0.2
$0.1V_{max}$	0.1
$V_{min}=10^{-18}$ cm/s ≈ 0	0

} $V_{avg}=0.01V_{max}$ from geometric mean

Figure 6. 3, Mean Velocity Calculation for Analytical Modeling

Table 6.5, Maximum Velocities Occured in the Runs

Runs	3a	3b	3c	
Maximum Velocity, cm/s	7.01×10^{-6}			
Runs	4a	4b	4c	
Maximum Velocity, cm/s	7.01×10^{-6}			
Runs	5a	5b	5c	
Maximum Velocity, cm/s	7.01×10^{-6}			
Runs	6a	6b	6c	6d
Maximum Velocity, cm/s	7.01×10^{-8}	7.01×10^{-7}	7.01×10^{-6}	7.01×10^{-5}
Runs	7a	3b	7c	
Maximum Velocity, cm/s	1.40×10^{-5}	7.01×10^{-6}	4.67×10^{-6}	

6.1.2.1 Effect of Dispersivity on CO₂ Saturation (analytical model)

In Figures 6.4, 6.5, and 6.6, the effect of dispersivity on CO₂ dissolution is presented in convection dominated system. In Figure 6.4, the CO₂ saturation for early time region (200 years) is shown. The effect of dispersivity on CO₂ transport is analyzed. When the dispersivity increases, more CO₂ is spreaded through the aquifer in early time region. In Figure 6.5, the CO₂ saturation for middle time region (750 years) is shown. In the middle time region, at the top of the aquifer more CO₂ is accumulated with lower dispersivity values for aquifers. After a point, this turns out to be opposite and more CO₂ is accumulated at the

deeper parts of the aquifer for higher dispersivity as in the early time region. In Figure 6.6, the CO₂ saturation for late time region (6000 years) is shown. At the end of the dissolution process in the aquifer, the dissolved CO₂ amount in the aquifer increases with lower dispersivity values.

Although the dissolved CO₂ amount is more in the early time of the whole transport in higher dispersivity value, the complete dissolution takes place earlier in lower dispersivity value.

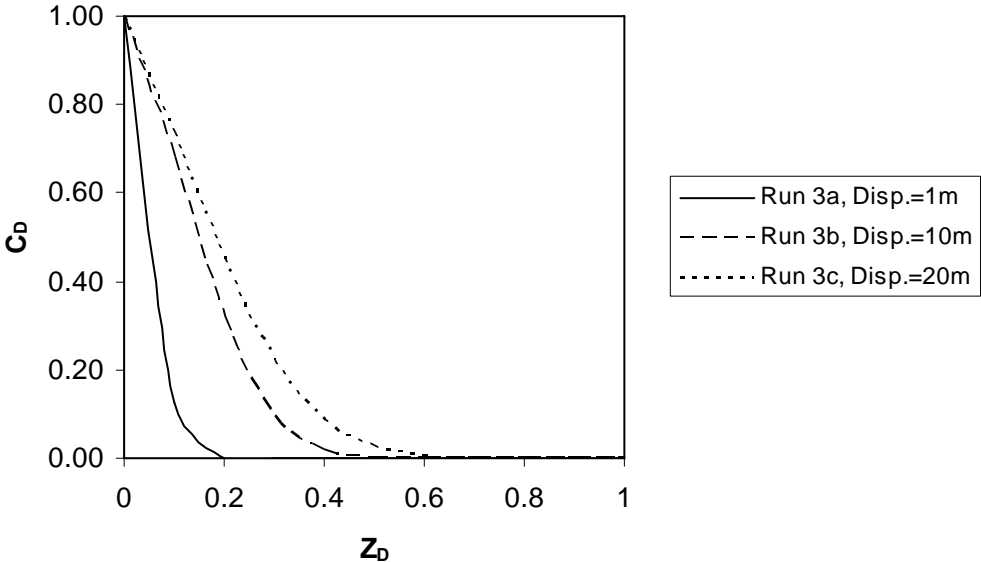


Figure 6. 4. Effect of Dispersivity on CO₂ Saturation (200 years, analytical model)

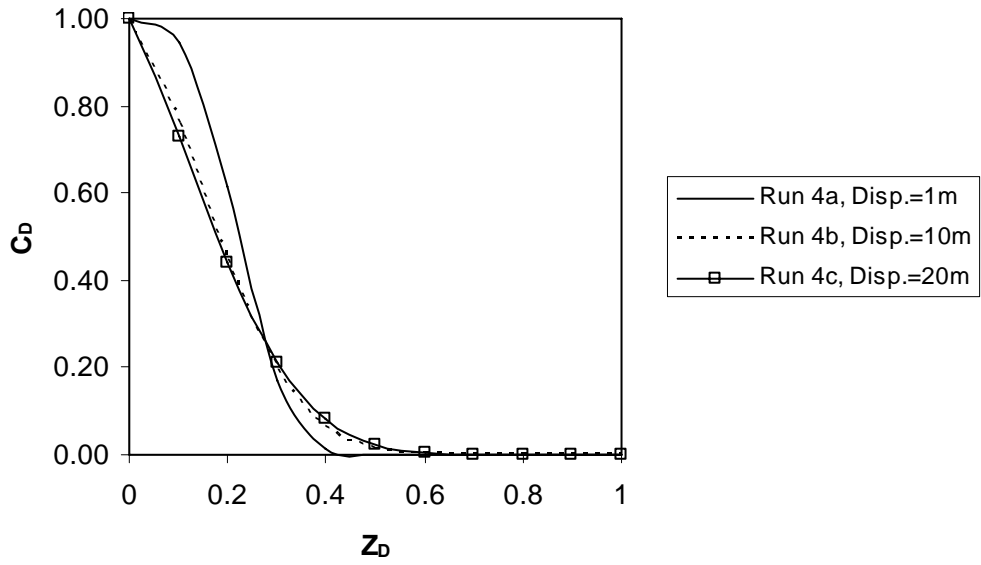


Figure 6. 5. Effect of Dispersivity on CO₂ Saturation (750 years, analytical model)

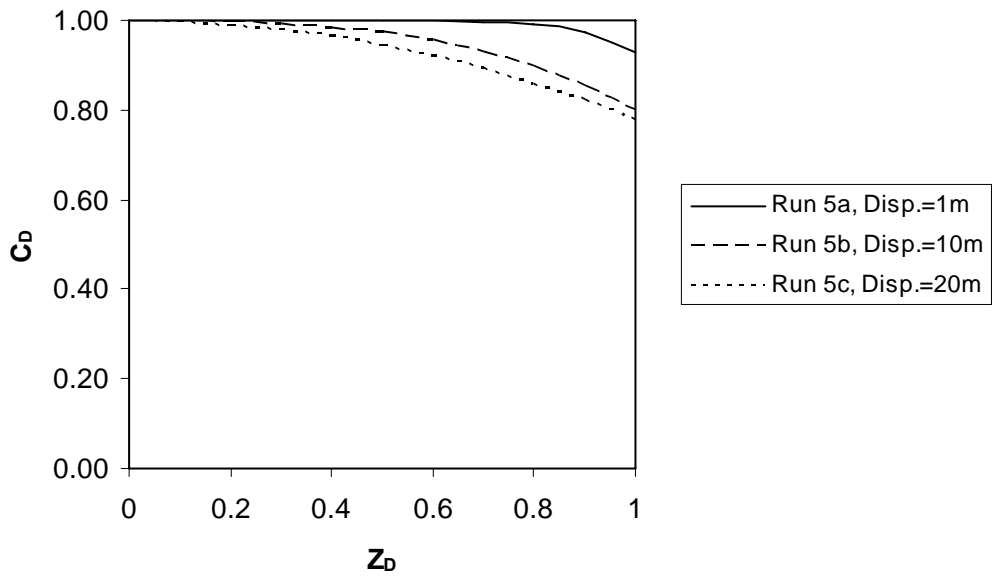


Figure 6. 6. Effect of Dispersivity on CO₂ Saturation (6000 years, analytical model)

6.1.2.2 Effect of Permeability on CO₂ Saturation (analytical model)

In Figure 6.7, the effect of permeability on CO₂ dissolution in convection dominated system is presented. As the permeability of the aquifer increases, the convection rate increases due to increased velocity. As shown in Figure 6.7, the saturated CO₂ amount increases with increased permeability.

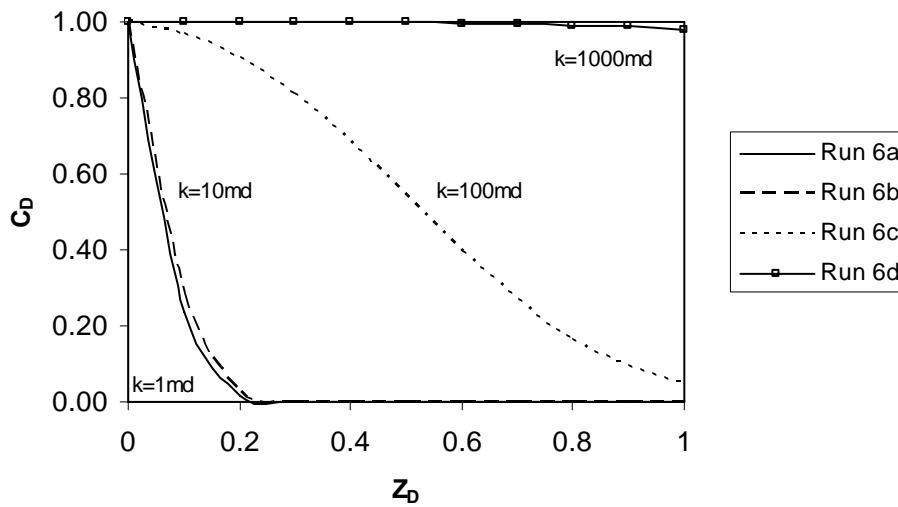


Figure 6. 7. Effect of Permeability on CO₂ Saturation (1000 years, analytical model)

6.1.2.3 Effect of Porosity on CO₂ Saturation (analytical model)

In Figure 6.8, the effect of porosity on CO₂ dissolution in convection dominated systems is presented. In convection dominated systems, at low porosity convection rate is faster due to higher interstitial velocity. So, with increase in porosity the convection rate of the transport decreases as shown in Figure 6.8.

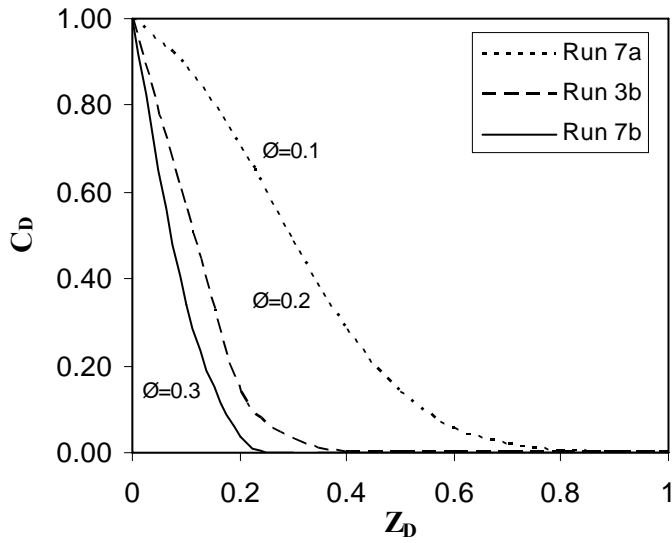


Figure 6. 8. Effect of Porosity on CO₂ Saturation (200 years, analytical model)

6.2 The Results of Numerical Modeling Study

6.2.1 Numerical Modeling of Molecular Diffusion Mechanism

6.2.1.1 Effect of Duration on CO₂ Saturation (numerical model)

In Figure 6.9, the distribution of CO₂ in aquifer in a diffusion dominated system is presented and the trend is similar as in Figure 6.1. The dissolved CO₂ amount in aquifer increases with time. Due to diffusion dominated system, the dissolution rate is very slow. After 10,000,000 years the aquifer is just about saturated with CO₂. The visual distribution of CO₂ in the aquifer by numerical simulator could be viewed in Figures 6.10, 6.11, 6.12, 6.13, and 6.14.

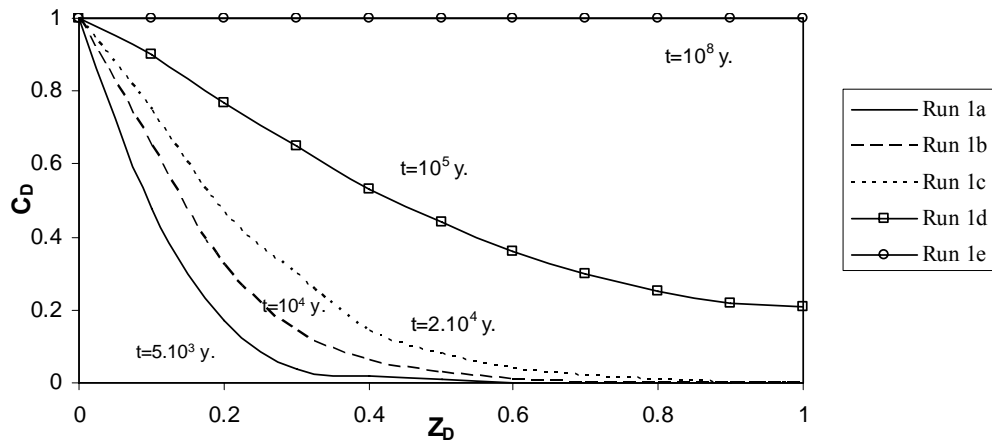


Figure 6. 9. Effect of Duration on CO₂ Saturation ($\phi=0.2$, numerical model)

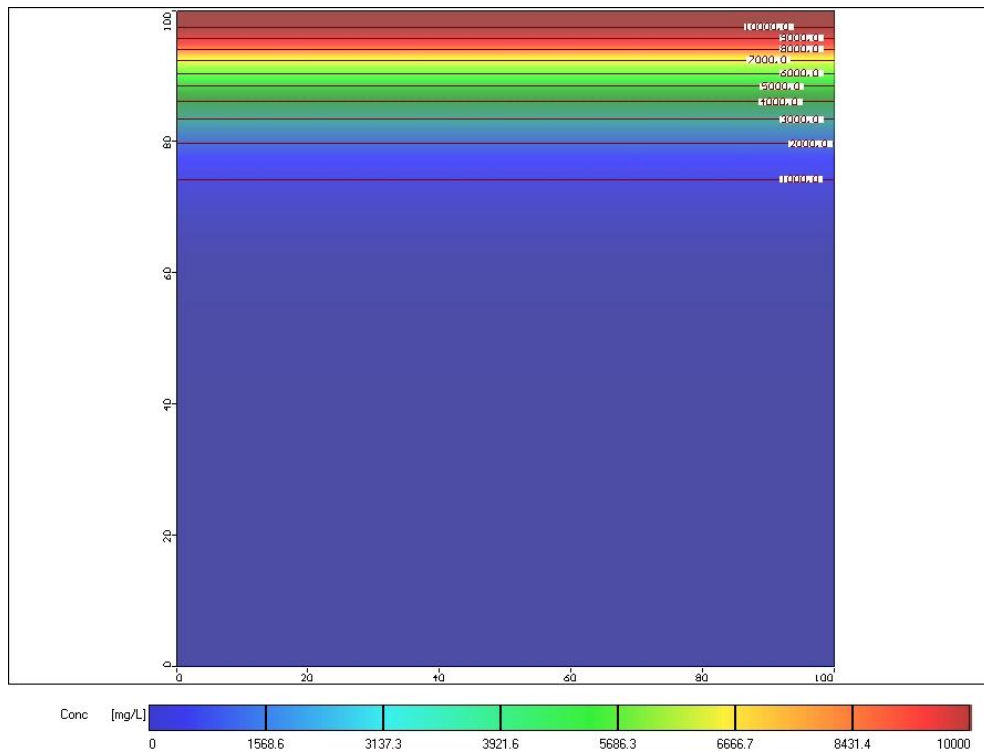


Figure 6. 10. Map of CO₂ Saturation in an Aquifer for Run 1a (5000 years, numerical modeling)

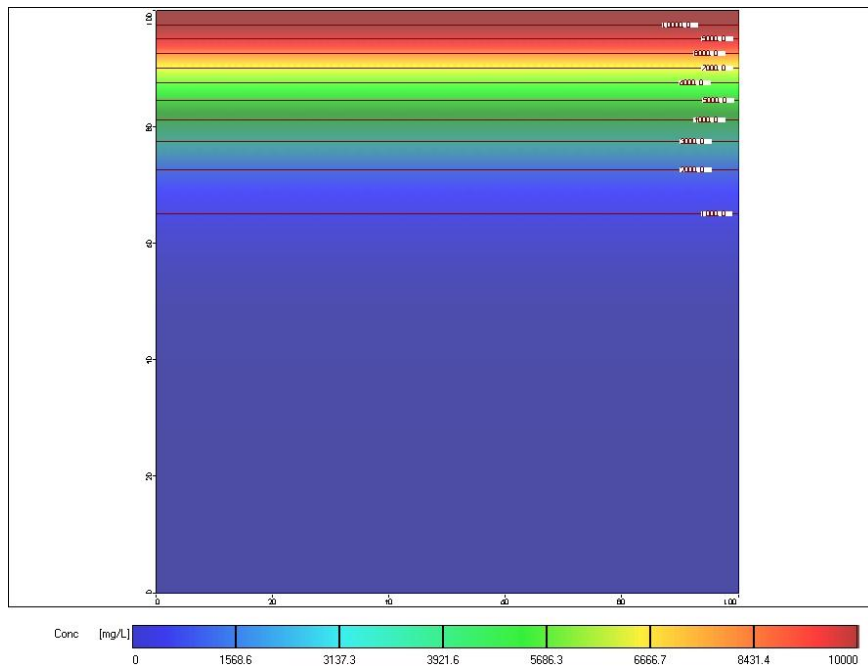


Figure 6. 11. Map of CO₂ Saturation in an Aquifer for Run 1b, (10000 years, numerical modeling)

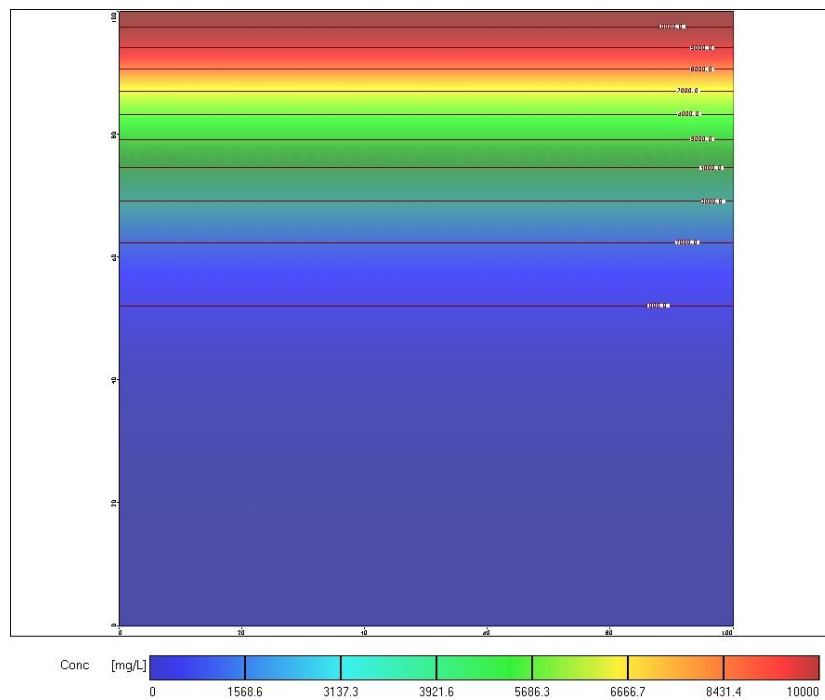


Figure 6. 12. Map of CO₂ Saturation in an Aquifer for Run 1c, (20000 years, numerical modeling)

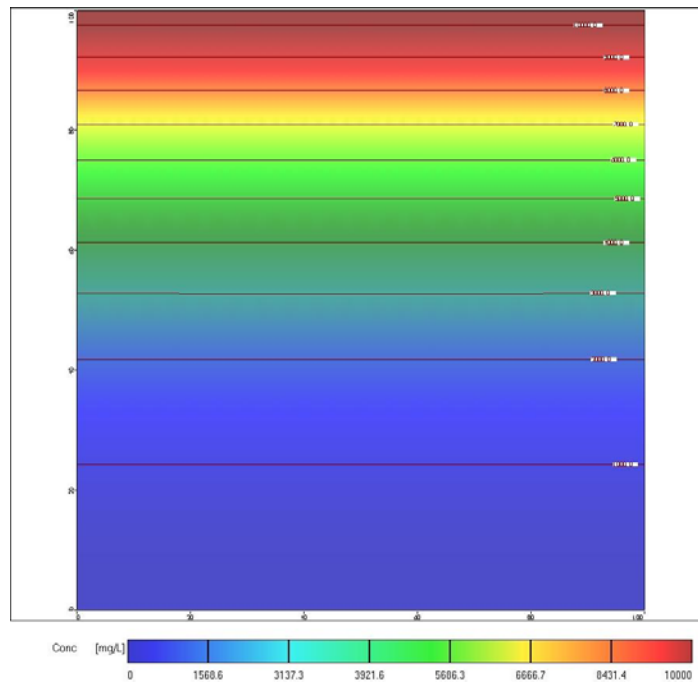


Figure 6. 13. Map of CO₂ Saturation in an Aquifer for Run 1d, (100000 years, numerical modeling)

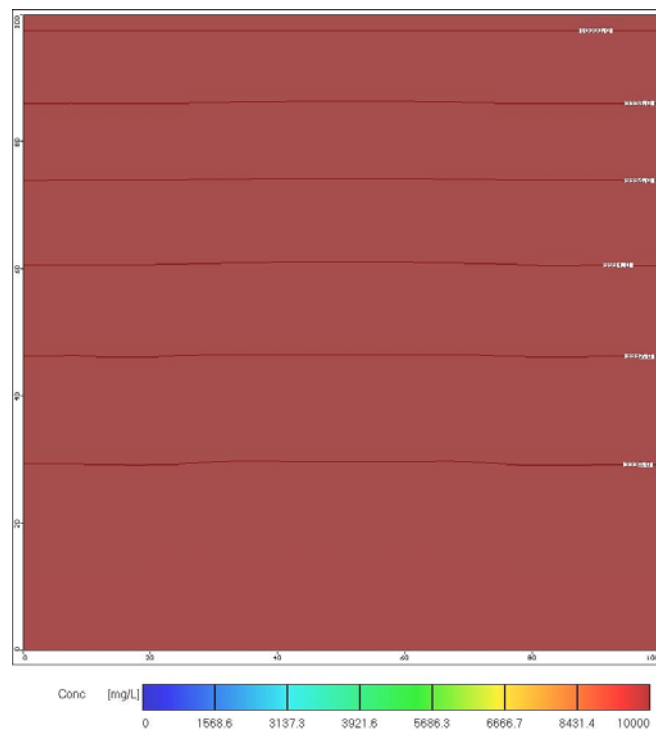


Figure 6. 14. Map of CO₂ Saturation in an Aquifer for Run 1e (10000000 years, numerical modeling)

6.2.1.2 Effect of Porosity on CO₂ Saturation (numerical model)

In Figure 6.15, the effect of porosity in diffusion dominated system is presented and the trend is similar to that of Figure 6.2. Due to the increase in the porosity of aquifer, the effective diffusion coefficient of solute in the brine increases (equation 3.3). So, dissolution becomes faster in higher porosity systems. The visual distribution of CO₂ in the aquifer by numerical simulator could be viewed in Figures 6.16 and 6.17.

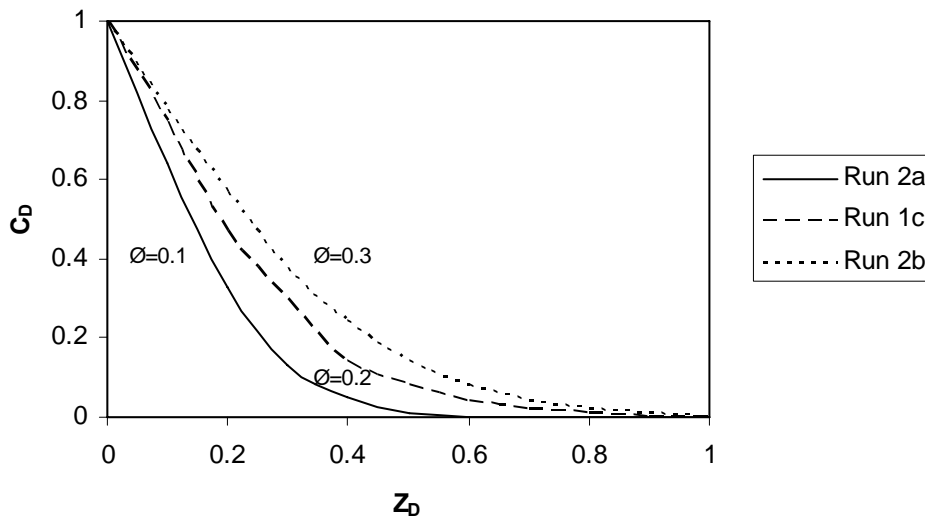


Figure 6. 15. Effect of Porosity on CO₂ Saturation (2.10⁴ years, numerical model)

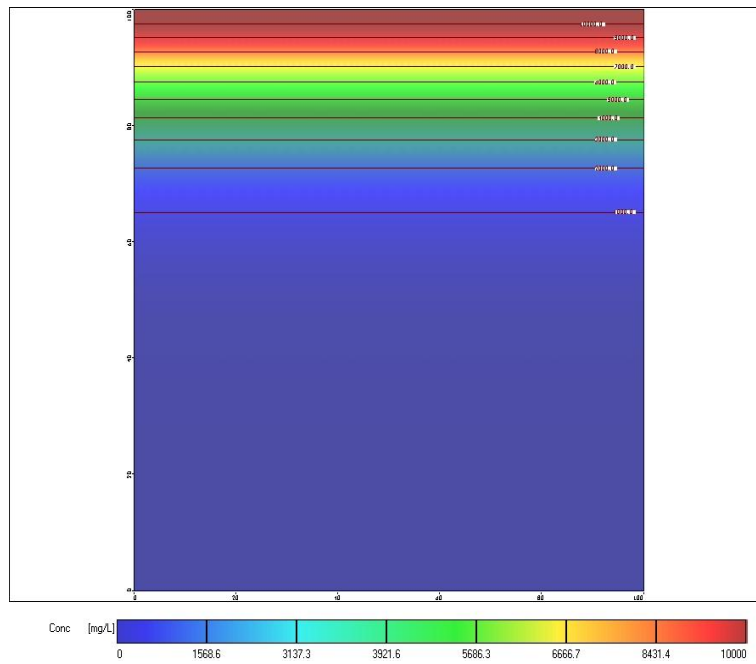


Figure 6. 16. Map of CO₂ Saturation in an Aquifer for Run 2a, $\phi=0.1$ ($2 \cdot 10^4$ years, numerical modeling)

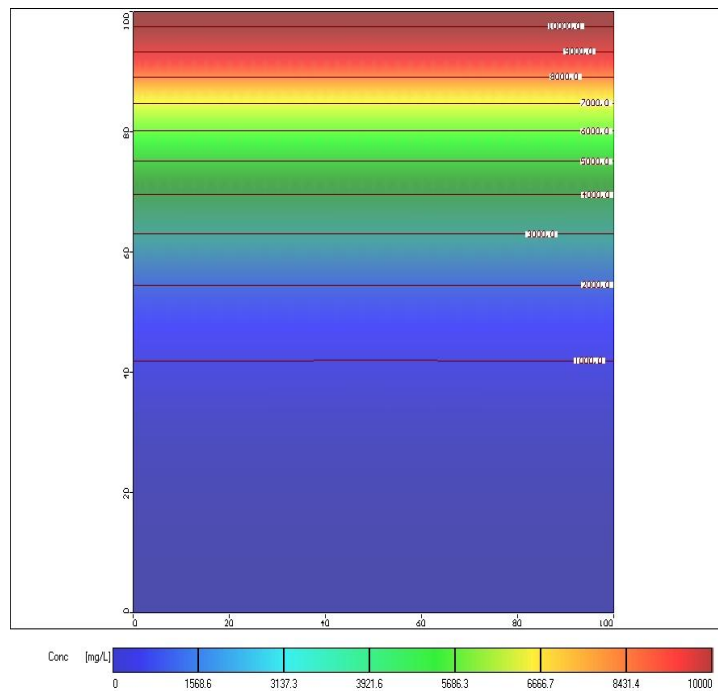


Figure 6. 17. Map of CO₂ Saturation in an Aquifer for Run 2b, $\phi=0.3$ ($2 \cdot 10^4$ years, numerical modeling)

6.2.2 Numerical Modeling of Convection Dominant Mechanism

6.2.2.1 Effect of Dispersivity on CO₂ Saturation (numerical model)

In Figures 6.18, 6.22, and 6.26, the effect of dispersivity on CO₂ dissolution is presented. In Figure 6.18, the CO₂ saturation for early time region (200 years) is shown. When the dispersivity of an aquifer increases, more solutes are spreaded through the aquifer in early time region as in the analytical modeling in figure 6.4. The visual distribution of CO₂ in the aquifer for early time region by numerical simulator could be viewed in Figures 6.19, 6.20, and 6.21.

In Figure 6.22, the CO₂ saturation for middle time region (750 years) is shown. In the beginning of the aquifer more CO₂ is accumulated with lower dispersivity values for aquifers. After a time (750 years), this turns out to be opposite and more CO₂ is accumulated at the end of the aquifer for higher dispersivity aquifers as in the early time region. This trend is nearly same with analytical results in Figure 6.5 with some deviations. This is possibly due to the different distribution of CO₂ plume after the deposition in the bottom of the aquifer. The visual distribution of CO₂ in the aquifer for middle time region by numerical simulator could be viewed in Figure 6.23, 6.24, and 6.25.

The CO₂ saturation for late time region (6000 years) is presented in Figure 6.26 for numerical modeling. The trend is again similar with analytical one in figure 6.5. The dissolution is faster at the end of the dissolution process for lower dispersivity aquifers. The visual distribution of CO₂ in the aquifer for late time region by numerical simulator could be viewed in Figures 6.27, 6.28, and 6.29.

The numerical results are same with analytical results. The total dissolution of the aquifer is quicker in low dispersivity aquifers in the end.

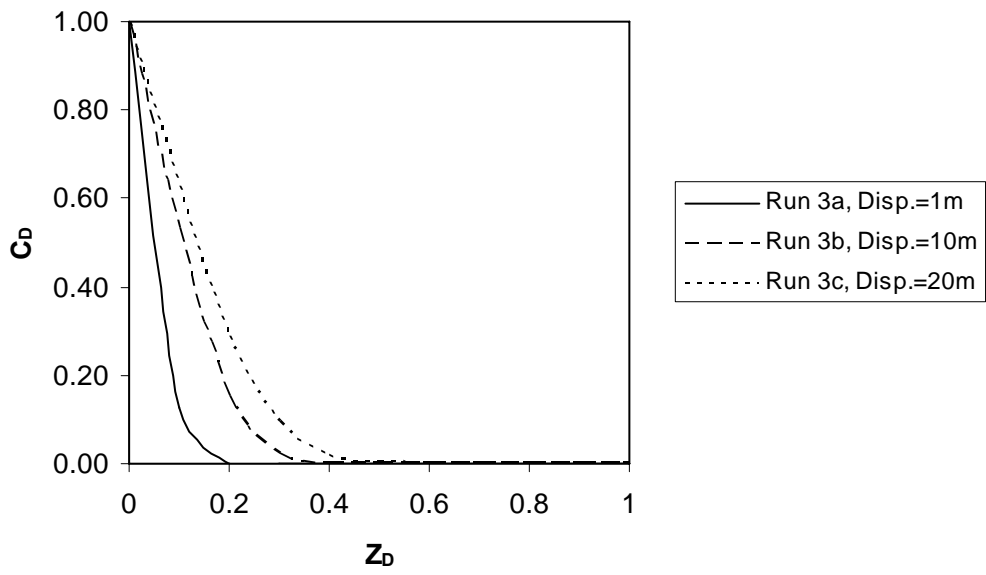


Figure 6. 18. Effect of Dispersivity on CO₂ Saturation (200 years, numerical model)

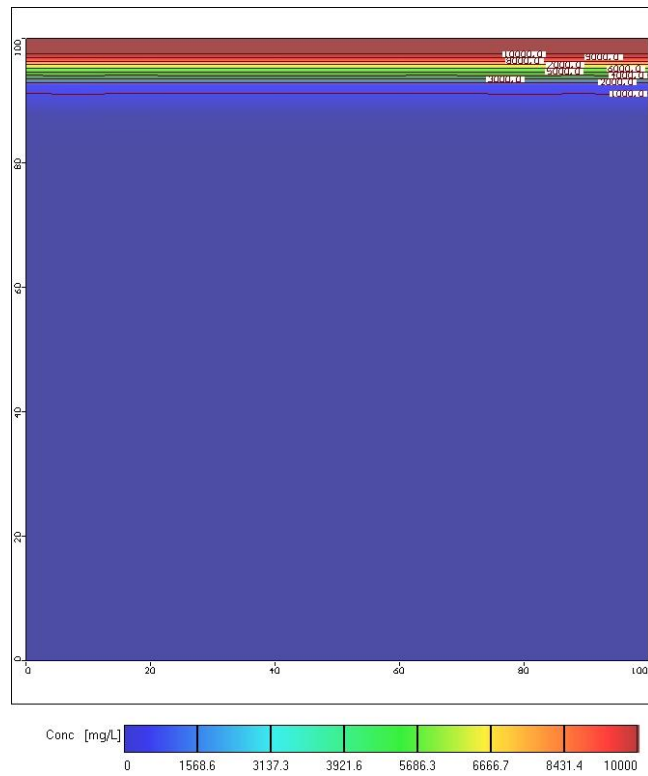


Figure 6. 19. Map of CO₂ Saturation in an Aquifer for Run 3a, $\alpha=1$ m (200 years, numerical model)

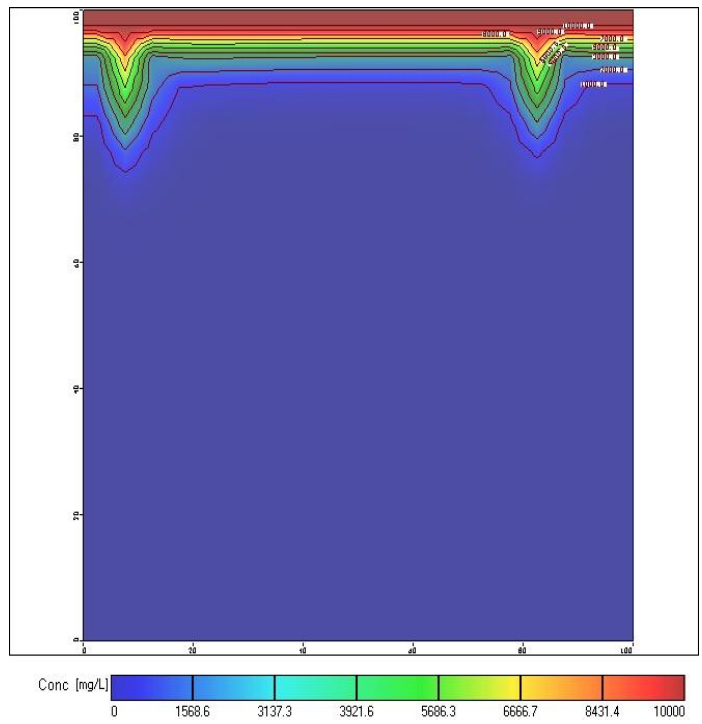


Figure 6. 20. Map of CO₂ Saturation in an Aquifer for Run 3b, $\alpha=10$ m (200 years, numerical model)

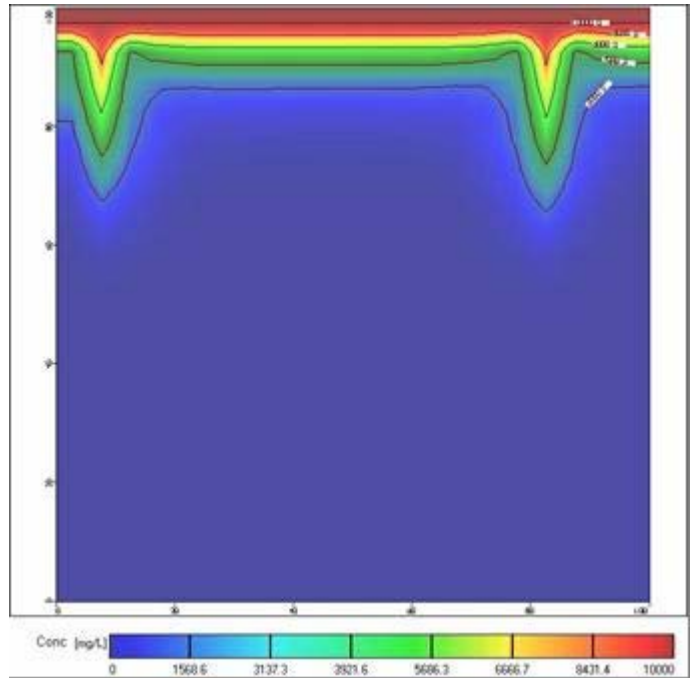


Figure 6. 21. Map of CO₂ Saturation in an Aquifer for Run 3c, $\alpha=20$ m (200 years, numerical model)

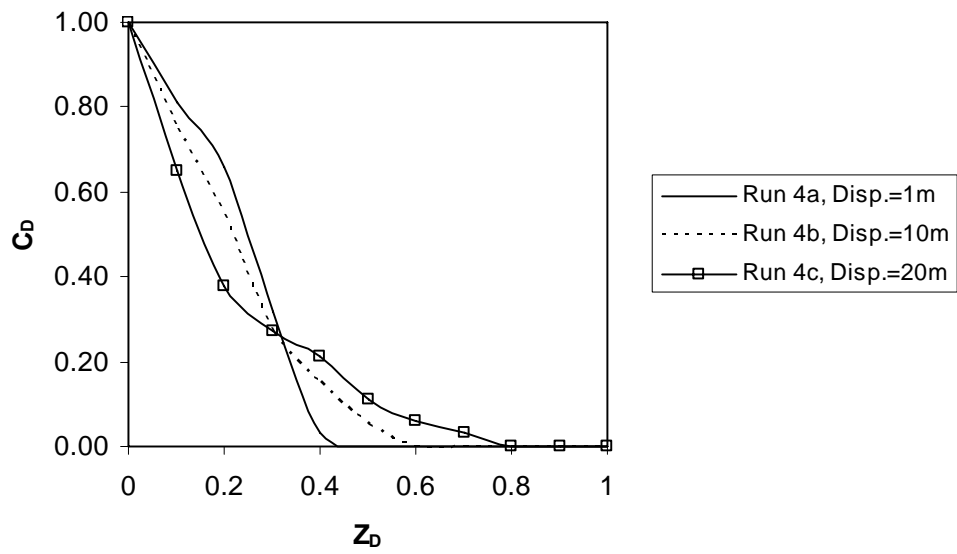


Figure 6. 22. Effect of Dispersivity on CO₂ Saturation (750 years, numerical model)

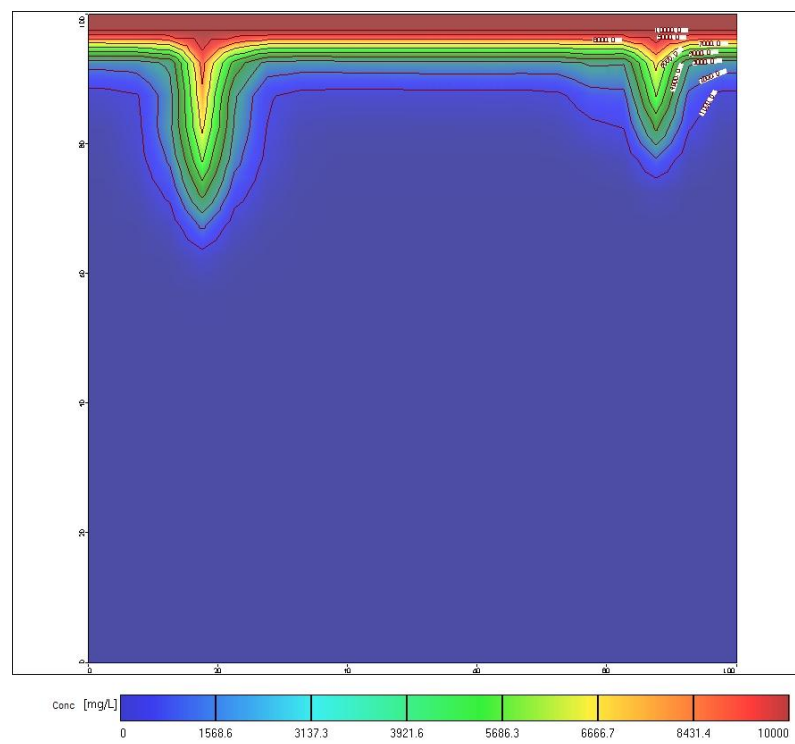


Figure 6. 23. Map of CO₂ Saturation in an Aquifer for Run 4a, $\alpha=1$ m (750 years, numerical model)

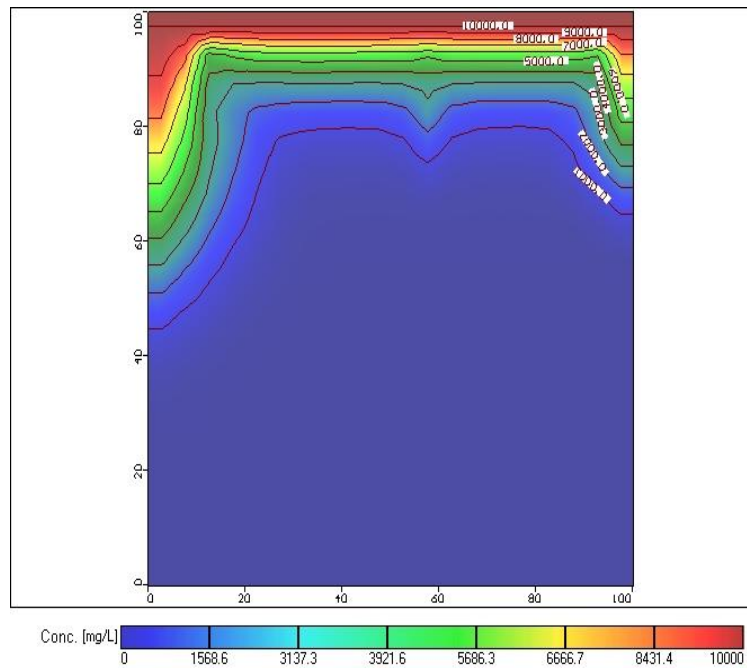


Figure 6. 24. Map of CO₂ Saturation in an Aquifer for Run 4b, $\alpha=10$ m (750 years, numerical model)

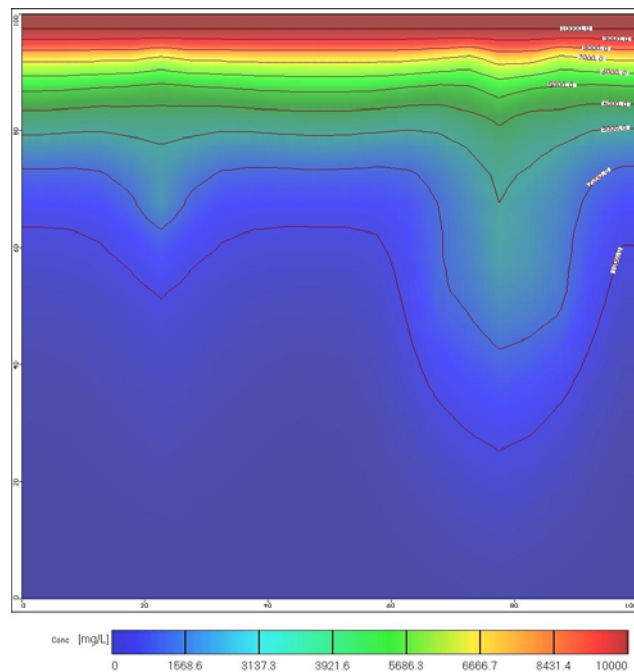


Figure 6. 25. Map of CO₂ Saturation in an Aquifer for Run 4c, $\alpha=20$ m (750 years, numerical model)

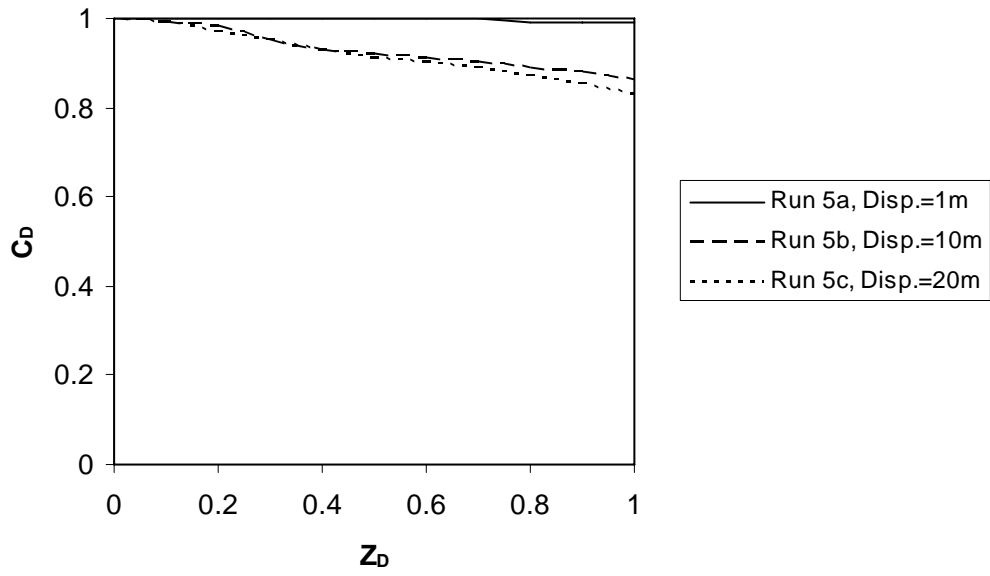


Figure 6. 26. Effect of Dispersivity on CO₂ Saturation (6000 years, numerical model)

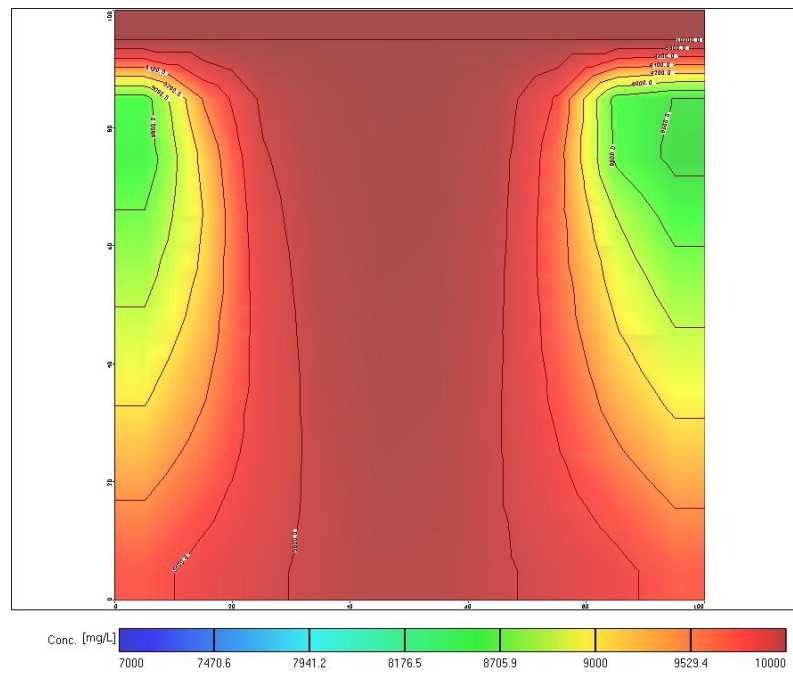


Figure 6. 27. Map of CO₂ Saturation in an Aquifer for Run 5a, $\alpha=1$ m (6000 years, numerical model)

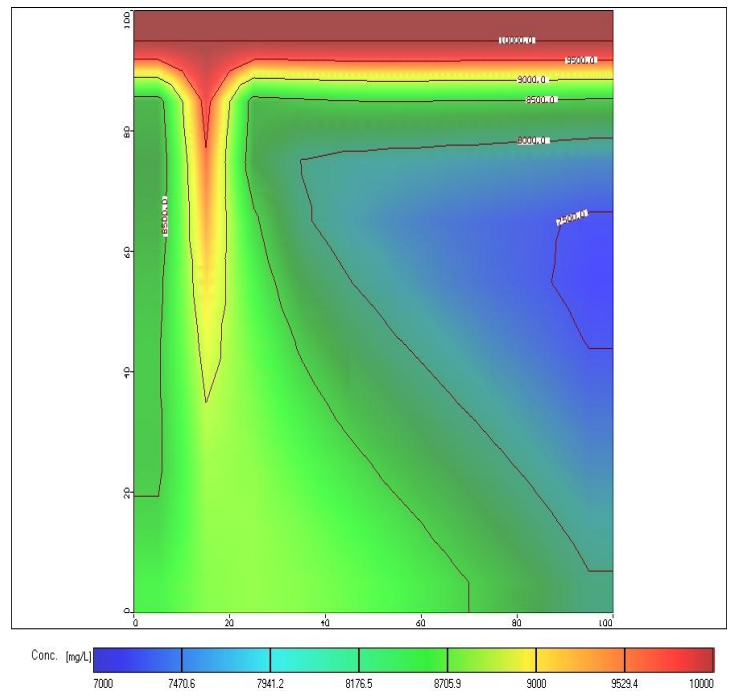


Figure 6. 28. Map of CO₂ Saturation in an Aquifer for Run 5b, $\alpha=10$ m (6000 years, numerical model)

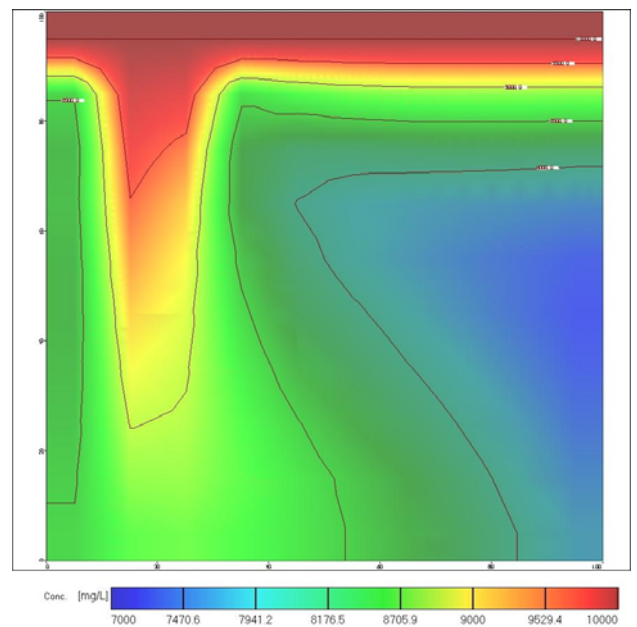


Figure 6. 29. Map of CO₂ Saturation in an Aquifer for Run 5c, $\alpha=20$ m (6000 years, numerical model)

6.2.2.2 Effect of Permeability on CO₂ Saturation (numerical model)

In Figure 6.30, the effect of permeability on CO₂ dissolution is presented. The effect of high permeable aquifer on dissolution in the studied time period can be seen in Figure 6.30. There is a slight change between 1md and 10md permeability aquifers. As the permeability of aquifer increases, the saturated CO₂ amount increases due to increased brine velocity. The trend is same with the analytical one. The visual distribution of CO₂ in the aquifer by numerical simulator could be viewed in Figures 6.31, 6.32, 6.33, and 6. 34.

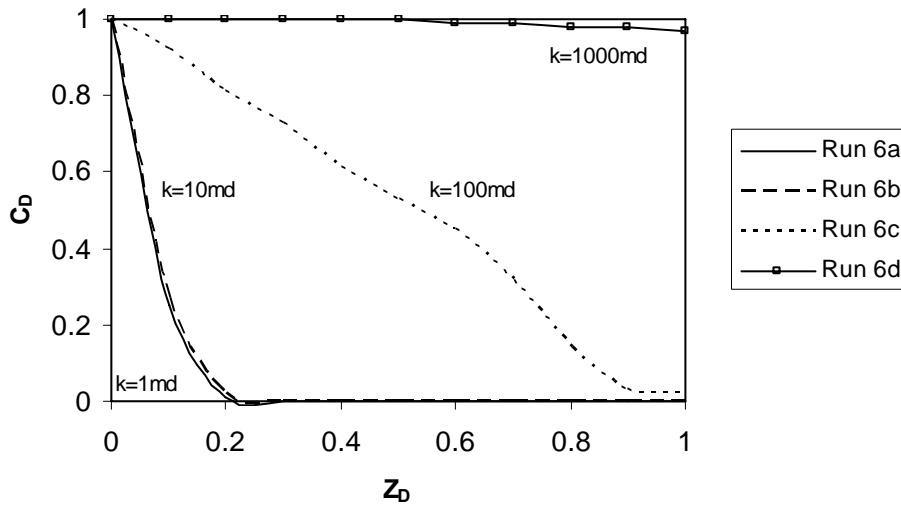


Figure 6. 30. Effect of Permeability on CO₂ Saturation (1000 years, numerical model)

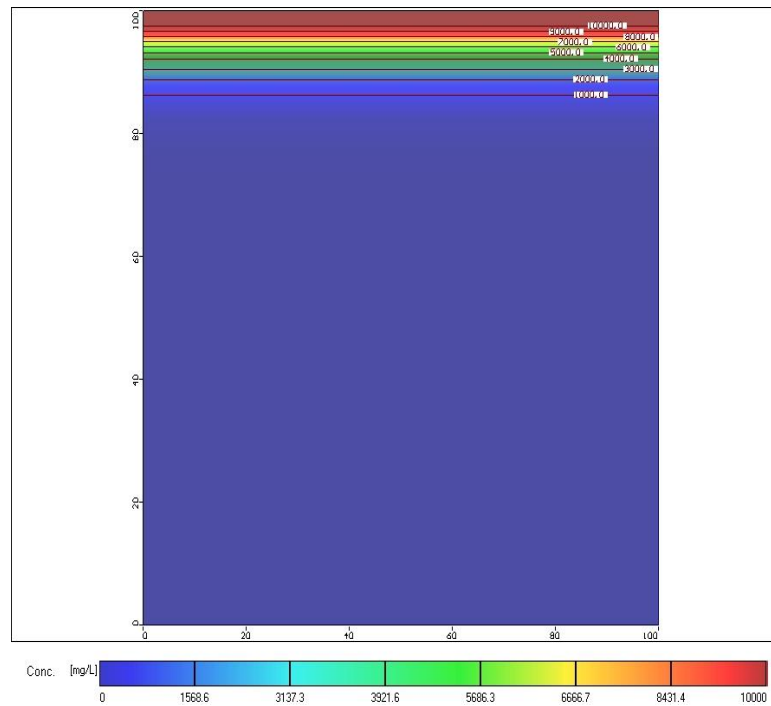


Figure 6. 31. Map of CO₂ Saturation in an Aquifer for Run 6a, k=1 md (1000 years, numerical model)

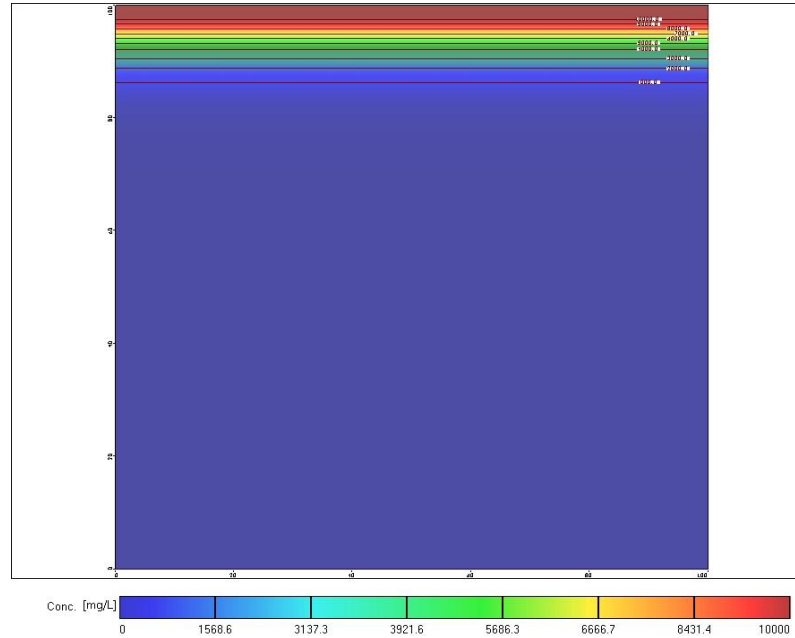


Figure 6. 32. Map of CO₂ Saturation in an Aquifer for Run 6b, k=10 md (1000 years, numerical model)

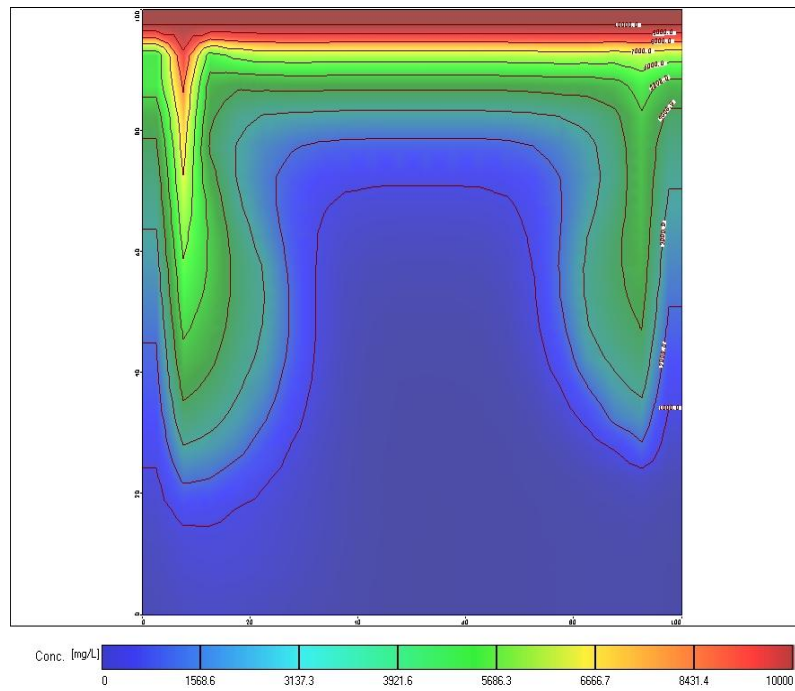


Figure 6. 33. Map of CO₂ Saturation in an Aquifer for Run 6c, k=100 md (1000 years, numerical model)

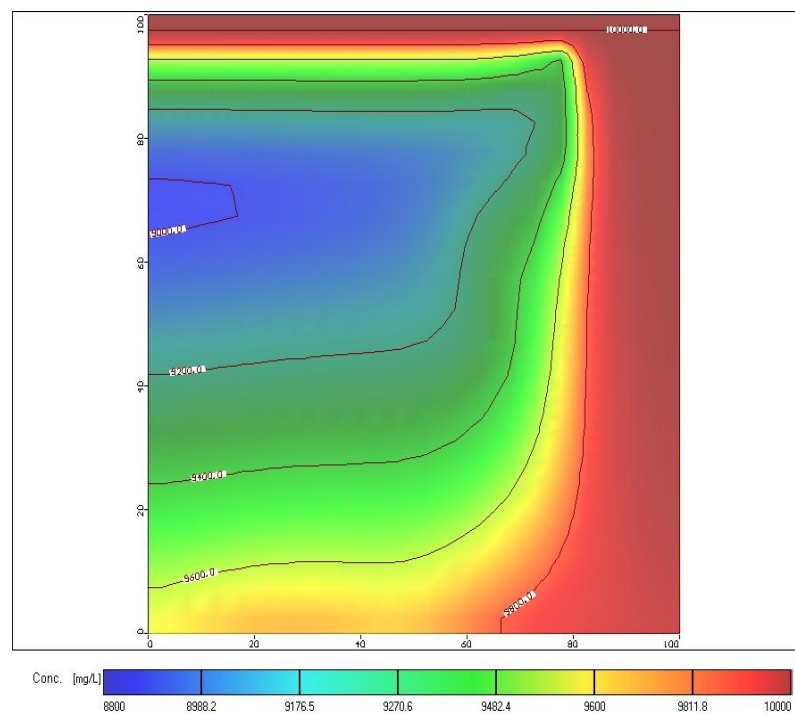


Figure 6. 34. Map of CO₂ Saturation in an Aquifer for Run 6c, k=1000 md (1000 years, numerical model)

6.2.2.3 Effect of Porosity on CO₂ Saturation (numerical model)

In Figure 6.35, the effect of porosity on CO₂ dissolution in convection dominated systems is presented. In convection dominated system, at low porosity convection rate is faster due to higher interstitial velocity. So, with porosity increase the convection rate of the transport decreases by numerical model as in the analytical results shown in Figure 6.8. The visual distribution of CO₂ in the aquifer for different porosities by numerical model can be viewed in Figure 6.36, 6.37, and 6.38. As shown, convective plume is large in lower porosity aquifers.

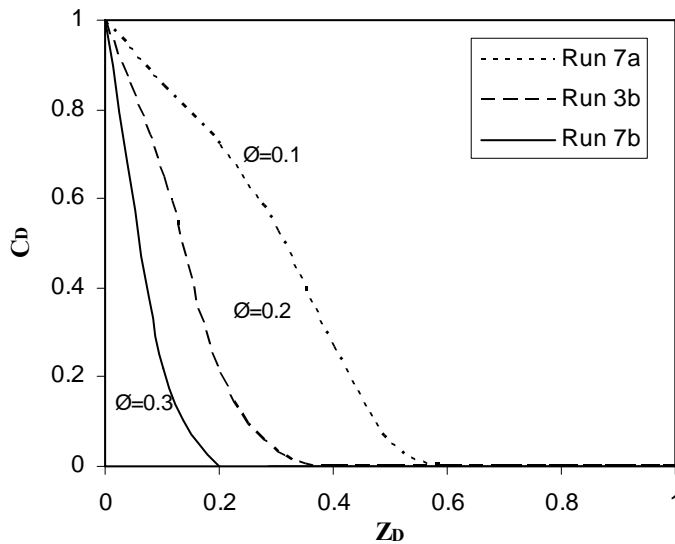


Figure 6. 35. Effect of Porosity on CO₂ Saturation (200 years, numerical model)

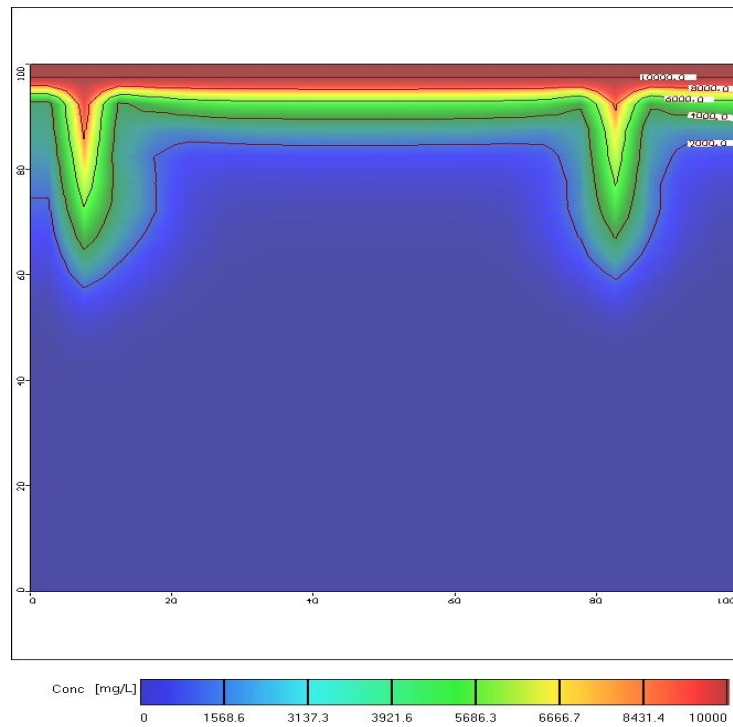


Figure 6. 36. Map of CO₂ Saturation in an Aquifer for Run 7a, $\phi=0.1$ (200 years, numerical model)

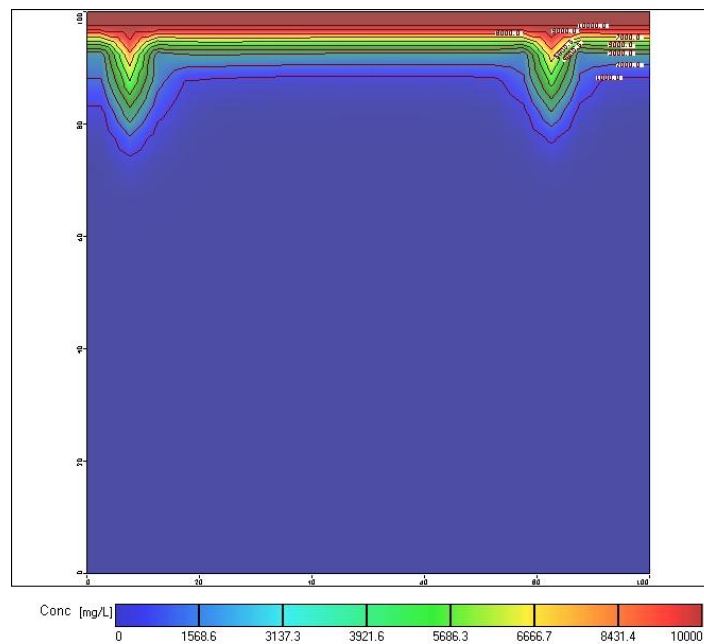


Figure 6. 37. Map of CO₂ Saturation in an Aquifer for Run 3b, $\phi=0.2$ (200 years, numerical model)

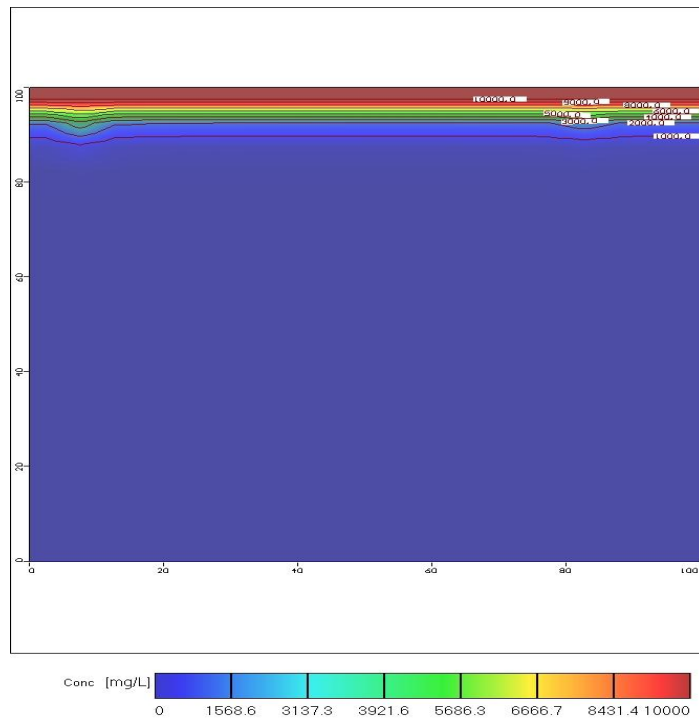


Figure 6. 38. Map of CO₂ Saturation in an Aquifer for Run 7b, $\phi=0.3$ (200 years, numerical model)

6.3 Comparison of Results for Analytical and Numerical Models

6.3.1 Molecular Diffusion Mechanism

6.3.1.1 Effect of Duration on CO₂ Saturation

In Figure 6.39, it could be seen that the results of analytical and numerical models match very well for diffusion dominated system. However, after many years such as in Run 1d and Run 1e, there are some deviations. This is possibly due to the round off and truncation errors that grow after many years in the numerical simulation. The dissolution of CO₂ in aquifer increases with time. But it takes about 10^7 years to saturate whole aquifer with CO₂ under only diffusion dominated system.

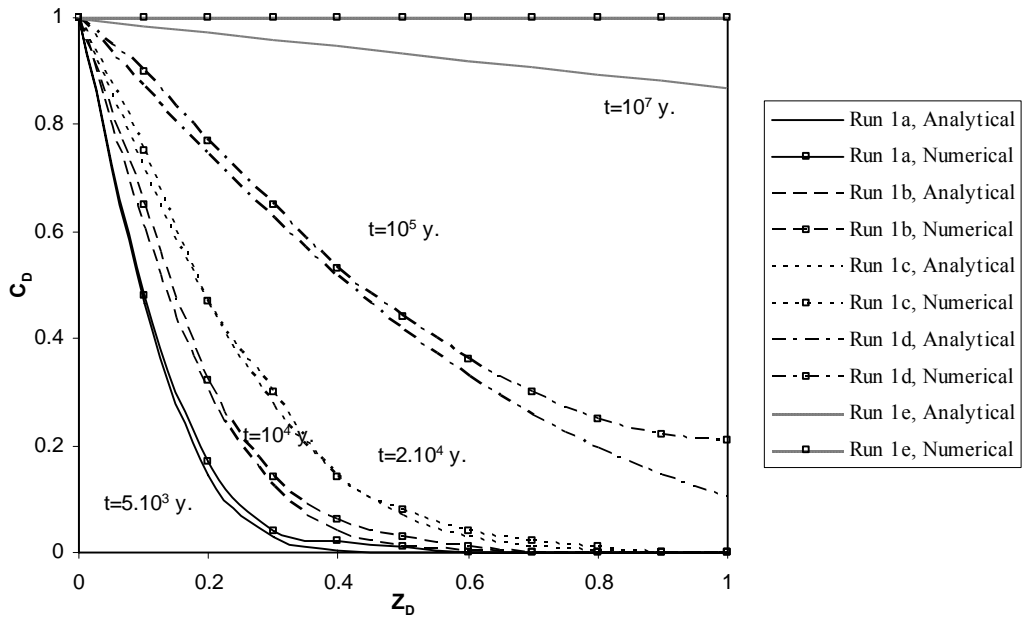


Figure 6. 39. Effect of Duration ($\phi=0.2$, comparison)

6.3.1.2 Effect of Porosity on CO₂ Saturation

In Figure 6.40, the results of analytical and numerical models match very well for Runs 2a and 2b. With porosity increase in diffusion dominated system, dissolution of CO₂ increases, because of increase in contacted water volume with CO₂.

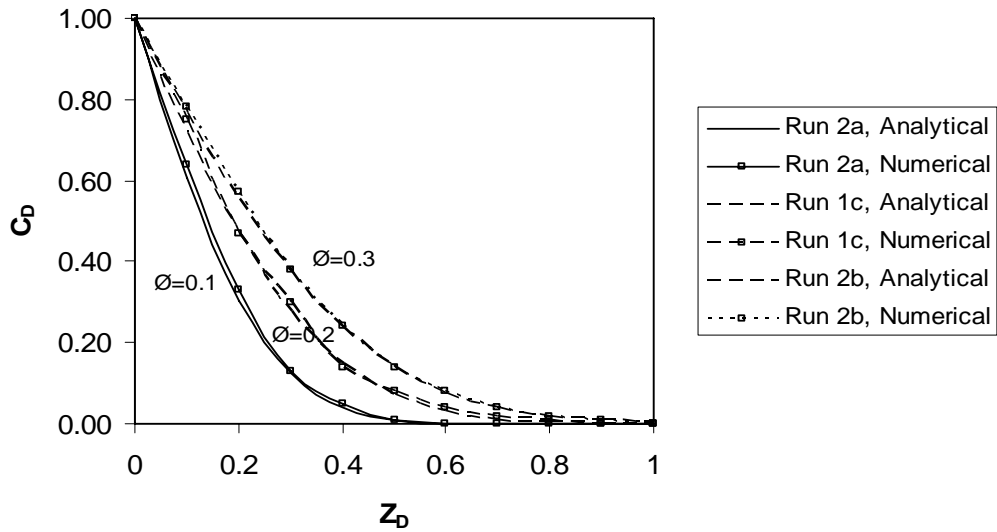


Figure 6. 40. Effect of Porosity, ($2 \cdot 10^4$ years, comparison)

6.3.2 Convection Dominated Process

6.3.2.1 Effect of Dispersivity on CO₂ Saturation

In Figures 6.41, 6.42, 6.43, 6.44, and 6.45, the comparison is presented between the results of analytical and numerical models of the dispersivity effect. The results of both models match very well generally, especially for early (200 years) and late time (6000 years) regions. However, for the middle time (750 years) region (the transition part from early to late time region) there are small deviations. This might be attributed to the movement of CO₂ saturated volume (plume) through the lower part of the aquifer to lateral direction at bottom. The analytical model doesn't take into account this movement at the bottom of the aquifer.

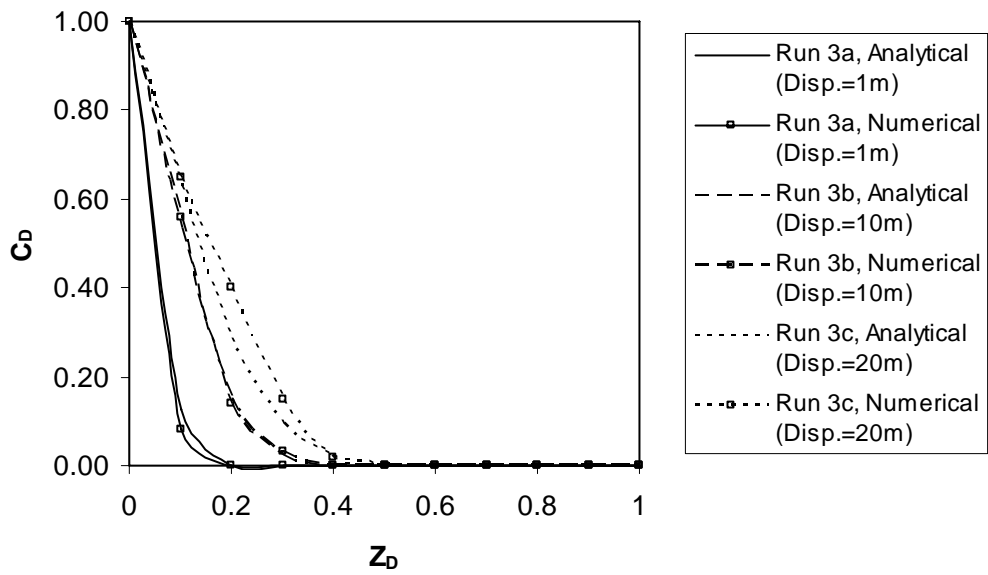


Figure 6. 41. Effect of Dispersivity (200 years, comparison)

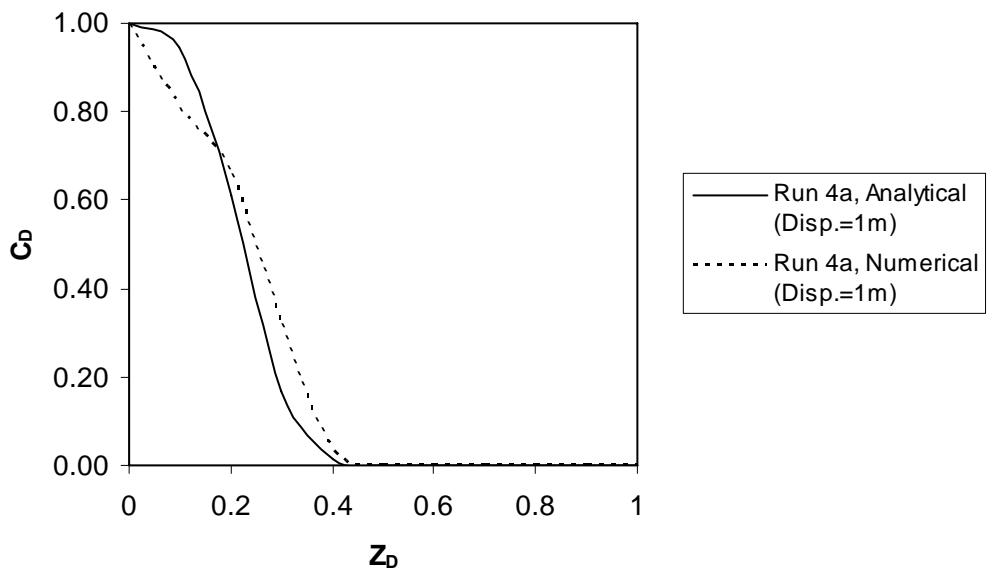


Figure 6. 42. Effect of Dispersivity (750 years, comparison)

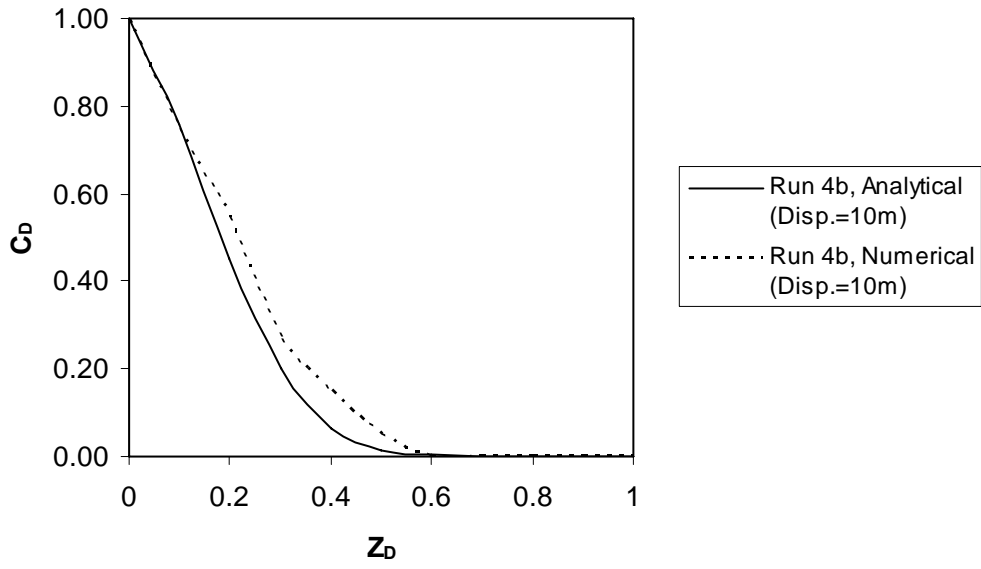


Figure 6. 43. Effect of Dispersivity (750 years, comparison)

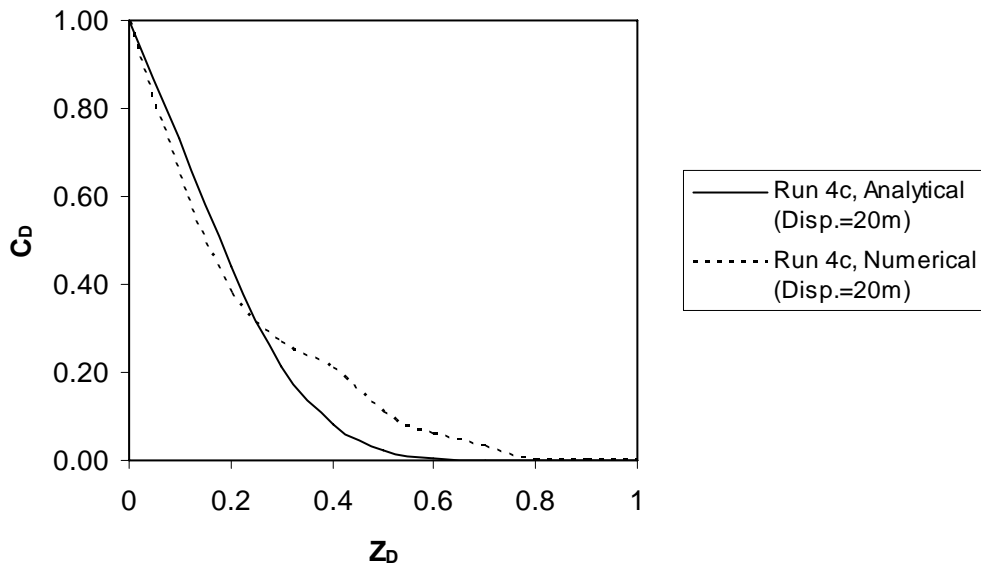


Figure 6. 44. Effect of Dispersivity (750 years, comparison)

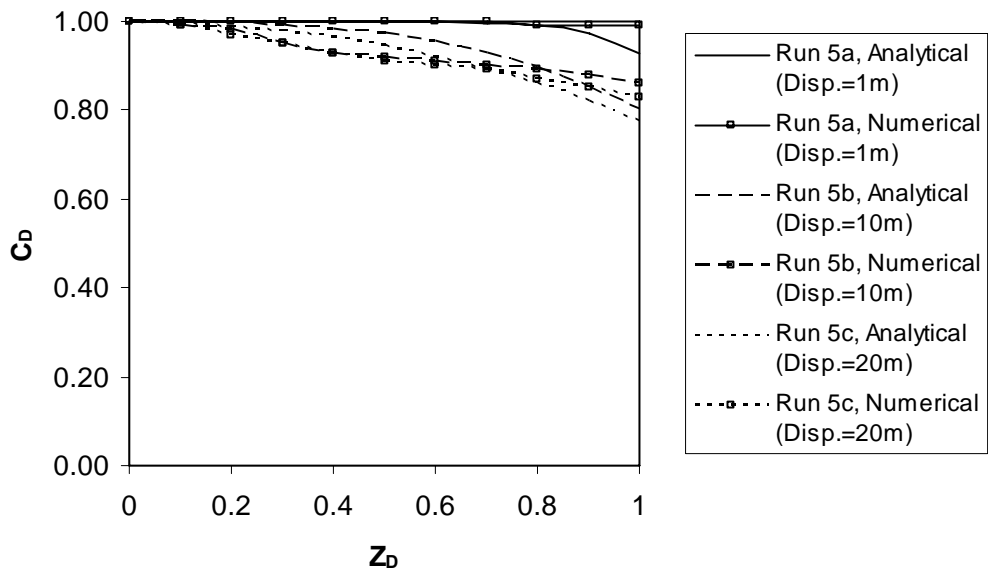


Figure 6. 45. Effect of Dispersivity (6000 years, comparison)

6.3.2.2 Effect of Permeability on CO₂ Saturation

The comparison of analytical and numerical modeling is made for permeability effect in Figures 6.46 and 6.47 for Run 6a, Run 6b, Run 6c and Run 6d. The results match very well. The higher permeability increases the convective transport of CO₂ into the aquifer; as a result more volume of water becomes saturated with CO₂.

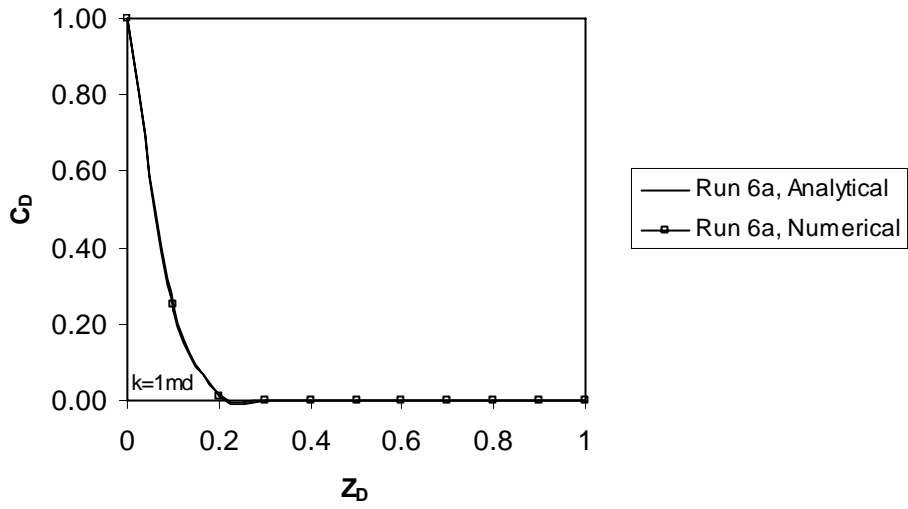


Figure 6. 46. Effect of Permeability (1000 years, comparison)

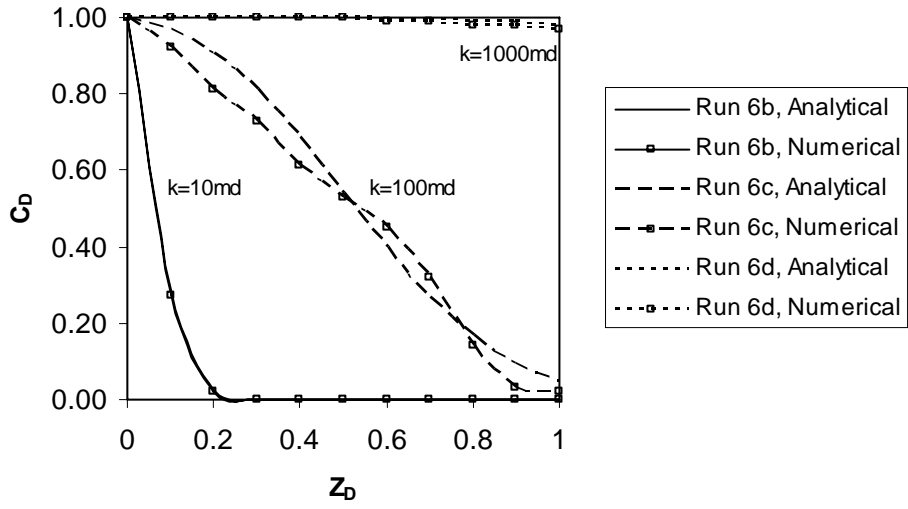


Figure 6. 47. Effect of Permeability (1000 years, comparison)

6.3.2.3 Effect of Porosity on CO₂ Saturation

The comparison of analytical and numerical modeling is made for porosity effect in Figure 6.48 for Run 7a, Run 3b, and Run 7b. The results are in good agreement.

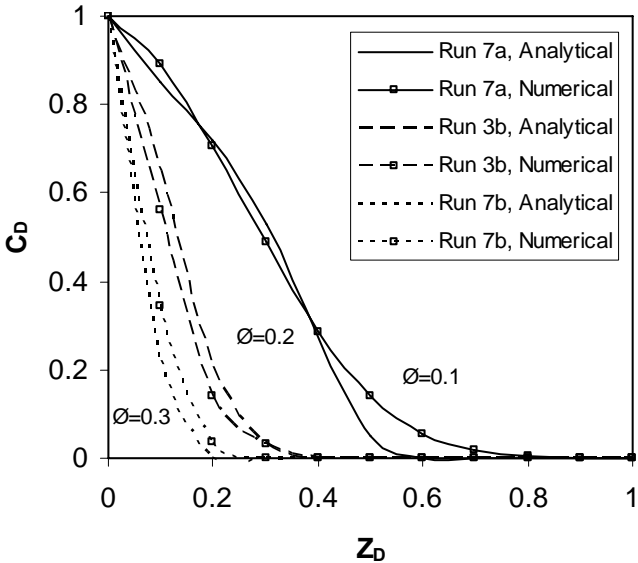


Figure 6. 48. Effect of Porosity (200 years, comparison)

6.3.2.4 Root Mean Square Error (RMSE)

The most common accuracy measurement between two different data is the Root Mean Square Error (RMSE) technique. The RMSE is sensitive to interpolation, phase error and the general variability or anomaly. To compare errors between the results of analytical and numerical models, the “Root Mean Square Error” equation 6.2 is used. RMSE of one shows the maximum error which is complete difference and zero value shows the exact match between data.

$$RMSE = \sqrt{\left(\frac{1}{n}\right) \times \left(\sum_{i=1}^n (C_{analytical} - C_{numerical})^2\right)} \quad (6.2)$$

Table 6. 6, RMSE values for Runs

1a	1b	1c	1d	1e
0.01	0.02	0.01	0.05	0.08
2a			2b	
0.01			0.01	
3a	3b		3c	
0.01	0.03		0.04	
4a	4b		4c	
0.04	0.02		0.04	
5a	5b		5c	
0.02	0.04		0.03	
6a	6b	6c	6d	
0	0	0.03	0.01	
7a		7b		
0.04		0.04		

The RMSE values of run cases are given in table 6.6. The values are between 0 and 0.08. The RMSE values are generally very low and in some cases zero which is a very good match. However, in some cases the RMSE value is slightly higher than that of others, especially for very long duration simulations and for the transition zones in the transport.

6.4 Determination of Mixing Zone Length by Using the Results of Analytical Modeling

The dimensionless mixing (transition) zone, Equation 6.3, is defined as the difference between two points where $C_D=0.1$ and $C_D=0.9$ [28]. This is the fraction of the total system length that lies between defined concentration limits at a given time. Because the results of analytical and numerical models are in good agreement which is supported by RMSE method, the analytical model is only used to find mixing zone lengths. Some run cases (Run 1e, 5a, 5b, 5c, and 6d) are omitted due to lowest value of C_D greater than 0.1 which is out of definition in dimensionless mixing zone.

$$\Delta z_D = z_D \Big|_{C_D=0.1} - z_D \Big|_{C_D=0.9} \quad (6.3)$$

6.4.1 Molecular Diffusion Process

6.4.1.1 Effect of Time on Mixing Zone Length

The mixing zone length increases with time as seen in Figure 6.49 in diffusion dominated system.

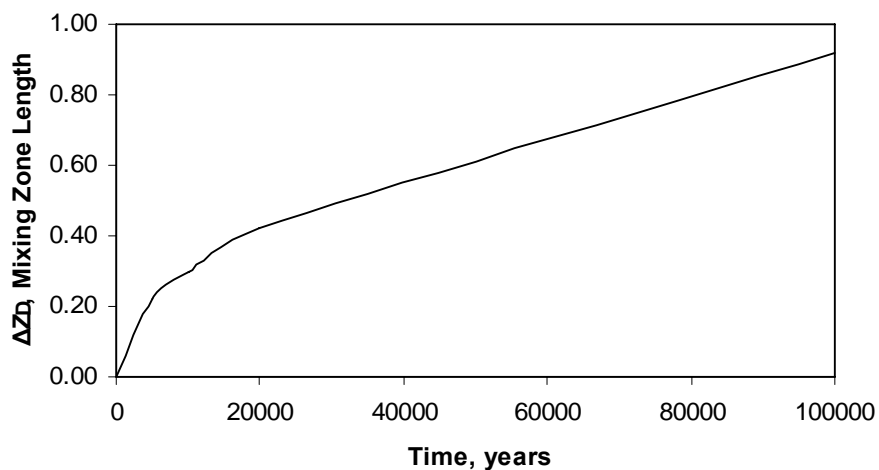


Figure 6. 49. Variation of Mixing Zone with Time for Diffusion Dominated System

6.4.1.2 Effect of Porosity on Mixing Zone Length

The mixing zone length increases with porosity as seen in Figure 6.50 in diffusion dominated system.

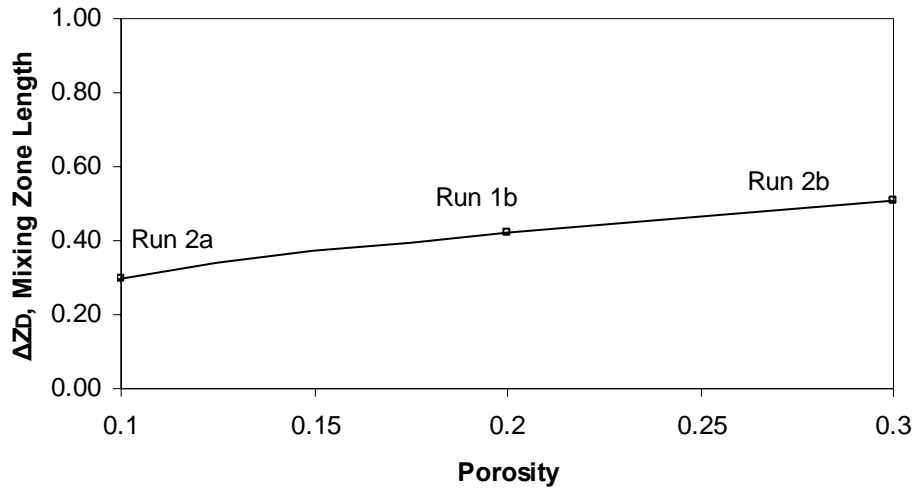


Figure 6. 50. Variation of Mixing Zone with Porosity for Diffusion Dominated System (20000 years)

6.4.2 Convection Process

6.4.2.1 Effect of Dispersivity on Mixing Zone Length

The mixing zone length increases with dispersivity as seen in Figure 6.51 in convection dominated system.

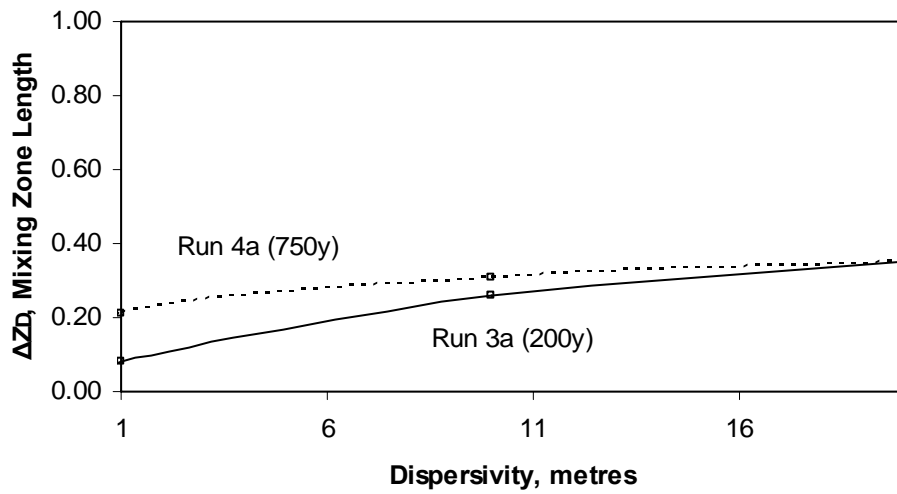


Figure 6. 51. Variation of Mixing Zone with Dispersivity for Convection Dominated System

6.4.2.2 Effect of Permeability on Mixing Zone Length

The mixing zone length increases with permeability after a point as seen in Figure 6.52 in convection dominated system. This point is the sign of the beginning of convection in the system.

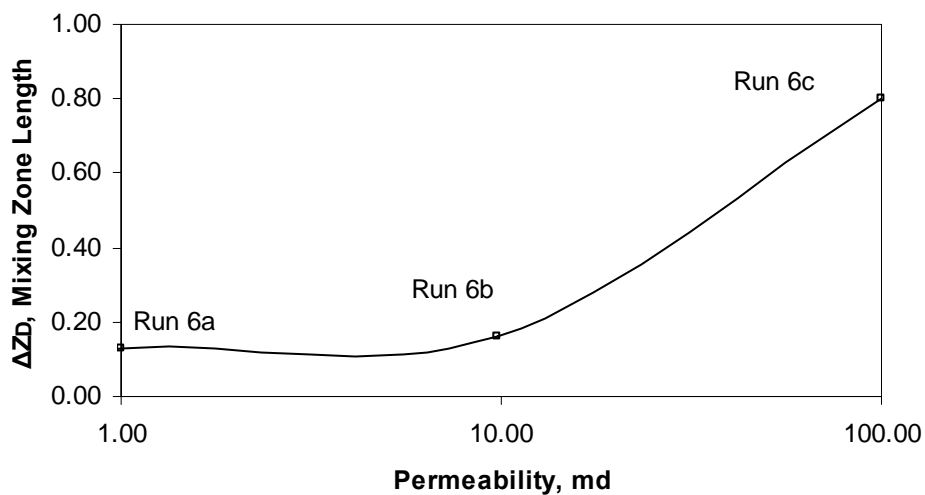


Figure 6. 52. Variation of Mixing Zone with Permeability for Convection Dominated System (1000 years)

6.4.2.3 Effect of Porosity on Mixing Zone Length

The mixing zone length decreases with porosity as seen in Figure 6.53 in convection dominated system.

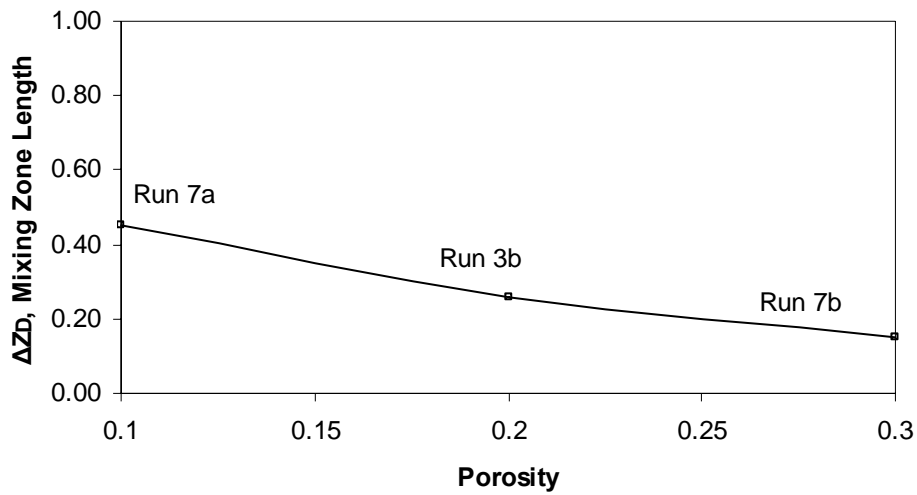


Figure 6. 53. Variation of Mixing Zone with Porosity for Convection Dominated System (200 years)

6.5 CO₂ Saturated Part of the Aquifer

The CO₂ saturated part of the aquifer is calculated by integrating equations of all C_D vs Z_D curves obtained from analytical models (equation 6.4). The CO₂ saturated part of the saturated aquifer is determined in dimensionless unit. It can be considered as a fraction of total aquifer volume. The equation of the curves is a polynomial type shown in table 6.7. The constant of the polynomial equations are given in table 6.7. All “r²” values are in the range of 0.99 and 1.

$$\text{CO}_2 \text{ Saturated Part of the Aquifer (fraction)} = \int_0^{Z_D(\max)} C_D \cdot dZ_D \quad (6.4)$$

$$C_D = b_1 Z_D^5 + b_2 Z_D^4 + b_3 Z_D^3 + b_4 Z_D^2 + b_5 Z_D + n \quad (6.5)$$

Table 6.7, Constants for Polynomial Equation of C_D vs z_D Curves

Run	b_1	b_2	b_3	b_4	b_5	n	Figure
1a	0	6.7	-17.91	17.12	-6.96	1	6.1
1b	0	0	-3.16	6.74	-4.59	1	6.1
1c	0	0	-1.5	3.99	-3.5	1.01	6.1
1d	0	0	0.15	0.32	-1.36	1	6.1
1e	0	0	0.0006	7.10^{-6}	-0.13	1	6.1
2a	0	0	-3.16	6.74	-4.59	1	6.2
2b	0	0	-0.7	2.5	-2.8	1.01	6.2
3a	-36.06	105.44	-115	57.42	-12.8	0.99	6.4
3b	4.41	-5.61	-5.65	12.12	-6.27	1.01	6.4
3c	9.95	-23.46	15.5	1.21	-4.2	1	6.4
4a	40.89	-112.3	108.1	-40.1	2.41	1	6.5
4b	15.51	-42.02	38.38	-11.12	-1.75	1	6.5
4c	10.65	-28.76	25.56	-6.06	-2.4	1	6.5
5a	0	-0.61	0.88	-0.4	0.06	1	6.6
5b	0	0.02	-0.23	0.03	-0.02	1	6.6
5c	0	0.05	-0.16	-0.07	-0.04	1	6.6
6a	-25.24	76.22	-86.85	46.11	-11.25	1	6.7
6b	-20.52	63.4	-74.39	41.06	-10.55	1	6.7
6c	-3.1	7.73	-4.88	-0.45	-0.25	1	6.7
6d	0	0	-0.04	0.02	-0.01	1	6.7
7a	3.91	-15.4	20.71	-10.04	0.19	1	6.8
7b	-14.68	47.54	-59	34.81	-9.67	1	6.8

Table 6.8, CO_2 Saturated Part of the aquifer (fraction), analytical modeling

Run 1a	Run 1b	Run 1c	Run 1d	Run 1e
0.12	0.15	0.22	0.46	0.94
Run 2a	Run 1c		Run 2b	
0.15	0.22		0.27	
Run 3a	Run 3b		Run 3c	
0.05	0.12		0.15	
Run 4a	Run 4b		Run 4c	
0.23	0.20		0.20	
Run 5a	Run 5b		Run 5c	
0.99	0.95		0.92	
Run 6a	Run 6b	Run 6c	Run 6d	
0.07	0.08	0.54	1	
Run 7a	Run 3b		Run 7c	
0.31	0.16		0.08	

6.6 Rayleigh and Peclet Numbers

Rayleigh numbers for each run are calculated with equation 3.6 and presented in Table 6.9. Rayleigh number gives an idea about the occurrence of convection. Since the velocity changes in the system as a function of space and time, the average velocities are used for the calculation of Rayleigh numbers. As seen in Table 6.9, Rayleigh numbers of runs 6a and 6b are below the critical Rayleigh number which is about 39.5, [23].

Table 6.9, Rayleigh Numbers

Run 3a	Run 3b	Run 3c	
116	233	233	
Run 4a	Run 4b	Run 4c	
146	81	58	
Run 5a	Run 5b	Run 5c	
116	116	116	
Run 6a	Run 6b	Run 6c	Run 6d
6	8	233	1164
Run 7a	Run 3b	Run 7c	
582	233	77	

Peclet numbers for each run are calculated with equation 3.7 and given in Table 6.10. Peclet Number gives the ratio of convective forces to dispersive forces. Peclet numbers are nearly same for each run except for Run 6a and Run 6b in which the diffusion mechanism is dominated.

Table 6.10, Peclet Numbers

Run 3a	Run 3b	Run 3c	
9.2	9.6	9.6	
Run 4a	Run 4b	Run 4c	
9.4	8.9	8.5	
Run 5a	Run 5b	Run 5c	
9.2	9.2	9.2	
Run 6a	Run 6b	Run 6c	Run 6d
3.7	4.5	9.6	9.9
Run 7a	Run 3b	Run 7c	
9.8	9.6	8.9	

6.7 Comparison between Numerical Results of Molecular Diffusion and Dispersion

In this part, the lower limit of permeability required for the beginning of convective flow is investigated. Equation 5.1 is used for convection dominated runs (Run 9) and Equation 5.2 is used for diffusion dominated runs (Run 8). Then, these results are compared.

In Figure 6.54, the comparison of Runs 8a and 9a is done by matching their results. The similar results are obtained. The effect of convection is so little that the transport of CO₂ could be due to diffusion dominated mechanism for a system having a permeability of 1 md.

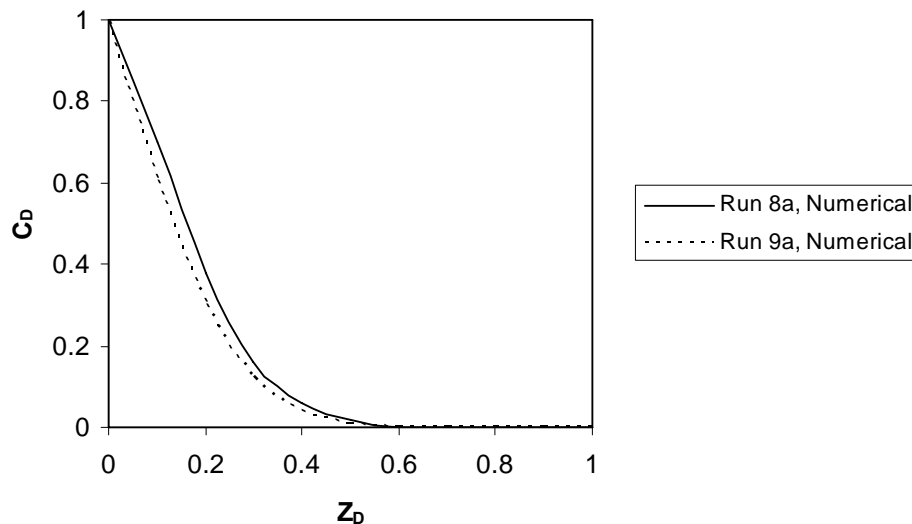


Figure 6. 54. Comparison of Results for Runs 8a and 9a, t=10000 y and k=1 md

In Figure 6.55, the results of two runs, Run 8b and Run 9b, are again similar. Also for 10md systems, the effect of convection is so little that the transport could be accepted as diffusion dominated mechanism for a system having a permeability of 10 md.

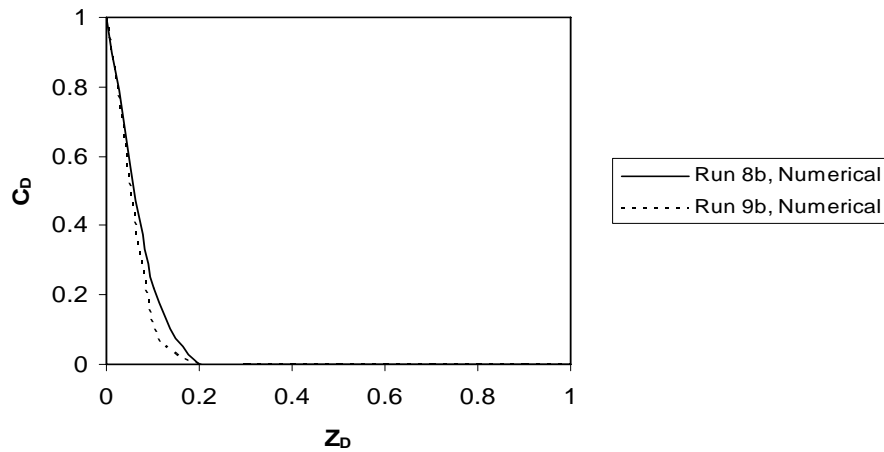


Figure 6. 55. Comparison of Results for Runs 8b and 9b, $t=1000$ y and $k=10$ md

In Figure 6.56, the system starts to be gradually convection dominated for a system having a permeability of 20 md although the aid of the diffusion is significant. It is shown that convection begins to occur after 20 md permeability; however the system is neither diffusion nor convection dominated in Run 8c and Run 9c.

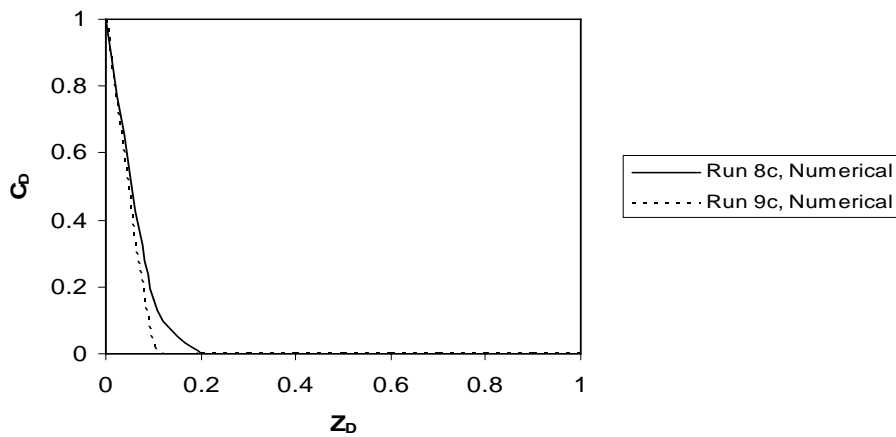


Figure 6. 56. Comparison of Results for Runs 8c and 9c, $t=500$ y and $k=20$ md

In Figure 6.57, the system behaves as convection dominated system having a permeability of 50md. The diffusion has no significant contribution to the

transport in Run 8d and Run 9d because there is no dissolved CO₂ even in the upper part of the aquifer.

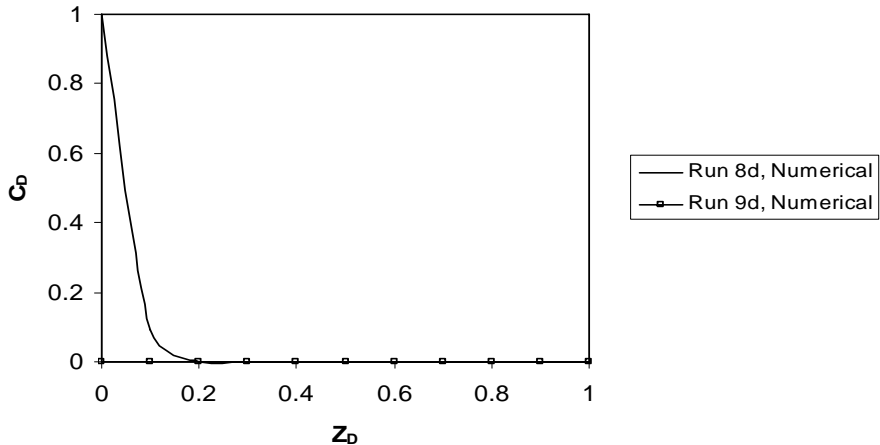


Figure 6. 57. Comparison of Results for Runs 8d and 9d, t=200 y and k=50 md

In Figure 6.58, the system behaves as convection dominated in 100md aquifer. The diffusion has no contribution to the transport in Run 8e and Run 9e because there is no dissolved CO₂ even in the upper part of the aquifer.

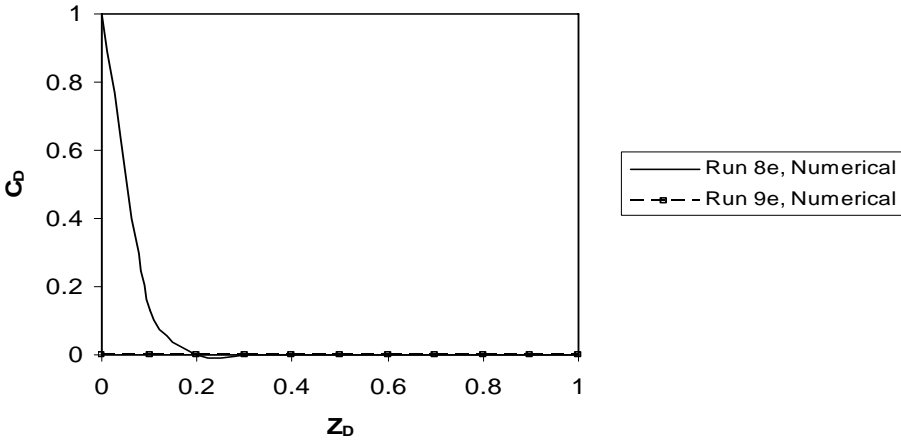


Figure 6. 58. Comparison of Results for Runs 8e and 9e, t=100 y and k=100 md

In Figure 6.59, the system behaves as convection dominated in 1000md aquifer. The diffusion has no contribution to the transport in Run 8f and Run 9f because there is no dissolved CO₂ even in the upper part of the aquifer.

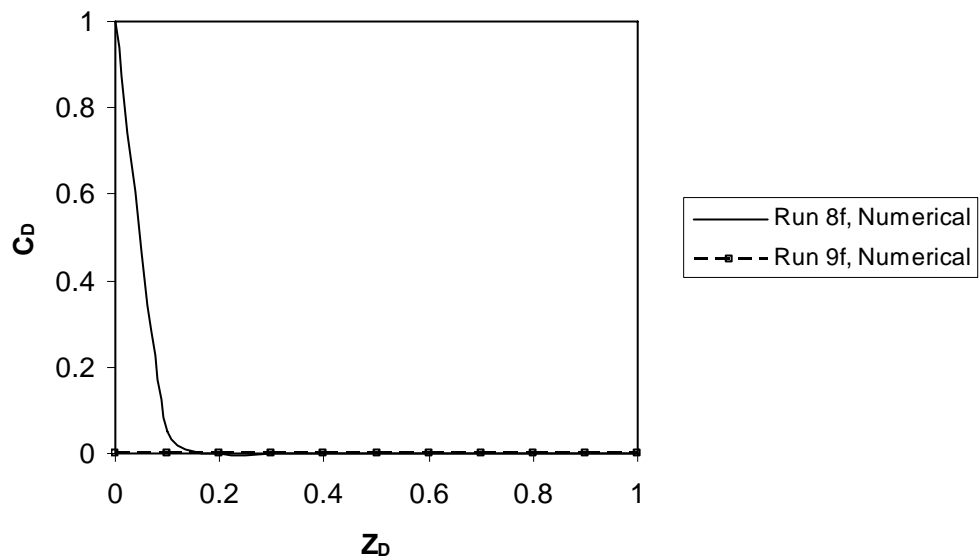


Figure 6. 59. Comparison of Results for Runs 8f and 9f, t=10 y and k=1000 md

CHAPTER 7

CONCLUSIONS

A comparison is made between analytical and numerical modeling of CO₂ solute transport in a hypothetical deep saline aquifer in this thesis. The effects of aquifer properties on transport mechanisms are evaluated in one dimensional vertical system.

The following remarks are concluded after having the results of analytical and numerical models:

- The complete dissolution of CO₂ in the aquifer by only diffusion takes thousands, even millions of years. In diffusion dominated system, an aquifer with 100 m thickness becomes just about saturated after 10,000,000 years. Whereas, this time is much smaller in the convective dominant systems.
- In diffusion dominant process, dissolution of CO₂ in aquifer increases with porosity increase; however, in convection dominant process dissolution of CO₂ in aquifer decreases with porosity. Because the increase in porosity decreases the velocity of brine in the aquifer.
- The increase in permeability accelerates the dissolution of CO₂ in aquifer significantly, which might be due to increasing velocity.
- Dispersivity increases the spreading and the transport distance of CO₂ in the aquifer. At the end of the dissolution process in the aquifer, the dissolved CO₂ amount in the aquifer increases with lower dispersivity values.
- The results of convective dominant mechanism in aquifers with 1md and 10md permeability values are so near in that of diffusion dominated system. After 10md, the convection mechanism begins to dominate

gradually and it becomes totally convection dominated for 50 md and higher permeability values. These results are also verified by Rayleigh number and mixing zone lengths.

- Rayleigh number gives an idea about the occurrence of convection. The runs having Rayleigh numbers that are above the critical Rayleigh number of 39.5 are considered as convection dominated systems.
- The mixing zone length increases with porosity and time in diffusion dominated system. However, the mixing zone length decreases with porosity and it increases with dispersivity and permeability higher than 10 md in convection dominated system.

This study is important step to select the candidate aquifer for CO₂ sequestration. For the aquifer having 0.2 porosity and 100 m x 100 m x 100 m dimensions in 50° C temperature and 75 atm pressure, 4,000 tonnes of CO₂ could be sequestered. For more typical dimensions, such as 1000 m x 1000 m x 1000 m aquifer, 4,000,000 tonnes of CO₂ could be sequestered. Besides aquifer's storage capacity, its transmissivity is also important. If the quick dissolution rate of CO₂ is wanted, the aquifers higher than 50 md permeability are good alternatives.

RECOMMENDATIONS

For CO₂ sequestration in Turkey, the inventory of deep saline aquifers should be prepared. After this inventory, the candidate aquifer with high storage capacity and quick dissolution property could be determined for CO₂ sequestration in the next step.

REFERENCES

- 1) IEA Greenhouse Gas R&D Programme, "Capture and Storage of CO₂", <http://www.ieagreen.org.uk> (accessed February 02, 2006)
- 2) IEA Greenhouse Gas R&D Programme, "CO₂ Storage in Deep Salt Water Reservoirs", <http://www.ieagreen.org.uk> (accessed February 02, 2006)
- 3) Noh, M., Lake, L. W., Bryant, S. L., and Araque-Martinez, A.: "Implications of Coupling Fractional Flow and Geochemistry for CO₂ Injection in Aquifers", paper SPE 89341 presented at SPE/DOE 14th Symposium on Improved Oil Recovery, Tulsa, U.S.A, 2004
- 4) Justus, J. R., and Fletcher, S. R., Global Climate Change, Congressional Research Service, March 2006
- 5) Wikipedia contributors, "Global warming," *Wikipedia, The Free Encyclopedia*, http://en.wikipedia.org/w/index.php?title=Global_warming&oldid=58192104 (accessed June 12, 2006)
- 6) NASA (National Aeronautics and Space Administration), The Satellite view of Arctic Sea Ice in 1979 and 2003, http://earthobservatory.nasa.gov/Newsroom/NewImages/images.php3?img_id=16340 (accessed January 12, 2006).
- 7) IEA Greenhouse Gas R&D Programme, "Geological Storage of CO₂", <http://www.ieagreen.org.uk> (accessed February 02, 2006).
- 8) Gorelick, S. M., Freeze, R. A., Donohue, D., Keely, J. F., *Groundwater Contamination: Optimal Capture and Containment*, CRC Press LLC, 1993.
- 9) Todd, D. K., and Mays, L. W., *Groundwater Hydrology*, 3rd Edition, John Wiley & Sons, 2005
- 10) Wikipedia contributors, "Aquifer," *Wikipedia, The Free Encyclopedia*, <http://en.wikipedia.org/w/index.php?title=Aquifer&oldid=59645732> (accessed July 31, 2006)

- 11) Bouwer, H., *Groundwater Hydrology*, McGraw-Hill, 1978
- 12) Domenico, P. A., Schwartz, F. W., Physical and chemical hydrogeology, 2nd Edition, John Wiley & Sons, 1998
- 13) Wikipedia contributors, "Fick's law of diffusion," *Wikipedia, The Free Encyclopedia*, http://en.wikipedia.org/w/index.php?title=Carbon_dioxide&oldid=65904787 (accessed June 03, 2006)
- 14) Cussler, E. L., Diffusion : mass transfer in fluid systems, 2nd edition, Cambridge University Press, 1997
- 15) Unver, A., Himmelblau, D. M., "Diffusion Coefficients of CO₂, C₂H₄, C₃H₆, and C₄H₈ in Water from 6° to 65°C", *Journal of Chemical and Engineering Data*, Vol. 9, No. 3, July 1964
- 16) Hirai, S., Okazaki, K., Yazawa, H., Ito, H., Tabe, Y., Hijikata, K., "Measurement Of CO₂ Diffusion Coefficient And Application Of Lif In Pressurized Water", *Energy*, Vol. 22, No. 2/3, pp. 363-367, 1997
- 17) Wikipedia contributors (2005), "Laser-induced Fluorescence", *Wikipedia, The Free Encyclopedia*. Retrieved October 1, 2005 from http://en.wikipedia.org/wiki/Laser-induced_fluorescence
- 18) Wilke, C. R, Chang, P., *Am. Inst. Chem. Eng. J.* 1, 264-270, 1955
- 19) Shimizu, K., Kikkawa, N., Nagashima, A., *Proc. 4th Asian Thermophysical Properties Conferences* 3, 771 (1995)
- 20) Onda K., Okamoto T., and Yamaji Y., *Chemical Engineering*, Vol. 24, page 918, 1960
- 21) Tang Y.P., and Himmelblau D.M., "Effect of solute concentration on the diffusivity of carbon dioxide in water", *Chemical Engineering Sciences*, Vol. 20, page 7-14, 1965
- 22) Bedient, P.B., Rifai, H.S., Newell, C.J., *Groundwater Contamination: Transport and Remediation*, Prentice Hall, 1994
- 23) Weatherill, D., Simmons, C. T., Voss, C. I., and Robinson, N. I., "Testing density-dependent groundwater models: Two-dimensional

- steady state unstable convection in infinite, finite and inclined porous layers” , *Advances in Water Resources*, 2004
- 24) Fetter, C.W., *Applied Hydrogeology*, Macmillan College Publishing Company, 3rd Edition, 1994
 - 25) Holzbecher, E., *Modeling Density-Driven Flow in Porous Media: principles, numerics, software*, Springer-Verlag, 1998
 - 26) Wikipedia contributors, "Porosity," *Wikipedia, The Free Encyclopedia*, <http://en.wikipedia.org/w/index.php?title=Porosity&oldid=64943455> (accessed July 31, 2006)
 - 27) Wikipedia contributors, "Permeability (fluid)," *Wikipedia, The Free Encyclopedia*, http://en.wikipedia.org/w/index.php?title=Permeability_%28fluid%29&oldid=66636583 (accessed July 31, 2006)
 - 28) Lake, L. W., *Enhanced Oil Recovery*, New Jersey: Prentice-Hall, 1989
 - 29) Nofziger, D. L., and Wu, J., Lecture Notes, <http://soilphysics.okstate.edu/software/cde/document.pdf> (accessed May 05, 2006)
 - 30) Anderson, M.A., 1984. Movement of contaminants in groundwater: Groundwater transport-Advection and dispersion. In: *Groundwater Contamination*, National Academy Press, Washington D.C.: 37-45.
 - 31) Gelhar, L. W., C. Welty and K. R. Rehfeldt, A critical review of data on field-scale dispersion in aquifers, *Water Resources Research*, 28(7): 1955-1974, 1992
 - 32) Neuman, S.P., Universal scaling of hydraulic conductivities and dispersivities in geologic media, *Water Resources Research*, v. 26, no. 8, pp. 1749-1758, 1990
 - 33) Price, M., *Introducing Groundwater*, Chapman & Hall, 2nd Edition, 1996
 - 34) Ebbing, D. D., and Gammon, S. D., *General Chemistry*, Houghton Mifflin Company, 6th Edition, 1999
 - 35) Modified from <http://www.cbu.edu/~mcondren/c115e503.htm> (accessed June 06,2006)

- 36) Enick, R.M., Klara, S.M., "CO₂ Solubility in Water and Brine under Reservoir Conditions", Chem. Eng. Comm., Vol. 90, pp. 23-33, 1990
- 37) Dodds, W. S., Stutzman, L. F., and Sollami, B. J., "Carbon Dioxide Solubility in Water", Industrial and Engineering Chemistry, Vol. 1, No. 1, 1956
- 38) Batzle, M. and Wang, Z., Seismic properties of pore fluids: Geophysics, Vol. 57, No. 11, p. 1396-1408, 1992
- 39) McCain, W. D. Jr, Reservoir fluid property correlations-state of the art. SPE Reservoir Engineering, 6, pp. 266-272, 1991
- 40) Garcia, J. E., "Density of Aqueous Solutions of CO₂", Report LBNL-49023, Lawrence Berkeley National Laboratory, CA 2001. 8 p.
- 41) Bachu, S., Adams, J. J., "Sequestration of CO₂ in geological media in response to climate change: capacity of deep saline aquifers to sequester CO₂ in solution", Energy Conversion and Management, Vol. 44, pg. 3151-3175, 2003
- 42) Tumasjan, A. B., Panteleev, V. G., Mejncer, G. P., "Influence de l' Anhydride Carbonique Sur Les Propriétés Physiques du Pétrole et de l'eau", Nefteprom. delo. n2, pp. 20-23, 1969
- 43) Farouq, A.S.M., *Oil Recovery by Steam Injection*, Producers Publishing Company, 1970
- 44) Langevin, C.D., Shoemaker, W.B., and Guo, W., MODFLOW-2000, the U.S. Geological Survey Modular Ground-Water Model-Documentation of the SEAWAT-2000 Version with the Variable-Density Flow Process (VDF) and the Integrated MT3DMS Transport Process (IMT): U.S. Geological Survey Open-File Report 03-426, 43 p., 2003
- 45) Guo, W., and Langevin, C.D., User's guide to SEAWAT: A computer program for simulation of three-dimensional variable-density ground-water flow: Techniques of Water-Resources Investigations of the U.S. Geological Survey, Book 6, Chapter A7, 77 p., 2002

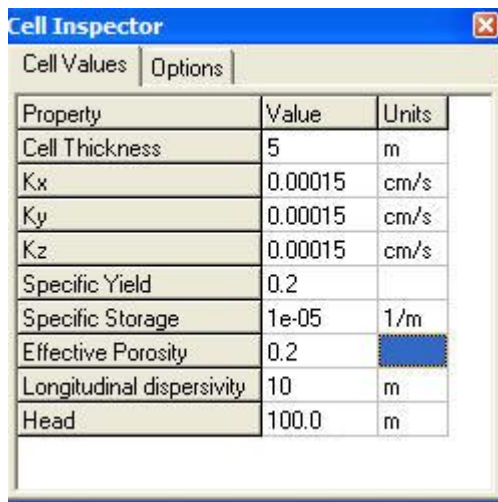
- 46) Dirik, I., Bülül, S., Altıntaş, A. and Gümrah, F.: “Analytical Modeling of CO₂ Sequestration in Saline Aquifers”, Proceedings of Canadian International Petroleum Conference, 55th Annual Technical Meeting, June 8-10, 2004, Calgary, Alberta, Canada
- 47) İzgeç, Ö.: “Experimental and Numerical Investigation of Carbon Dioxide Sequestration in Deep Saline Aquifers”, A MSc Thesis Submitted to Graduate School of Middle East Technical University, 2005
- 48) Başbuğ, B.: “Modeling of Carbon Dioxide Sequestration in a Deep Saline Aquifer”, A MSc Thesis Submitted to Graduate School of Middle East Technical University, 2005

APPENDIX

Input Data for Numerical Model (VISUAL MODFLOW):

- Number of Grid Blocks in x-direction = 20
- Number of Grid Blocks in y-direction = 20
- Number of Grid Blocks in z-direction = 20
- Length of Each Grid Block = 5 meters
- Density/Concentration Slope = 0.2357

For the variation of brine density with CO₂ saturation, “0.2357” is taken as density/concentration slope which is obtained from Figure 3.15. Concentration readings of numerical results are made through the direction of plume. Some images could be viewed in Figure A.1, A.2, A.3, A.4, A.5, and A.6 about the numerical simulator (Visual MODFLOW) for the input and run parts. The hydraulic conductivity (K) values were calculated by using equation 3.10 for convection dominated systems. The values are given in Figure A.7. Viscosity and brine density were taken as 0.7 cp and 1.05 g/cm³, respectively.



Property	Value	Units
Cell Thickness	5	m
Kx	0.00015	cm/s
Ky	0.00015	cm/s
Kz	0.00015	cm/s
Specific Yield	0.2	
Specific Storage	1e-05	1/m
Effective Porosity	0.2	
Longitudinal dispersivity	10	m
Head	100.0	m

Figure A.1. Input Data for Run 3b

Constant Variant Parameters

Model Params

Name	Designation	Description	Value	Units
DENSEREF	DENSEREF	Reference fluid density	1060	kg/m ³
DENSEMIN	DENSEMIN	Minimum fluid density	1060	kg/m ³
DENSEMAX	DENSEMAX	Maximum fluid density	1070	kg/m ³
DENSESLP	DENSESLP	Density/concentration slope	0.2357	

OK Cancel Help

Figure A.2. Input Data for all Density-dependent Runs

Dispersion Package

Edit columns

Layer #	Horiz./Long. Dispersivity [-]	Vert./Long. Dispersivity [-]	Diff Coeff [m ² /yr]
1	0.1	0.01	0.019
2	0.1	0.01	0.019
3	0.1	0.01	0.019
4	0.1	0.01	0.019
5	0.1	0.01	0.019
6	0.1	0.01	0.019
7	0.1	0.01	0.019
8	0.1	0.01	0.019
9	0.1	0.01	0.019
10	0.1	0.01	0.019
11	0.1	0.01	0.019
12	0.1	0.01	0.019
13	0.1	0.01	0.019
14	0.1	0.01	0.019
15	0.1	0.01	0.019
16	0.1	0.01	0.019
17	0.1	0.01	0.019
18	0.1	0.01	0.019
19	0.1	0.01	0.019
20	0.1	0.01	0.019

OK Cancel

Figure A.3. Options for layers of Aquifer about dispersivity and diffusion coefficient terms

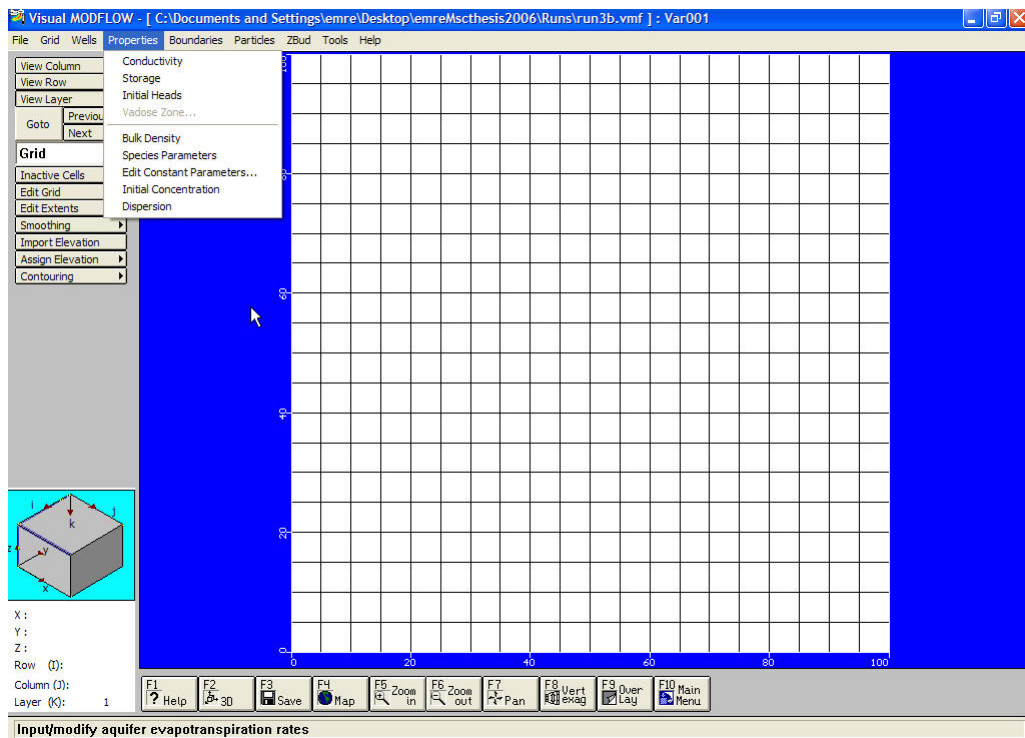


Figure A.4. User Interface Screen to Enter Inputs

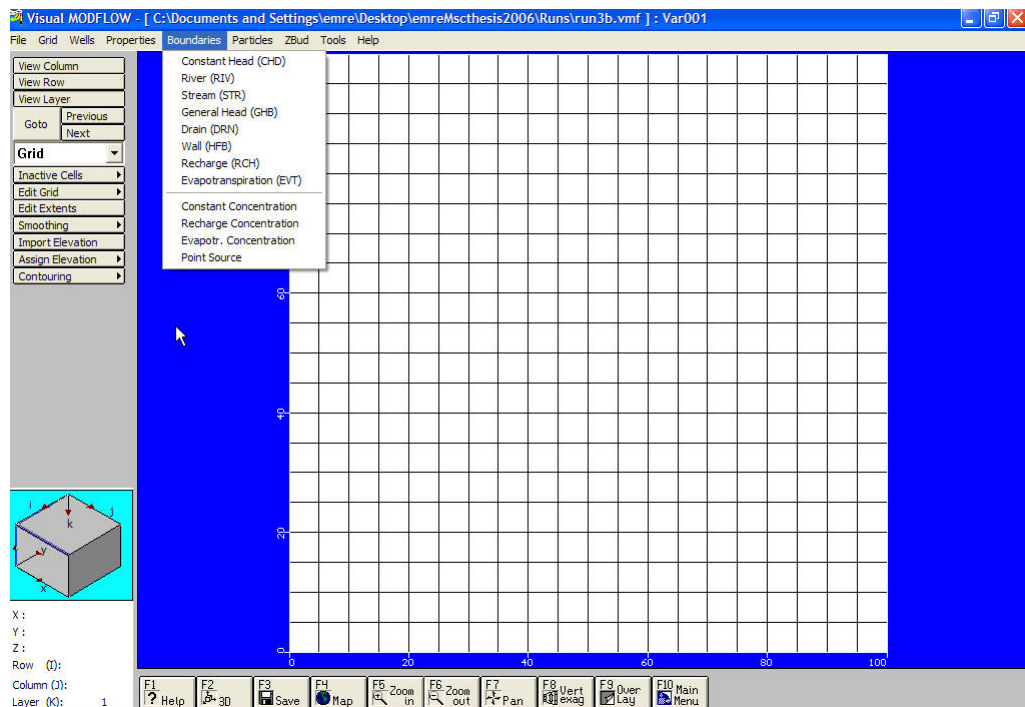


Figure A.5. User Interface Screen to Enter Inputs

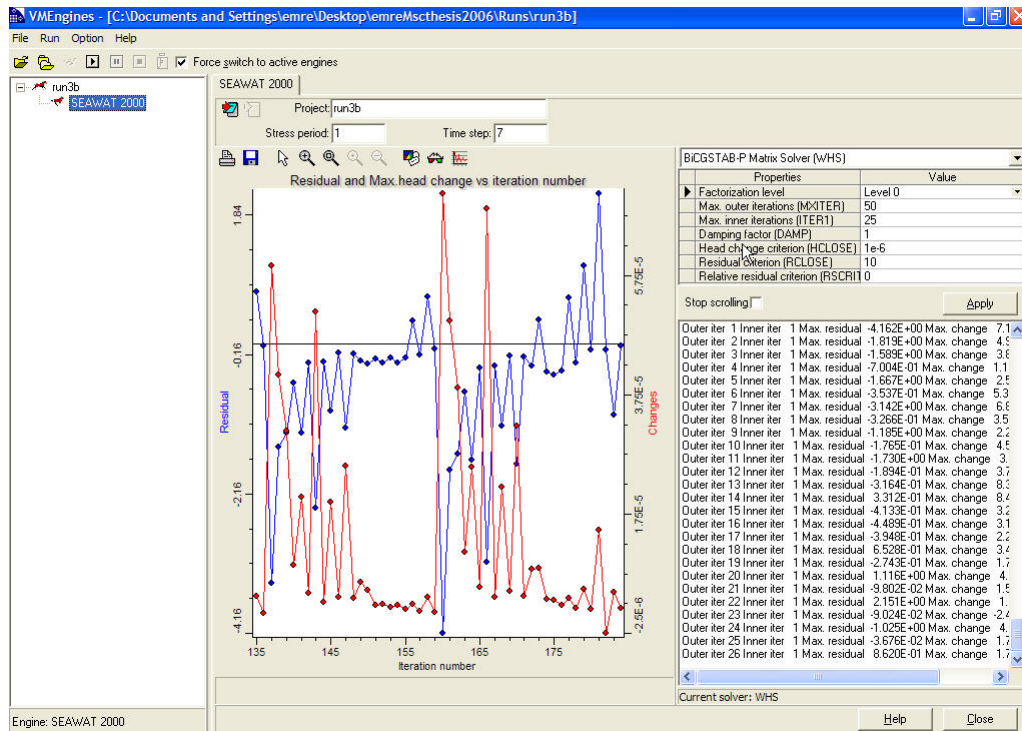


Figure A.6. Engine to Run the Given Inputs

Run Numbers	Hydraulic Conductivity, cm/s
3	$1.5 \cdot 10^{-4}$
4	$1.5 \cdot 10^{-4}$
5	$1.5 \cdot 10^{-4}$
6a	$1.5 \cdot 10^{-6}$
6b	$1.5 \cdot 10^{-5}$
6c	$1.5 \cdot 10^{-4}$
6d	$1.5 \cdot 10^{-3}$
7	$1.5 \cdot 10^{-4}$

Figure A.7, Hydraulic Conductivities for Each Run